

Best Practices for Radio Propagation Measurements

Chriss Hammerschmidt
Robert T. Johnk
Paul M. McKenna
Christopher R. Anderson



technical memorandum

Best Practices for Radio Propagation Measurements

**Chriss Hammerschmidt
Robert T. Johnk
Paul M. McKenna
Christopher R. Anderson**



U.S. DEPARTMENT OF COMMERCE

David J. Redl
Assistant Secretary for Communications and Information

November 2018

DISCLAIMER

Certain commercial equipment and materials are identified in this report to specify adequately the technical aspects of the reported results. In no case does such identification imply recommendation or endorsement by the National Telecommunications and Information Administration, nor does it imply that the material or equipment identified is the best available for this purpose.

CONTENTS

| | |
|--|-----|
| Figures..... | vi |
| Tables..... | xi |
| Abbreviations/Acronyms | xii |
| 1. Introduction..... | 1 |
| 2. Comparison of Five Channel-Sounder Architectures..... | 4 |
| 3. Measurement Basics | 7 |
| 3.1 General Remarks..... | 7 |
| 3.2 Connections | 7 |
| 3.3 Accurate Measurement of System Losses | 11 |
| 4. Component Measurements..... | 13 |
| 4.1 Signal Generator Output Power Variability..... | 14 |
| 4.2 The Transmit Power Amplifier..... | 16 |
| 4.3 Receiver Preselector/Preamplifier | 18 |
| 4.4 Bandpass Filter | 24 |
| 4.5 Directional Couplers..... | 25 |
| 4.6 Antenna Pattern Characterization..... | 26 |
| 4.7 Antenna Directionality Considerations..... | 27 |
| 5. System Measurements | 31 |
| 5.1 Detection Algorithms and System Noise Floor | 31 |
| 5.2 System Noise Floor Measurement..... | 35 |
| 5.3 System Dynamic Range..... | 38 |
| 5.4 EMI/EMC Problems | 40 |
| 6. Benchtop Testing | 44 |
| 6.1 Link Budget | 44 |
| 6.2 Benchtop Testing – Single Power Level..... | 45 |
| 6.3 Benchtop Testing – Simulated Fading Environments | 46 |
| 7. In-Situ (Radiated Signal) System Testing..... | 50 |
| 7.1 NLOS Drive Route—Rayleigh Fading..... | 50 |
| 7.2 LOS drive route—Rician fading..... | 55 |
| 7.3 Measurement System Repeatability Measurements | 59 |
| 8. Summary of Best Practices | 60 |
| 9. References..... | 61 |
| Acknowledgements..... | 65 |

| | |
|--|----|
| Appendix A —Measurement System Uncertainties | 66 |
| Appendix B —Antenna Characterization | 69 |
| B.1 Far-field Characteristics of Some Common Antennas..... | 69 |
| B.2 Anechoic Chamber Measurements | 70 |
| B.3 Open Area Test Site (OATS) | 70 |
| B.4 Free-Field Antenna Measurements | 71 |
| B.5 Turntable Measurements at Table Mountain | 72 |
| B.6 General Test Procedure for Other Situations | 76 |
| Appendix C —Measurement System Uncertainties | 78 |
| C.1 Mobile Measurement Repeatability Analysis | 78 |
| C.2 Static Measurement Repeatability Analysis..... | 86 |
| C.3 Parameter Dependencies on Propagation Measurements | 88 |

FIGURES

| | |
|--|----|
| Figure 1. Multipath environment experienced by signals propagating between a transmitter and receiver..... | 4 |
| Figure 2. Type N (precision, distinguished by solid inner conductor) and SMA male RF connectors. Photo courtesy of en.wikipedia.org. | 8 |
| Figure 3. Test setup used to show comparison between hand tightening and torque wrench tightening of an N connector..... | 9 |
| Figure 4. S11 magnitude variations for repeated hand-tightened connections. | 9 |
| Figure 5. S11 magnitude variations for repeated torqued connections..... | 10 |
| Figure 6. S21 magnitude variations for hand-tight connections. | 10 |
| Figure 7. S21 magnitude variations for torqued connections. | 11 |
| Figure 8. Type N female connector. Photo from Aerial.net website (https://www.aerial.net/shop/product_info.php?products_id=780). | 11 |
| Figure 9. Schematic showing how the transmitting side of the ITS propagation measurement system was measured with a VNA versus a signal generator/power meter combination. | 12 |
| Figure 10. ITS transmitter equipment configuration used in conducting propagation measurements..... | 13 |
| Figure 11. ITS receiver equipment configuration for measuring RF propagation attenuation..... | 14 |
| Figure 12. Schematic for signal generator output power testing. | 15 |
| Figure 13. Equipment setup for power amplifier testing. | 17 |
| Figure 14. Input power (dBm) vs. Output power (Watts) for 3 different power amplifiers. | 17 |
| Figure 15. Power amplifier harmonic measurement. The second harmonic is at -88 dBm which is approximately 45 dB below the fundamental. The third harmonic is about 60 dB down from the fundamental..... | 18 |
| Figure 16. Preselector/preamplifier schematics for a broadband spectrum measurement system. | 19 |
| Figure 17. Receiving system block diagram for Long-Term Evolution (LTE) aggregate measurement..... | 20 |

| | |
|--|----|
| Figure 18. Carrier RSL and system noise floor (kTB) for different component configurations. | 22 |
| Figure 19. C/N versus LNA gain. | 24 |
| Figure 20. Equipment setup for measuring insertion loss a bandpass filter. | 25 |
| Figure 21. VNA measurement of a bandpass filter from 1755 to 1780 MHz. | 25 |
| Figure 22. Magnetic declination of the earth’s magnetic field in North America. See https://maps.ngdc.noaa.gov/viewers/historical_declination/index.html (accessed 8/24/2018). | 28 |
| Figure 23. Using a directional antenna to make measurements in the Martin Acres neighborhood. | 29 |
| Figure 24. Misaligned directional antenna used to make measurement in the Martin Acres neighborhood. | 29 |
| Figure 25. RBW vs. RSL for system noise and a CW signal. | 31 |
| Figure 26. RBW vs. RSL for system noise and band-limited Gaussian noise with a bandwidth of 6 kHz. | 33 |
| Figure 27. Measured CW signal showing the effect of various detection algorithms for a system noise floor of -104 dBm. | 35 |
| Figure 28. ITS measurement system testing with a variable attenuator. | 36 |
| Figure 29. VSA measurement results for the ITS system as a function of attenuation. | 37 |
| Figure 30. VSA measurement results for the ITS system as a function of attenuation both with and without the noise floor points. | 38 |
| Figure 31. Illustration showing the dynamic range of a receiver and its relationship to the noise floor and saturation power. | 39 |
| Figure 32. Dynamic range for an SA (blue trace) and a VSA (red trace). | 40 |
| Figure 33. EMI problems—two signals through power amplifier. | 41 |
| Figure 34. EMI problems—power amplifier in Faraday cage, and common ground circuit. | 42 |
| Figure 35. Link budget parameters. | 45 |
| Figure 36. Received signal power in dB for a simulated 20 dB path loss and 90 dB path loss. | 46 |

| | |
|---|----|
| Figure 37. Simulated Rayleigh fading channel measured with a VSA. The fast-fading data (blue trace) and the slow-fading data (red trace) calculated using a 1 second moving average..... | 47 |
| Figure 38. Normalized Rayleigh fading channel and the PDF for the simulated channel..... | 48 |
| Figure 39. Simulated power spectrum for a Rayleigh channel..... | 49 |
| Figure 40. NLOS drive path in Martin Acres next to the Boulder Laboratories. The transmitter is shown by the red + and the street chosen for analysis is shown by the blue line. The yellow arrow is the location of a wave-guiding street..... | 52 |
| Figure 41. NLOS environment in the Martin Acres neighborhood. The blue trace is the fast-fading data and the red trace is the slow-fading data which is a 1 second windowed average..... | 53 |
| Figure 42. Linear signal envelope and dB signal envelope for the run from 659 to 671 seconds..... | 53 |
| Figure 43. Slow-fading dB signal envelope and the Doppler frequency spectrum from 659 to 671 seconds..... | 54 |
| Figure 44. PDF for the NLOS drive run in Martin Acres from 659 to 671 seconds..... | 54 |
| Figure 45. Power spectrum for a NLOS drive test showing a Doppler frequency spectrum from approximately -104 Hz to $+104$ Hz..... | 55 |
| Figure 46. LOS drive path in Martin Acres next to the Boulder Laboratories. The transmitter is shown by the red + and the street chosen for analysis is shown by the blue line..... | 56 |
| Figure 47. LOS environment in the Martin Acres neighborhood. The blue trace is the fast-fading data and the slow-fading data which is shown by the red trace using a 1 second windowed average..... | 57 |
| Figure 48. Slow-fading dB signal envelope and the Doppler frequency spectrum for the LOS condition on Lashley Lane in Martin Acres..... | 57 |
| Figure 49. Linear signal envelope and dB signal envelope for the run from 505 to 515 seconds for the LOS condition on Lashley Lane..... | 58 |
| Figure 50. Slow-fading dB signal envelope and the Doppler frequency spectrum from 505 to 515 seconds for the LOS condition on Lashley Lane..... | 58 |
| Figure 51. PDF for the LOS drive route in Martin Acres from 505 to 515 seconds..... | 59 |

| | |
|---|----|
| Figure A-1. Reflection coefficient definitions for uncertainty terms. | 67 |
| Figure B-1. Schematic showing a measurement of an antenna in an anechoic chamber..... | 70 |
| Figure B-2. Photo of an antenna measurement at the NIST OATS facility at the Boulder Laboratories. | 71 |
| Figure B-3. Microwave absorber placement to minimize reflection into receiving antenna. | 72 |
| Figure B-4. Time-domain responses for antenna measurements on an OATS facility at various distances. | 72 |
| Figure B-5. LPDA reference measurement. | 74 |
| Figure B-6. Measurement of a log-periodic antenna on top of the van. | 75 |
| Figure B-7. (a) Manufacturer’s antenna radiation pattern at three different frequencies, (b) measured antenna radiation pattern at the Table Mountain facility..... | 76 |
| Figure B-8. Measurement of vehicle antenna. | 77 |
| Figure C-1. Table Mountain drive route for repeatability studies and static measurement locations..... | 78 |
| Figure C-2. Received power for all four runs at Table Mountain. | 79 |
| Figure C-3. Sample sizes of received power at each point for different size radius bins..... | 80 |
| Figure C-4. Standard deviation of received power at each point for different size radius bins. | 81 |
| Figure C-5. Boxplots of standard deviation of received power (dBm) by radius (all samples)..... | 82 |
| Figure C-6. Coefficient of variation of received power at each point for different size radius bins..... | 82 |
| Figure C-7. Coefficient of variation of received power (mW) at each point for different size radius bins. | 83 |
| Figure C-8. Figure showing three locations of high standard deviation..... | 84 |

| | |
|---|----|
| Figure C-9. Figure showing the location of three measurement points at the left-most intersection on Table Mountain (see yellow square in Figure C-8). Google Earth ® image, 2015. | 84 |
| Figure C-10. Northern-most location on Table Mountain where large standard deviations exits. | 85 |
| Figure C-11. Measured smoothed received power as a function of time for static position 1 on Table Mountain. | 87 |
| Figure C-12. Received power as a function of time for static position 2 on Table Mountain. | 87 |
| Figure C-13. Screening measurement drive route. Sections for analysis are shown by the green outlined regions. | 90 |
| Figure C-14. Received power levels for all screening measurement runs along Lashley Lane and Moorhead Ave. | 91 |
| Figure C-15. Boxplots of received power as a function of the screening variables. | 92 |
| Figure C-16. Plot of main screening effects (influence factors) as a function of the mean value of the received power level in dBm. | 93 |
| Figure C-17. Pareto chart showing the percentage influence of each main effect on the mean received power levels. | 94 |
| Figure C-18. Pareto chart showing the percentage influence of each main effect on the coefficient of variation (CV). | 95 |
| Figure C-19. Pareto chart showing the percentage influence of each main effect on the K-factor. | 95 |

TABLES

| | |
|--|----|
| Table 1. Advantages and disadvantages of various channel sounders..... | 5 |
| Table 2. Recorded output powers for signal generator..... | 15 |
| Table 3. System linearity measurements..... | 17 |
| Table 4. Power amplifier measurements of power contained in harmonics..... | 18 |
| Table 5. Noise figure calculations for system shown in Figure 17..... | 21 |
| | |
| Table A-1. Typical uncertainty sources and their values for the ITS measurement system..... | 66 |
| | |
| Table B-1. Various antennas, their largest aperture dimension, and the far-field distance for their lowest and highest frequencies..... | 69 |
| | |
| Table C-1. Summary of sample sizes by radius bin size..... | 80 |
| Table C-2. Summary statistics of received power standard deviations by radius bin size..... | 81 |
| Table C-3. Summary of received power coefficient of variation by radius bin size..... | 83 |
| Table C-4. Summary of basic transmission loss (dB) and distance difference (m) of three measurement files for the nearest neighbor..... | 85 |
| Table C-5. Summary of basic transmission loss (dB) and distance difference (m) of three measurement files for the closest mutual location..... | 86 |
| Table C-6. Summary of screening variables..... | 88 |
| Table C-7. Run chart for screening experiment..... | 88 |

ABBREVIATIONS/ACRONYMS

| | |
|-----------------------|--|
| 3D | 3-Dimensional |
| AC | Alternating current |
| AM | Amplitude modulation |
| AWS | Advanced Wireless Services |
| BP | Bandpass |
| C/N | Carrier-to-noise |
| COW | Cellular on wheels |
| CW | Continuous wave |
| dB | Decibel |
| dB_i | Decibel referenced to isotropic |
| dB_m | Decibel referenced to 1 mW |
| DC | Direct Current |
| DSO | Defense Spectrum Organization |
| DRG | Dual-ridged guided |
| EIRP | Equivalent isotropically radiated power |
| EMC | Electromagnetic compatibility |
| EMI | Electromagnetic interference |
| FCC | Federal Communications Commission |
| FSPL | Free-space path loss |
| GHz | Gigahertz |
| GPS | Global Positioning System |
| Hz | Hertz |
| IF | Intermediate frequency |
| I-Q | In-phase and quadrature |
| ITS | Institute for Telecommunication Sciences |
| J | Joules |
| JSON | Java-script object notation |
| K | Kelvin |
| kHz | kilohertz |
| LNA | Low-noise amplifier |
| LOS | Line-of-sight |
| LPA | Log-periodic antenna |
| LPDA | Log-periodic dipole antenna |
| LTE | Long-Term Evolution |
| MHz | Megahertz |
| NF | Noise figure |

| | |
|-------------|--|
| NLOS | Non-line-of-sight |
| NIST | National Institute of Standards and Technology |
| NTIA | National Telecommunications and Information Administration |
| OATS | Open Area Test Site |
| PA | Power amplifier |
| PDF | Probability distribution function |
| PN | Pseudo-random noise |
| PXA | Precision signal analyzer |
| RBW | Resolution bandwidth |
| RF | Radio frequency |
| RSL | Received signal level |
| RMS | Root mean square |
| RSS | Root sum-of-squares |
| SA | Spectrum analyzer |
| SNR | Signal-to-noise ratio |
| SMA | Subminiature Version A |
| UE | User equipment |
| UPS | Uninterruptable power supply |
| VNA | Vector network analyzer |
| VSA | Vector signal analyzer |
| W | Watts |

BEST PRACTICES FOR RADIO PROPAGATION MEASUREMENTS

Chriss Hammerschmidt, Robert T. Johnk, Paul M. McKenna,¹ Chris Anderson²

This report describes a set of best practices for the preparation and verification of radio propagation measurement systems. We discuss advantages and disadvantages of various channel sounders, the common components used in these systems, and measurement of these components. We then move to system verification measurements both on the benchtop and in some preliminary outdoor propagation measurements. The appendices discuss uncertainty analysis, antenna measurements, and system repeatability and sensitivity analysis measurements.

Keywords: measurements, radio propagation, radio propagation measurements, radio propagation measurement system, radio propagation uncertainties, radio measurement system performance verification

1. INTRODUCTION

In June 2010, the National Telecommunications and Information Administration (NTIA), in collaboration with the Federal Communications Commission (FCC), was tasked to make 500 MHz of Federal and nonfederal spectrum available for fixed and mobile wireless broadband services by 2020 [1]. One way to achieve this goal involves instituting spectrum sharing arrangements between Military Services and commercial wireless carriers [2] prior to transitioning Military Services out of the band. The Defense Spectrum Organization (DSO) has been tasked with managing the Advanced Wireless Services (AWS)-3 transition. A key part of the transition involves developing new propagation models for evaluating radio-frequency (RF) interference between military RF systems and commercial wireless systems sharing the same frequency bands.

An essential part of developing improved RF propagation models is conducting in-situ propagation measurements, both to gain insight into the physics of particular propagation regimes as well as to validate existing and new propagation models developed in support of spectrum sharing. It is vital that such propagation measurements be conducted in such a way that the measurement results are as accurate and repeatable as possible.

The Institute for Telecommunication Sciences (ITS) has a long history of conducting accurate, well-regarded propagation measurements. ITS has recently been tasked by the Defense Spectrum Organization (DSO) with sharing with the wider technical community its institutional knowledge of how to best measure and process RF propagation data.

¹ The authors are with the Institute for Telecommunication Sciences, National Telecommunications and Information Administration, U.S. Department of Commerce, Boulder, CO 80305.

² The author is with the Department of Electrical Engineering at the United States Naval Academy, Annapolis, MD 21402.

We have prepared this document in response to that challenge. Here, we describe best practices for the preparation, and performance verification of, RF propagation measurement systems prior to conducting propagation measurements at field locations. ITS has spent the last few years verifying the accuracy of their continuous wave (CW) channel sounder system. As part of this verification, we have been working with other agencies who have channel sounders to understand the uncertainty bounds [3].

We begin the report by briefly discussing (Section 2) the advantages and disadvantages of a variety of basic channel sounder system architectures: (1) a vector network analyzer (VNA), (2) a continuous-wave (CW) system, (3) a full-bandwidth, correlation-based system, (4) a direct pulse system, and (5) a sliding correlator system [3]-[5]. The five sounders considered have common elements; however, each has trade-offs that make it perform better (or worse) from one type of propagation environment to the next. We provide a table that describes these trade-offs on a system-by-system basis, and recommend suitable propagation measurement system designs as a function of propagation environment.

Five major sections follow. The first (Section 3) discusses instrument warm-up times; the selection of RF connector types; techniques for, and the importance of, making proper connections; and the difference between using a VNA versus using a power meter to measure losses within a measurement system.

Prior to conducting propagation measurements, component losses, characteristics, and operational bandwidths should be measured. These topics are discussed in Section 4. Once components of the system are understood, we can begin assembling the system and checking the characteristics of the system. Important system characteristics are discussed in Section 5. Section 6 discusses the importance of benchtop system testing and techniques that can be used to verify simulated real-world environments. This is an important step so that we understand various types of propagation environments prior to making in-situ, outdoor propagation measurements. The benchtop measurements can also be used to verify performance between various channel sounders [3].

Once a measurement system's performance has been verified on a benchtop, its performance needs to be checked in a real-world environment. Section 7 discusses this topic via an example of various types of propagation measurements that ITS has performed in a neighborhood adjacent to the laboratory. The example shows how testing was performed via both line-of-sight (LOS) paths and non-line-of-sight (NLOS) paths to give us insights into types of propagation channels that might be expected.

Appendix A explains various uncertainties associated with a typical measurement system. Appendix B discusses antenna measurements both in a general sense and for specific examples of measurement scenarios. Each scenario can be used to characterize the antenna pattern of an antenna. Some of these measurements will have increased accuracy, while others may have increased uncertainties associated with them. In Appendix B, we discuss antenna measurements by starting with the best measurement that can be made and ending with a very generalized approach that won't be as accurate, but may be the only option one has. Finally, Appendix C provides some further analysis that ITS undertook to understand the uncertainties associated with their measurement system which may be helpful for other researchers. We looked at both system

repeatability and a screening measurement that allows us to understand the dependence of propagation measurement results on various input parameters such as antenna height, ambient road traffic patterns, LOS streets versus streets in clutter fields,³ and transmitting power.

³ Transmitted signals reflect off physical objects in the environment, including terrain features, buildings, and vegetation. Such reflectors are collectively called clutter.

2. COMPARISON OF FIVE CHANNEL-SOUNDER ARCHITECTURES

When a signal is transmitted into some arbitrary environment, as shown in Figure 1, the signal can propagate along a direct path (red) to a receiver (e.g., a cell phone), it can be reflected from structures and terrain features (blue), and it can be scattered from or through vegetation (orange). Collectively, all of these paths considered together are called the multipath environment. Local interfering signals and RF noise can further complicate the situation by combining with the desired, transmitted propagation-probe signal inside the receiver.

To understand and characterize this variety of propagation paths, many types of channel sounders have been developed to measure impulse responses of propagation channels. A complete discussion of this topic is given in Chapter 2 of [5]; here we only compare different channel sounder architectures.

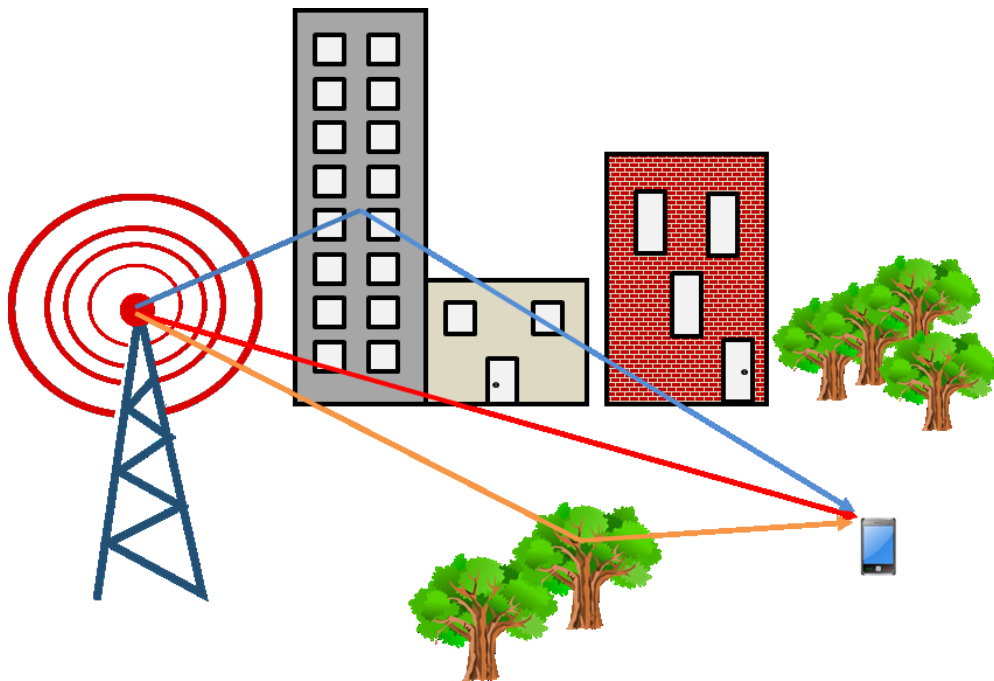


Figure 1. Multipath environment experienced by signals propagating between a transmitter and receiver.

There are five main channel sounder architectures:

- 1) CW, generates a single tone
- 2) Direct pulse, generates periodic pulses
- 3) Frequency domain (VNA), generates a series of frequencies at discrete steps
- 4) Correlation-based, generates a full-bandwidth, pseudo-random noise (PN) sequence
- 5) Swept time delay cross correlator (i.e., sliding correlator), generates a PN sequence and correlates in the analog domain to generate a narrowband signal at the receiver

Table 1 gives a summary of the advantages and disadvantages of each type of channel sounder.

Table 1. Advantages and disadvantages of various channel sounders.

| Channel Sounder Type | Advantages | Disadvantages | Best application |
|-------------------------------|---|---|--|
| CW | <ul style="list-style-type: none"> • Mobile • Simple architecture • Doppler spectra • High dynamic range • In-phase and quadrature (I-Q) information • Easy to obtain transmit authority • Large propagation range • Good audio sampling rates (kHz range) • Continuous data-record acquisition | <ul style="list-style-type: none"> • Does not preserve multipath time information • Requires accurate knowledge of link energy budget for post-processing • Requires clear spectrum at transmitting frequency • No root-mean square (RMS) delay spread | <ul style="list-style-type: none"> • Long-range outdoor environments • Short-range indoor measurements • Short-range indoor/outdoor building penetration measurements • Coherence time of channels • Best Doppler resolution • Imaging of local scatterers |
| Direct Pulse | <ul style="list-style-type: none"> • Simple architecture • Preserves time information • Doppler spectra | <ul style="list-style-type: none"> • Low dynamic range • Prone to jitter and drift • Limited propagation range • Wide receiver bandpass filtering tends to admit undesired in-band signals into the receiver • High-speed switch required • Requires high peak-to-average power ratio | <ul style="list-style-type: none"> • Limited mobility environments • Verification of other systems |
| Frequency Domain (VNA) | <ul style="list-style-type: none"> • Very accurate (NIST traceable) • Wideband • Moderate dynamic range • Limited susceptibility • Path loss • RMS delay spread • Highest resolution of timing/scattering information • Time-gating and deconvolution to enhance propagation parameter extraction • Good interference immunity • Low transmitting power | <ul style="list-style-type: none"> • Requires a physical connection between transmitting port and receiving port • Slow acquisition • Limited propagation range • No Doppler spectra • Limited to static channels • Some measurements require trigger connection | <ul style="list-style-type: none"> • Short-range outdoors • Indoor measurements • Verification of other systems • Shielding measurements |

| Channel Sounder Type | Advantages | Disadvantages | Best application |
|---------------------------|---|--|--|
| Correlation-based | <ul style="list-style-type: none"> • Mobile • Doppler spectra • Preserves time information • Processing gain provides some immunity to noise and interference • Coherence bandwidth • RMS delay spread • Path loss • Shadowing, fast-fading and Rician K-factor | <ul style="list-style-type: none"> • Low dynamic range • Limited range • Complex and time-consuming post-processing algorithms • Requires large measurement bandwidths • Requires higher equivalent isotropically radiated power (EIRP) (compared to CW) for a given propagation range • Large data file sizes | <ul style="list-style-type: none"> • Short-range mobile environments over all types of terrain • Short-range indoor measurements • Short-range indoor/outdoor building penetration measurements • Complex multipath environments |
| Sliding Correlator | <ul style="list-style-type: none"> • Mobile • Narrow post-processing bandwidth, thus smaller data file sizes • Preserves time information • Processing gain provides some immunity to noise and interference • Can resolve multipath components in time | <ul style="list-style-type: none"> • Limited temporal resolution • Requires large measurement bandwidths • Requires higher EIRP (compared to CW) for a given propagation range • Dynamic range depends on length of PN sequence • Susceptible to strong in-band interferers | <ul style="list-style-type: none"> • Mobile environments • Multipath environments |

Although each of these channel sounders uses a different technique to measure various channel parameters, they share some common elements: signal generator, power amplifier, receiver, and selected components (filters, low-noise amplifiers, mixers, cables, and antennas). Other common parameters are detection algorithms, system noise floor and system dynamic range, possible electromagnetic interference/compatibility (EMI/EMC) issues, and system uncertainties. In the sections that follow we will discuss the measurement and characteristics for each of these parameters.

3. MEASUREMENT BASICS

Verifying that the measurement system is operating properly and collecting data as expected prior to deployment at measurement locations is critically important. In this section, we discuss the importance of using appropriate connector types, best practices for using connectors, and the difference between performing system loss measurements using a highly accurate vector network analyzer versus a less accurate power meter. We also discuss measurement system warm-up times and recommended lengths and characteristics of RF cables. All of these influence the operation of the measurement system and, ultimately, the accuracy of the collected propagation data.

3.1 General Remarks

Before beginning any testing or measurements, it is important to allow adequate warm-up time for stabilization of components such as VNAs, power amplifiers, and receiving instrumentation. Most manufacturers suggest at least one-half hour for warm-up. Turning the equipment on 1–2 hours prior to any type of measurement activity will ensure that all internal components stabilize at their recommended operating temperatures. It is also important to keep equipment cool when operating in higher temperatures as this influences the accuracy of the measurement.

Cables for the transmitting and receiving sides of the system should be kept as short as possible. For the transmitting side, short cables allow for maximum radiated transmitter output power. If the transmitting antenna is placed on a mast, it is important to use low-loss, high phase stability cables to accommodate the longer cable lengths between the transmitting equipment and the antenna on the mast. On the receiving side, the noise figure of the receiving system is dominated by the first component in the system after the antenna, which is typically a cable. This will be discussed in greater detail in Section 4.3. Using minimum cable length between the receiver's antenna and its first amplifier will maximize signal-to-noise ratio, improving overall measurement sensitivity.

3.2 Connections

RF cables are used extensively in radio propagation measurements. Most RF cables used in the field have Type N, Subminiature Version A (SMA), or 3.5 mm connectors. The frequency range of a measurement largely determines the recommendation of which connector to use.

Type N connectors are used for frequencies below 18 GHz. There are two broad categories of N connectors: ordinary and precision. The ordinary connectors are less expensive than the precision type and should only be used at frequencies of 1 GHz or less. Precision N connectors can be used at any frequency up to 18 GHz. The two types are visually distinguished by their inner shields: ordinary N connectors have an inner shield with a flower-petal design consisting of about six little tongues of dull-looking pressed metal, whereas this shield is a solid piece of shiny, machined metal in precision N connectors. In general, precision N connectors are recommended at all frequencies below 18 GHz.

SMA connectors can be used for frequencies up to 26.5 GHz; 3.5 mm connectors look similar to SMA connectors and cover the same frequency range, except that the dielectric is air instead of Teflon®. Air dielectrics reduce cable losses. All of these connectors are used in a 50-ohm impedance environment. Figure 2 shows pictures of N and SMA connectors.

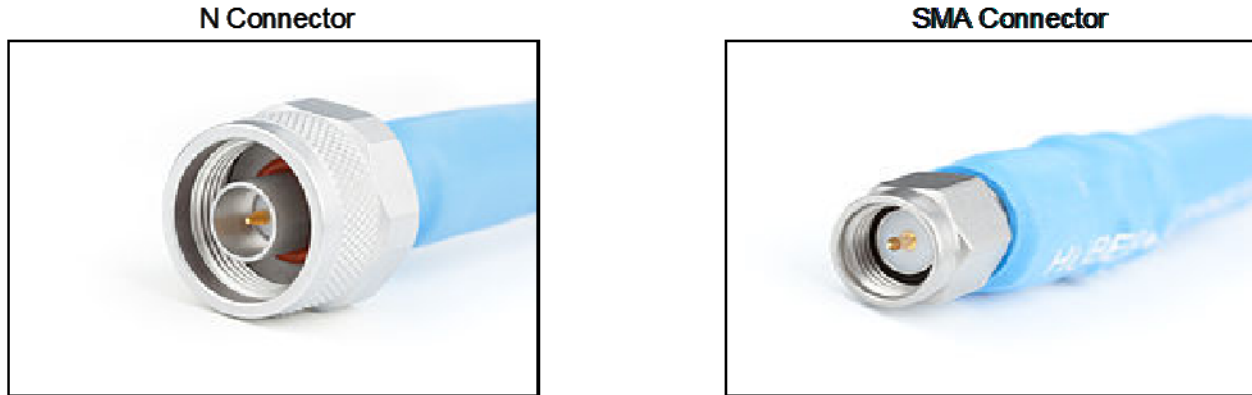


Figure 2. Type N (precision, distinguished by solid inner conductor) and SMA male RF connectors. Photo courtesy of en.wikipedia.org.

It is important to use the appropriate torque wrench to tighten all RF connectors. Using the appropriate torque wrench will reduce mismatch uncertainties, avoid loose connections, and improve repeatability. There are typically two torque values used for RF connectors, 8 in-lb (0.90 N-m) and 12 in-lb (1.36 N-m). The 8 in-lb torque should be used for connections at RF input ports on measurement instruments. The 12 in-lb should be used to tighten all cable-to-cable connections, which can otherwise fail due to insufficient torque.

To demonstrate the importance of using a torque wrench, ITS conducted a test using the setup shown Figure 3. This setup was used to measure the return loss (S_{11}) and the insertion loss (S_{21}) associated with an N female to N female adapter. The test involved hand tightening the two connections to the adapter and measuring S_{11} and S_{21} , then loosening, and then re-tightening the connection. This procedure was repeated six times. The measured values of the magnitude of S_{11} versus frequency is shown in Figure 4. The different curves correspond to the six different measurements (i.e., hand-tightening cycles). These results show that the return loss varies by about 3 dB when only hand tightening is used.

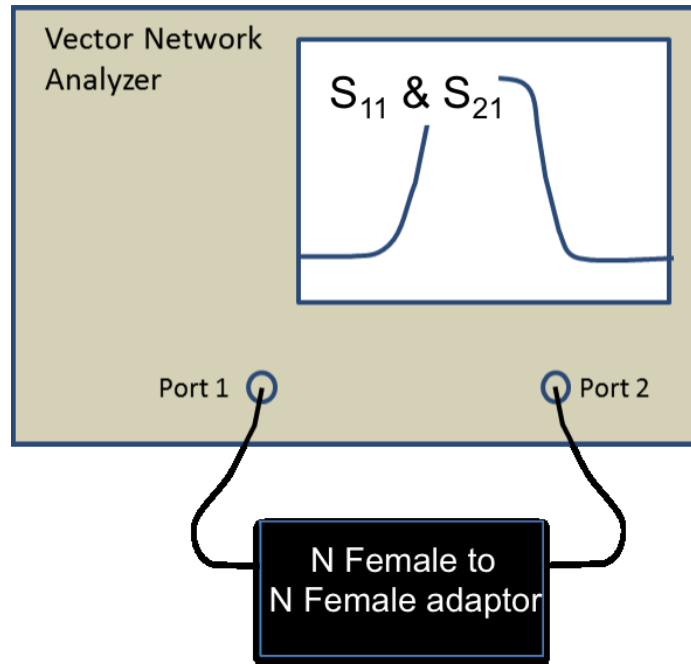


Figure 3. Test setup used to show comparison between hand tightening and torque wrench tightening of an N connector.

The same test was conducted using a 12 in-lb torque wrench (appropriate for Type-N cable connections). The measured S_{11} curves from those tests are shown in Figure 5. This figure shows that the variation in return loss is reduced to about 0.3 dB when a torque wrench is used. Similar comparisons are shown in Figures 6 and 7 for S_{21} . These results show the importance of using a torque wrench when making connections.

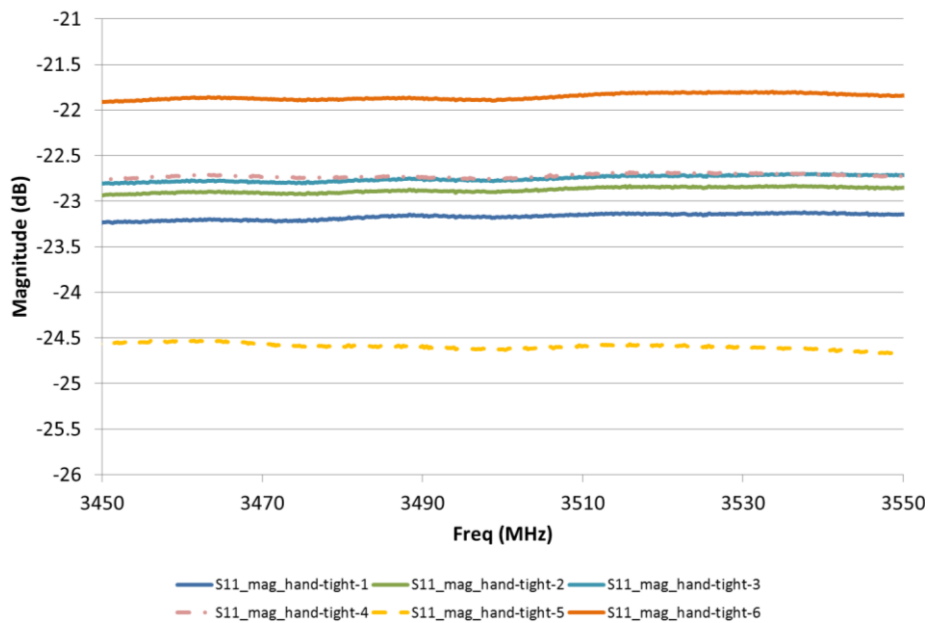


Figure 4. S_{11} magnitude variations for repeated hand-tightened connections.

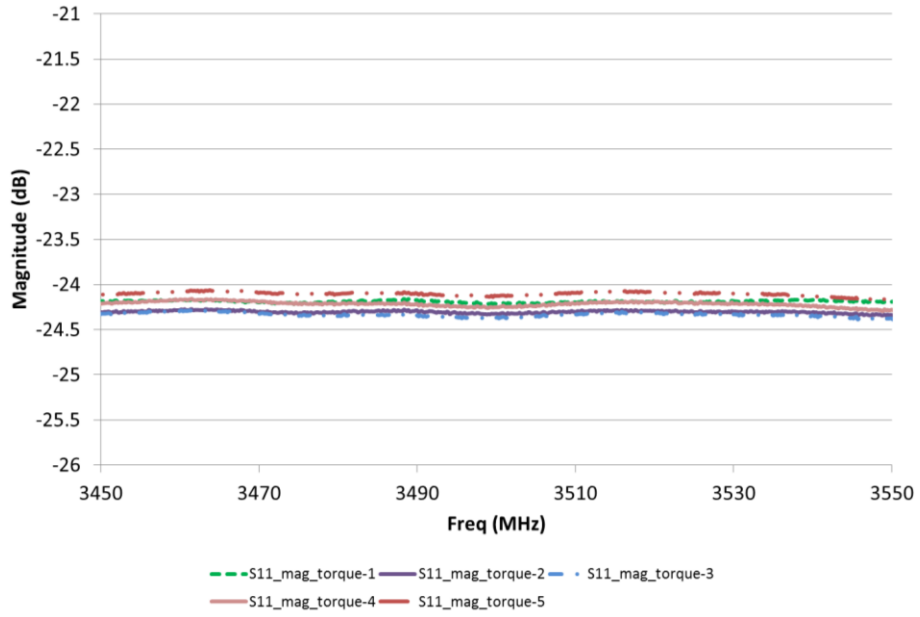


Figure 5. S_{11} magnitude variations for repeated torqued connections.

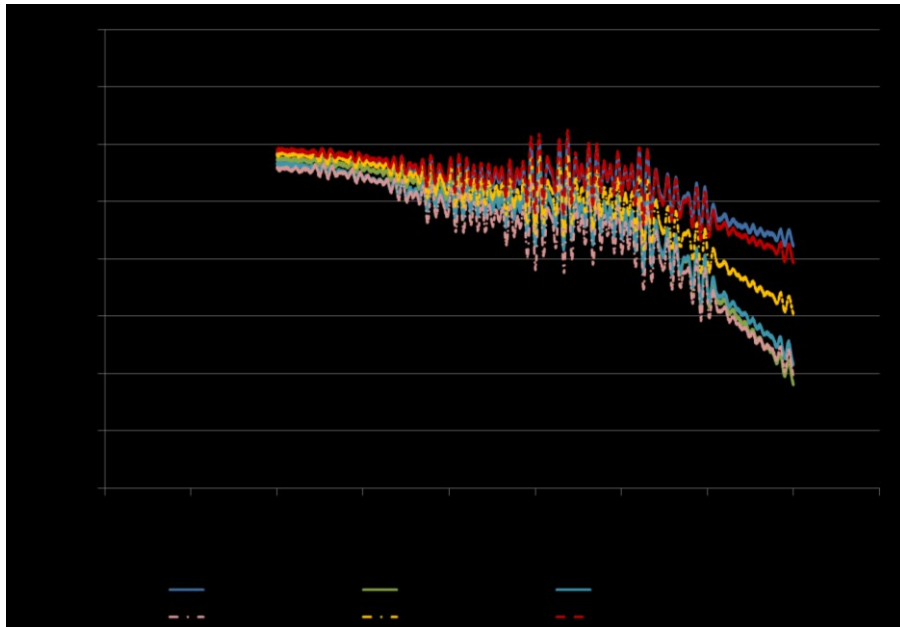


Figure 6. S_{21} magnitude variations for hand-tight connections.

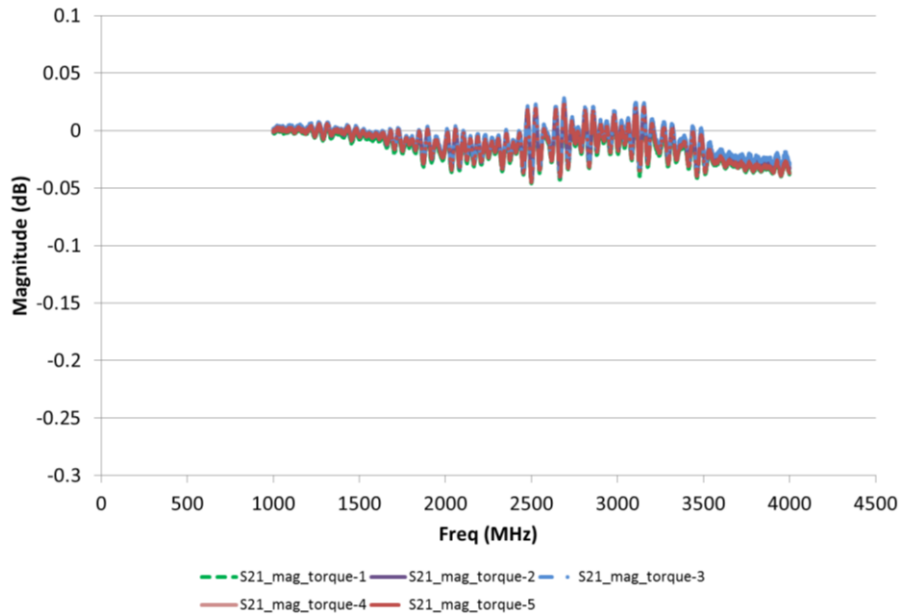


Figure 7. S₂₁ magnitude variations for torqued connections.

Another important consideration is to reduce the movement of cables at their connectors. If one looks closely at an N-type female connector, one can see that the inner connector is assembled using a slotted collar. The slots in the connector allow the male connector (see Figure 8) to provide a tight RF connection. The slotted design also allows slight movement of the connection. If this movement is too severe, it can damage the slots on the connector. Damage will increase the mismatch uncertainties and the losses per connection.



Figure 8. Type N female connector. Photo from Aerial.net website (https://www.aerial.net/shop/product_info.php?products_id=780).

3.3 Accurate Measurement of System Losses

System losses needed for calibration purposes can be measured in one of two ways: use a VNA that contains both a source and receiver inside the instrument, or a signal generator (the source) with a power meter (the receiver). Measuring insertion losses with a VNA is more accurate and useful because it measures both the magnitude and phase of the received signal and can account

for mismatches when properly calibrated. The power meter, in contrast, measures only the magnitude. VNAs are, however, more expensive (e.g., \$150,000, at the time publication) and therefore may not be available to all researchers, and so understanding the difference between measurements using both methods is important.

To illustrate the difference between the two instruments, we performed a set of measurements using the test configurations shown in Figure 9. The test involved measuring the insertion loss of a combination directional coupler, bandpass filter, and 15 meters of coaxial cable using a VNA (Figure 9(a)) versus using a power meter (Figure 9(b)). The results, shown in the figure, indicate that the VNA measures the loss to be 8.27 dB compared with 8.46 dB using a signal generator and power meter, a difference of only about 0.2 dB for this configuration. As mentioned previously the VNA will give the better accuracy and lower uncertainty, however, the difference in the measurement is small and the uncertainty of the power meter can be included in the uncertainty analysis.

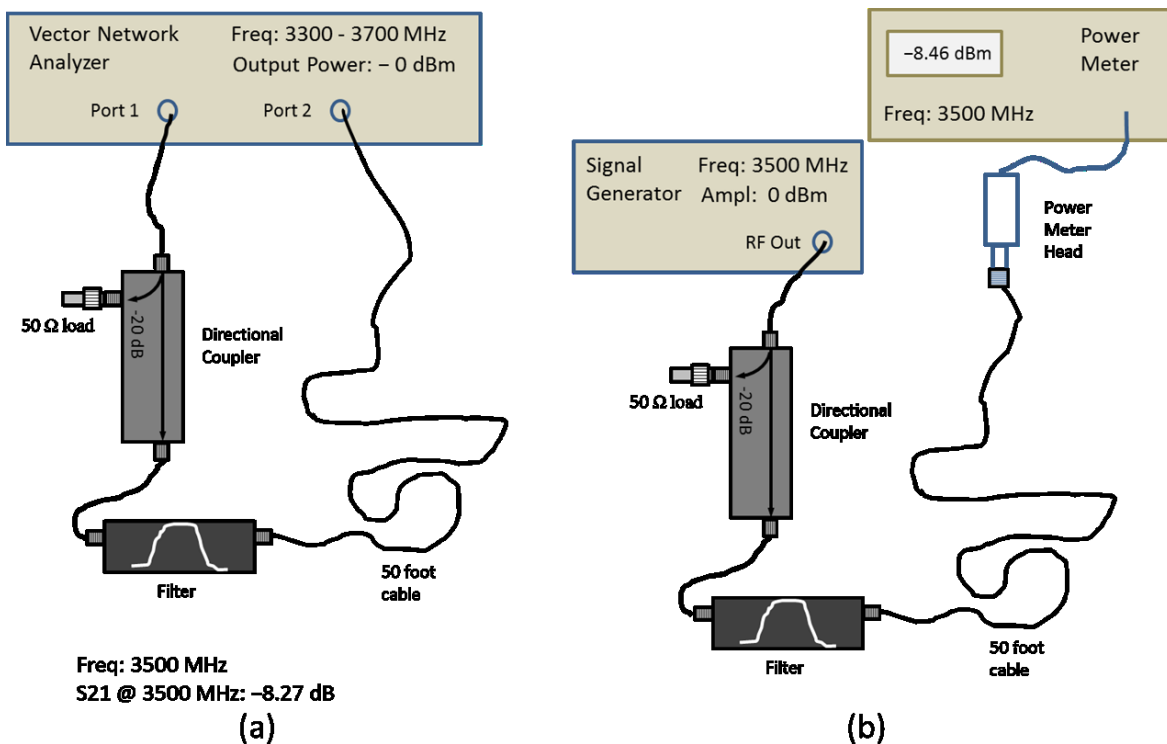


Figure 9. Schematic showing how the transmitting side of the ITS propagation measurement system was measured with a VNA versus a signal generator/power meter combination.

4. COMPONENT MEASUREMENTS

An important part of the test planning process is assembling, testing, and characterizing the hardware components that will be used to conduct the propagation measurements. Figures 10 and 11 show the ITS channel-sounder and the equipment layout for the transmitting side and the receiving side of the system [6]–[8]. The key equipment items that need to be characterized prior to conducting a propagation test are a) the transmit power amplifier; b) bandpass filters, c) directional couplers, d) antennas; and e) the vector signal analyzer (VSA). The measurement of each of these components is addressed in Sections 4.1 to 4.6. Most of these components are common to other types of propagation measurement systems.

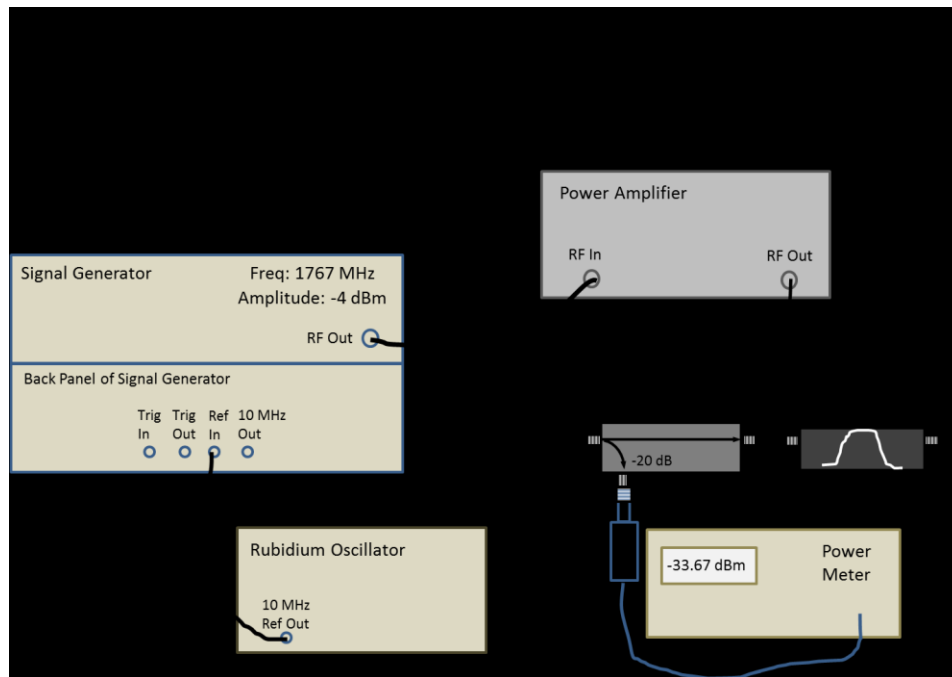


Figure 10. ITS transmitter equipment configuration used in conducting propagation measurements.

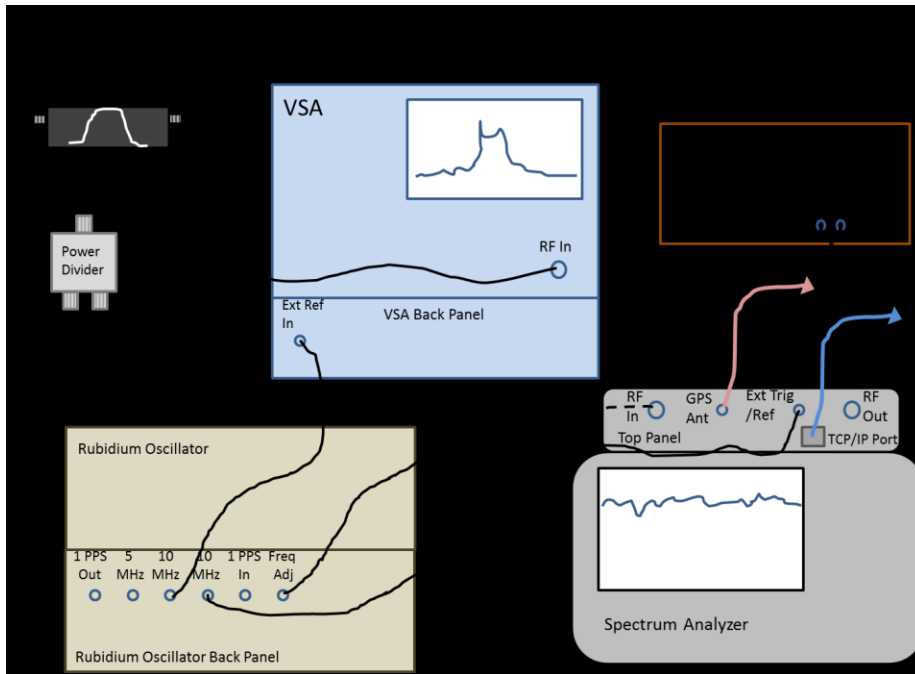


Figure 11. ITS receiver equipment configuration for measuring RF propagation attenuation.

4.1 Signal Generator Output Power Variability

Since all propagation measurement systems need to generate a carefully controlled, well-calibrated signal, it is important to characterize the variability of the output power of the measurement system's signal generator. This measurement needs to be performed using the same RF frequency or frequencies used during field measurements. A schematic of the system setup for measuring signal generator output power variability is shown in Figure 12.

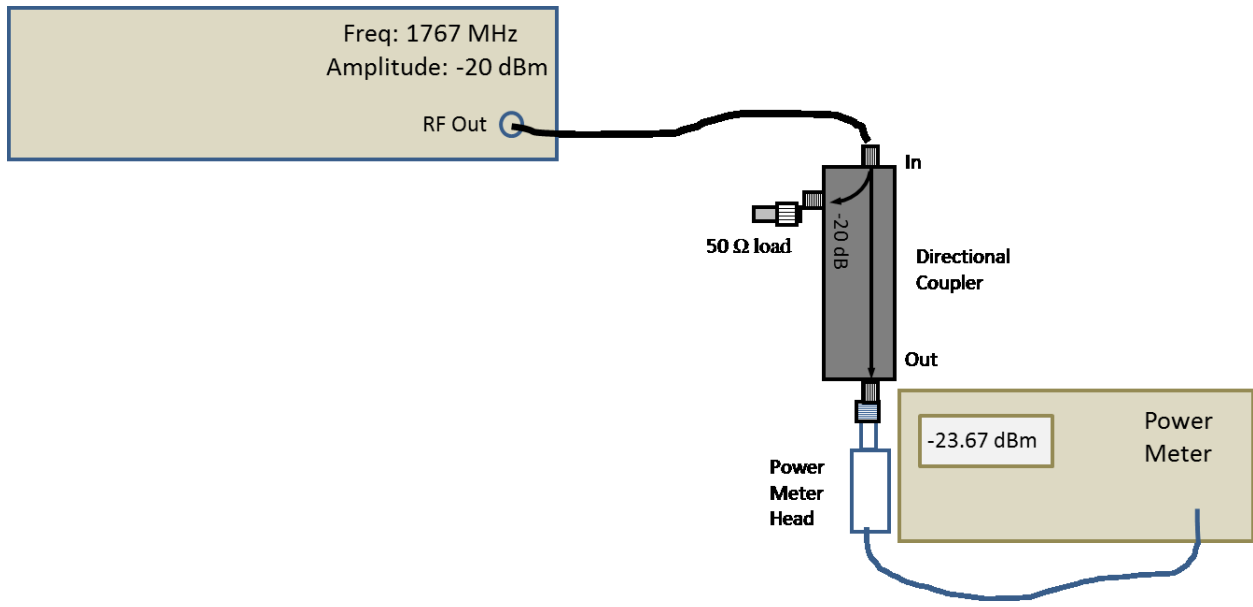


Figure 12. Schematic for signal generator output power testing.

Table 2 shows signal generator output power level measurements from a test conducted by ITS prior to one of its propagation measurement campaigns. The output power was recorded over five days at different times of day. The output power through the directional coupler is given in column 3 and the power read at the coupled port is shown in column 4. These results show that the mean (μ) of the 19 measurements in column 3 is -20.56 dBm and the standard deviation (σ) is 0.66 dBm. The reading at 3:24 p.m. on 4/11/2016 was the lowest reading of the measurement period and was lower than the next lowest by about 2.7 dBm. The reason for this anomaly is unknown, but if it is excluded, because it is a statistical outlier, the mean (μ) of 18 readings is -20.41 dBm and the standard deviation is 0.01 dBm. The standard deviation of the output power is used in the total end-to-end error budget, which is discussed in Appendix A. We also monitor this quantity in the field and this analysis helps us understand when the power amplifier is not behaving as expected.

Table 2. Recorded output powers for signal generator.

| Date | Time | Power-Output (dBm) | Coupled Port (dBm) | Temp (deg F) |
|-----------|------------|--------------------|--------------------|--------------|
| 4/11/2016 | 12:54 p.m. | -20.40 | -40.55 | -- |
| 4/11/2016 | 3:24 p.m. | -23.29 | -40.54 | -- |
| 4/12/2016 | 7:54 a.m. | -20.40 | -40.55 | -- |
| 4/12/2016 | 8:20 a.m. | -20.41 | -40.54 | -- |
| 4/12/2016 | 1:09 p.m. | -20.40 | -40.56 | -- |
| 4/12/2016 | 3:40 p.m. | -20.41 | -40.55 | -- |
| 4/13/2016 | 7:16 a.m. | -20.39 | -40.57 | -- |
| 4/13/2016 | 10:44 a.m. | -20.41 | -40.57 | -- |
| 4/13/2016 | 12:42 p.m. | -20.40 | -40.56 | -- |
| 4/13/2016 | 3:45 p.m. | -20.42 | -40.56 | -- |
| 4/14/2016 | 7:30 a.m. | -20.40 | -40.56 | 83 |
| 4/14/2016 | 8:19 a.m. | -20.40 | -40.54 | 83 |

| Date | Time | Power-Output (dBm) | Coupled Port (dBm) | Temp (deg F) |
|-----------|------------|--------------------|--------------------|--------------|
| 4/14/2016 | 8:48 a.m. | -20.40 | -40.56 | 83 |
| 4/14/2016 | 10:36 a.m. | -20.41 | -40.57 | 79 |
| 4/14/2016 | 3:15 p.m. | -20.42 | -40.57 | -- |
| 4/15/2016 | 7:20 a.m. | -20.41 | -40.56 | 77 |
| 4/15/2016 | 9:08 a.m. | -20.41 | -40.55 | 79 |
| 4/15/2016 | 12:23 p.m. | -20.42 | -40.57 | 83 |
| 4/15/2016 | 2:55 p.m. | -20.40 | -40.56 | 78 |
| μ | | -20.56 | -40.56 | |
| σ | | 0.66 | 0.01 | |

4.2 The Transmit Power Amplifier

The transmitter's power amplifier (PA) boosts the signal power before it is fed to the antenna. It is important to check the power amplifier for linearity (output power is directly proportional to input power) and to measure harmonic signal levels to ensure that the transmitted signal energy is not excessive outside the allowed band. Figure 13 shows the equipment setup used to characterize the PA. This testing involves feeding either a CW or broadband signal from a signal generator into the PA and then varying the output power of the signal generator. It is important to add attenuators to the path so that the output signal from the PA does not exceed the maximum allowed input power to the VSA or the spectrum analyzer (SA). For the ITS test configuration, the power amplifier maximum output power is about 50 Watts (W) (80 dBm), so a total of 90 dB of attenuation is placed in the path between the power amplifier and the VSA/SA. This results in an input power to the VSA/SA of only -10 dBm, which is within the tolerable range.

The results of the linearity testing of three different PAs are shown in Figure 14. This figure shows the PA output power values plotted versus the input power from the signal generator. All three PAs exhibit linear behavior for input power levels less than about -2 dBm. Therefore the output power of the signal generator in Figure 10 must not exceed -2 dBm when conducting propagation measurements. Figure 15 shows a screen capture from an actual measurement of PA-1 whose statistics are given in the first row of Table 4. For this amplifier (blue asterisks), the plot shows linear behavior for an input level between -5 and -1 dBm, and non-linear behavior above -1 dBm. The PA-2 exhibits linear behavior from -10 dBm to 0 dBm and PA-3 amplifier exhibits linear behavior between -10 to -2 dBm. Any input signal level at or below -2 dBm allows the PA to operate in its linear range.

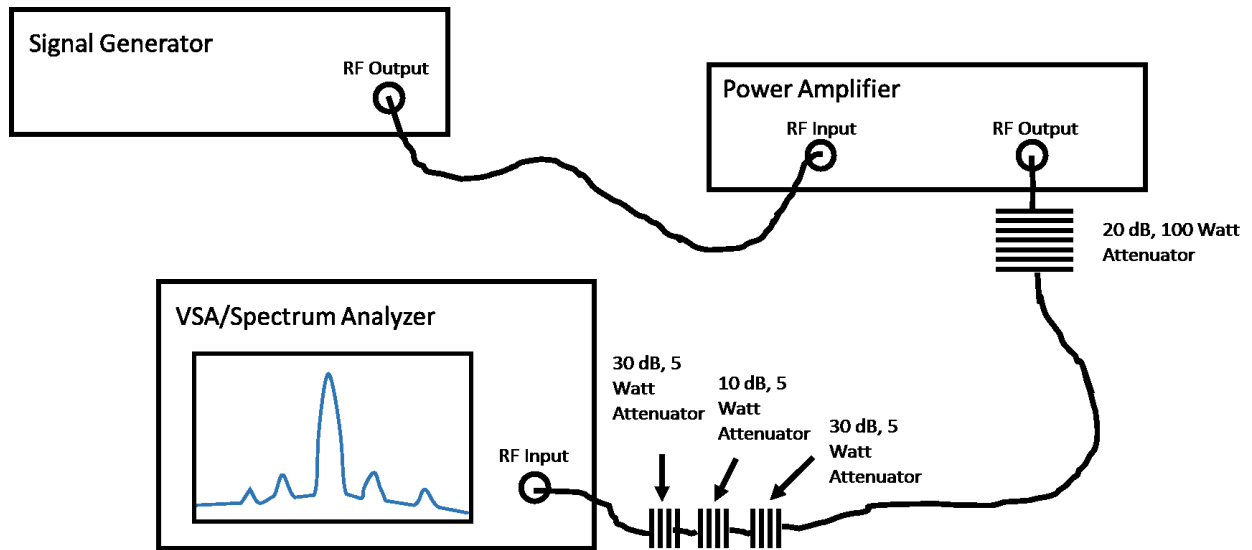


Figure 13. Equipment setup for power amplifier testing.

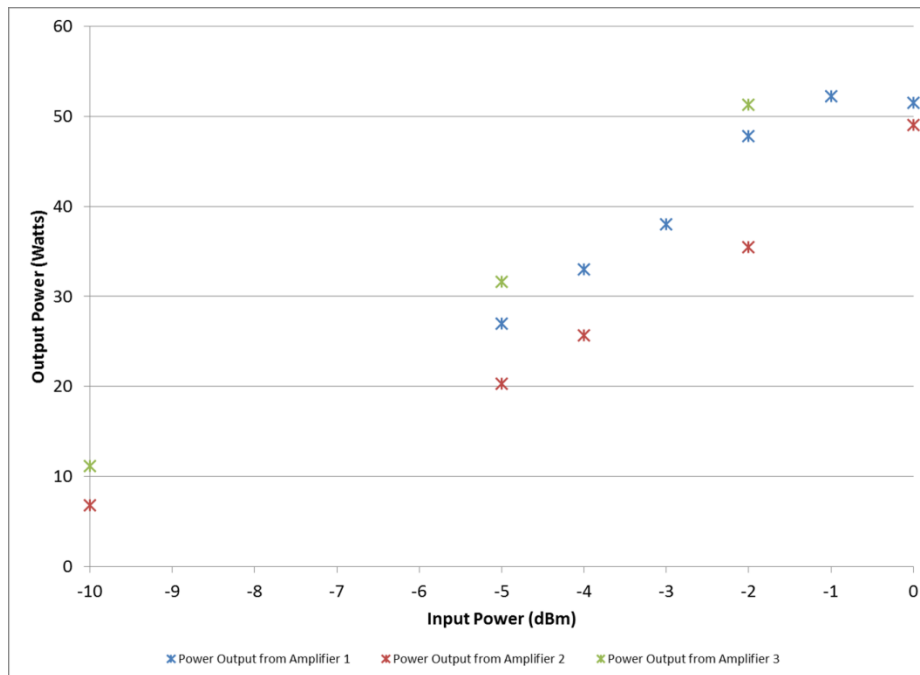


Figure 14. Input power (dBm) vs. Output power (Watts) for 3 different power amplifiers.

Table 3. System linearity measurements

| Signal Generator Output Power (dBm) | SA Measured Power (dBm) | Power (Watts) |
|-------------------------------------|-------------------------|---------------|
| -5 | -46.3 | 27 |
| -4 | -45.36 | 33 |
| -3 | -44.31 | 38 |
| -2 | -43.7 | 47.8 |
| -1 | -43.32 | 52.2 |
| 0 | -43.38 | 51.5 |

In addition to characterizing the linearity of the PA, it is also important to measure the power at harmonics of the transmit carrier frequency. Figure 15 shows an example of the measured power levels in the 1st, 2nd and 3rd harmonics of a PA.

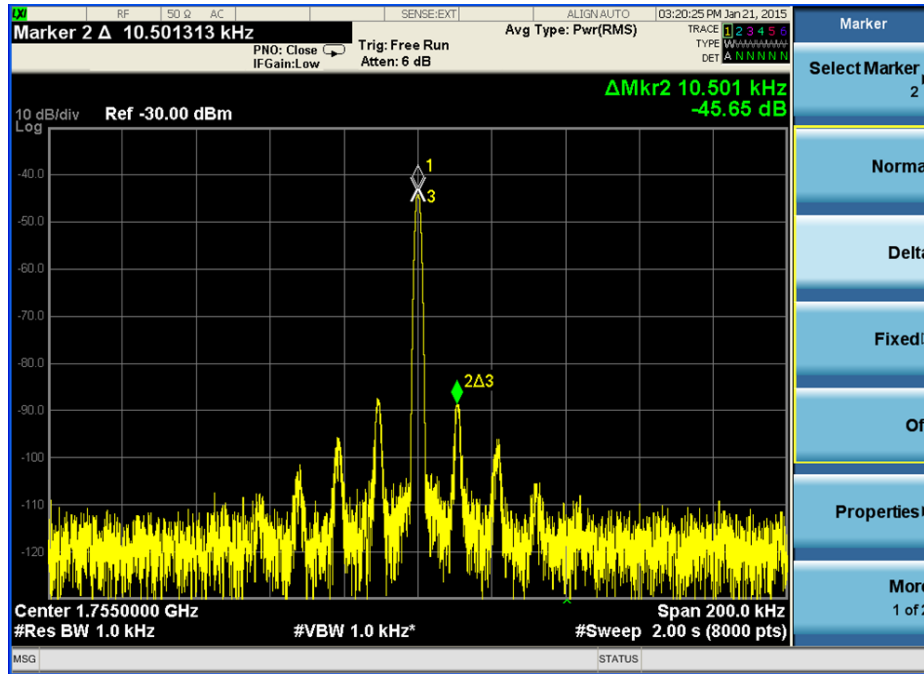


Figure 15. Power amplifier harmonic measurement. The second harmonic is at -88 dBm which is approximately 45 dB below the fundamental. The third harmonic is about 60 dB down from the fundamental.

Table 4. Power amplifier measurements of power contained in harmonics.

| | Power (dBm) at SA – 1 st harmonic | Power (dBm) at SA – 2 nd harmonic | Power (dBm) at SA – 3 rd harmonic |
|------------------------------|--|--|--|
| PA-1 (Input Power = - 1 dBm) | -43.3 | -88.9 | -103.0 |
| PA-2 (Input Power = - 2 dBm) | -54.5 | -80.2 | -78.5 |
| PA-3 (Input Power = - 2 dBm) | -52.9 | -73.9 | -81.0 |

4.3 Receiver Preselector/Preamplifier

A preselector/preamplifier unit at the receiver serves the dual purpose of improving the sensitivity and dynamic range of the system while reducing measurement system responses to signals outside the measurement band of interest. Two schematics of double heterodyne receiving systems with preselectors are shown in Figure 16 [9]. In both of these configurations, there is an adjustable RF attenuator, followed by a bank of fixed and/or tunable filters, and finally, low-noise amplifiers. The adjustable attenuator shifts the upper and lower bounds of the dynamic range of the measurement system, although instantaneous dynamic range is not

affected. More attenuation is used in bands where measured signals may overload the measurement system, and less attenuation is used in bands with weaker signals.

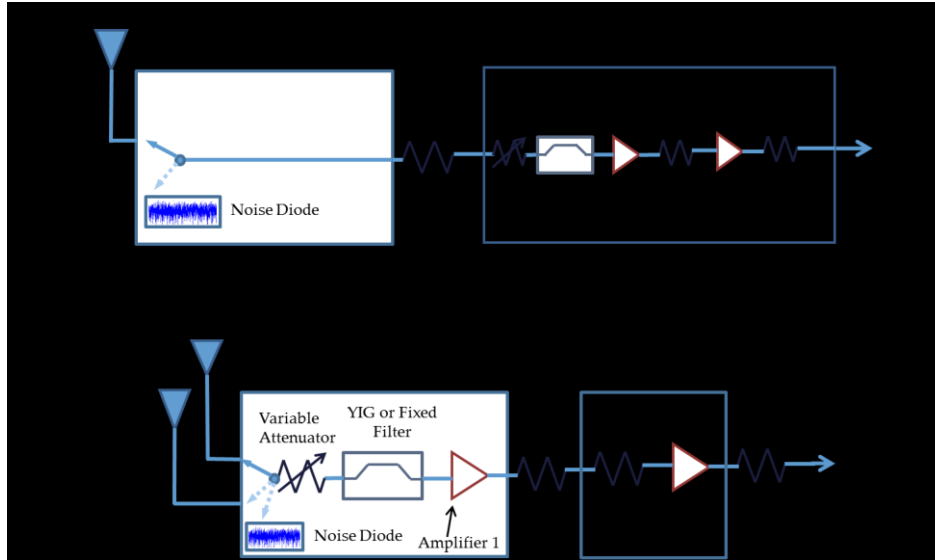


Figure 16. Preselector/preamplifier schematics for a broadband spectrum measurement system.

Bandpass filters also help prevent system overloads by decoupling the receiver from high-power out-of-band signals. Notch filters, low-pass filters, or high-pass filters may be used to reduce power levels from strong signals that may overload the front-end amplifiers or intermediate frequency (IF) stages of the measurement system receiver.

Low-noise amplifiers increase the receiver's sensitivity (decrease its overall internal thermal noise) so that weakly propagating signals are detectable above the overall noise of the receiver. The first amplifier is intended to overcome RF cable loss; the second amplifier is intended to increase the signal-to-noise ratio in the SA. The gain and compression points of the amplifiers are chosen so that the SA (or whatever the primary measurement instrument may be) is the first system component to overload when signals are too strong. Most modern spectrum analyzers can be queried for overload⁴ via the control software, thus automating the process of discarding bad data. More detailed analysis of RF receiver system design can be found in references [10] and [11]. A simplified analysis is given in the next paragraph.

System noise factor can be calculated with the well-known equation [12], [13]:

$$f = f_1 + \frac{f_2 - 1}{g_1} + \frac{f_3 - 1}{g_1 g_2} + \frac{f_4 - 1}{g_1 g_2 g_3} + \dots \quad (1)$$

⁴ If the SA's internal preamplifier is turned off, then SA overload typically occurs in the frequency conversion (mixer downconverter) stage or the log-amplification stage. If the SA's preamplifier is turned on, then it may also be a point of overload in the SA.

where f is the overall noise factor, a dimensionless quantity, and the noise factor and gain for the n^{th} component are f_n and g_n , respectively. We use the convention that lowercase f is the noise factor and uppercase NF is the noise figure, given by the following equation:

$$NF(dB) = 10 \log_{10} f \quad (2)$$

As a practical example, ITS has a receiving system to measure the signal aggregate of a large number of different cell phones or user equipment (UE). The system was designed to measure a very small input power using a high-gain, low-noise RF receiving chain. Its block diagram is shown in Figure 17. The RF characteristics of each component are given in the figure.

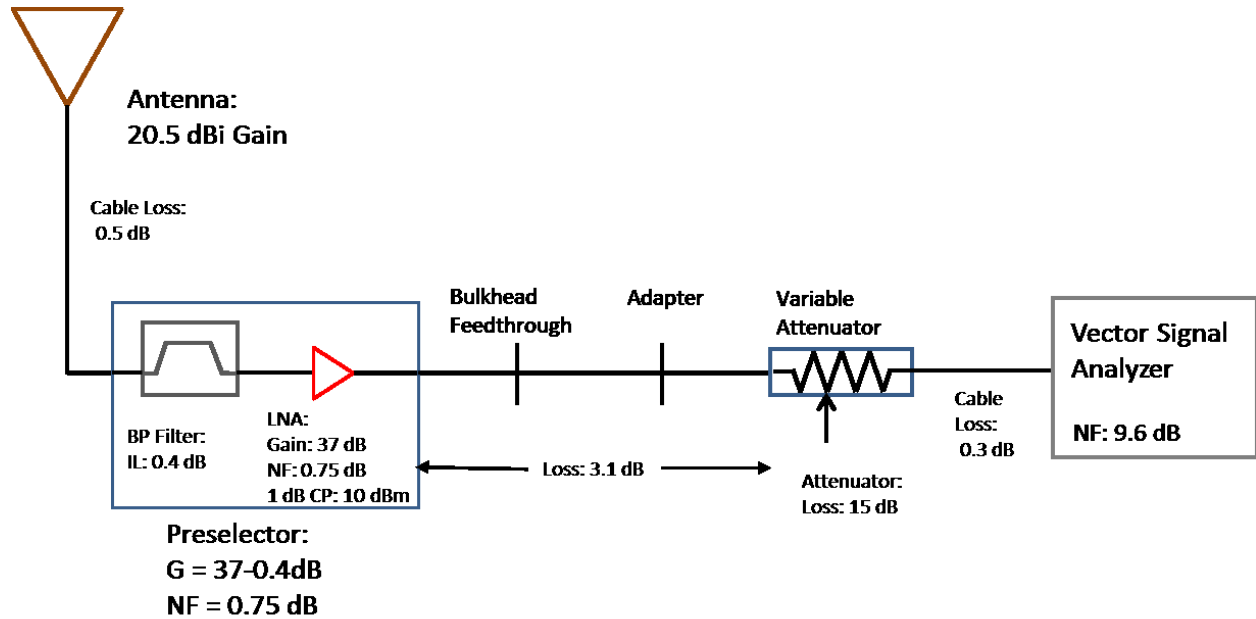


Figure 17. Receiving system block diagram for Long-Term Evolution (LTE) aggregate measurement.

The first component encountered after the antenna is a cable with a loss of 0.5 dB, the second component is a bandpass (BP) filter with an insertion loss of 0.4 dB, the third component is the low-noise amplifier (LNA) with a noise figure (NF) of 0.75 dB and a gain of 37 dB. The fourth component is a lumped series of losses from a cable and a variable attenuator totaling ~18.4 dB. The signal is then received by the vector signal analyzer which has a NF of approximately 9.6 dB.

If we used only the vector signal analyzer to receive the signal, then the overall noise figure of the system would be ~10 dB. This noise figure adds to the system noise floor which decreases the receiving system sensitivity. For example, suppose the vector signal analyzer is set up to measure at a resolution bandwidth of 180 kHz. The system noise floor is given by the following equation:

$$N_{sys} = kT_{sys}B \quad (3)$$

where k is Boltzmann's constant (1.38×10^{-23} J/K), T_{sys} is the system noise temperature (taken to be 290 K), and B is the bandwidth used to measure the signal(s). For this example, we will use $B = 180$ kHz. The system noise floor of this receiver configuration is -121.4 dBm. The calculations are broken down in Table 5.

Table 5. Noise figure calculations for system shown in Figure 17.

| Component data | Cable + Filter | LNA | Cable + Variable Attenuator | Receiver |
|---|----------------|----------------------------|-----------------------------|----------|
| Gain (dB) | -0.9 | 37 | -18.4 | -9.6 |
| NF (dB) | 0.9 | 0.75 | 18.4 | 9.6 |
| Linear values (=10^{(Gain (dB)/10)}) | | | | |
| Gain (linear) | 0.81 | 5011.87 | 0.01 | 0.11 |
| f (linear) | 1.23 | 1.19 | 69.18 | 9.12 |
| Cascaded Gains | | | | |
| Gain (linear) | 0.81 | 4073.80 | 58.88 | 6.46 |
| Noise factor by term | 1.23 | 0.23 | 0.02 | 0.14 |
| Cascaded noise factor and noise figure | | | | |
| f | 1.62 | 1.48 | | |
| Total NF (dB) | 2.09 | 1.70 | | |
| Total NF (dB) | 2.09 | All components | | |
| Total NF (dB) | 1.70 | For cable, filter, and LNA | | |

The NF for all components in the chain is 2.09 dB, and for only the first three components is 1.70 dB. This is much less than the 9.6 dB NF of the VSA, which increases dynamic range. This is shown in Figure 18. The blue line with triangles is the system noise floor ($kT_{\text{sys}}B$) of the VSA assuming NF = 0 dB. When we include the NF of the VSA then we obtain the result shown by the red line. Adding a preselector before the measurement instrument reduces the overall system noise floor to just above the noise floor of the VSA with a NF equal to 0 dB. The cable, attenuator, and VSA placed after the preselector only add a few tenths of a dB to the overall NF of the cable and preselector.

Placement of components in a preselector is very important. If the variable attenuator is placed before the filter and LNA and inserts 15 dB of attenuation to control overloads, then the overall NF of the system increases to 19.2 dB, which defeats the purpose of the preselector.

The cable between the antenna and the preselector should be as short as possible and have the lowest possible loss characteristic, so that its contribution to the noise figure is kept small.

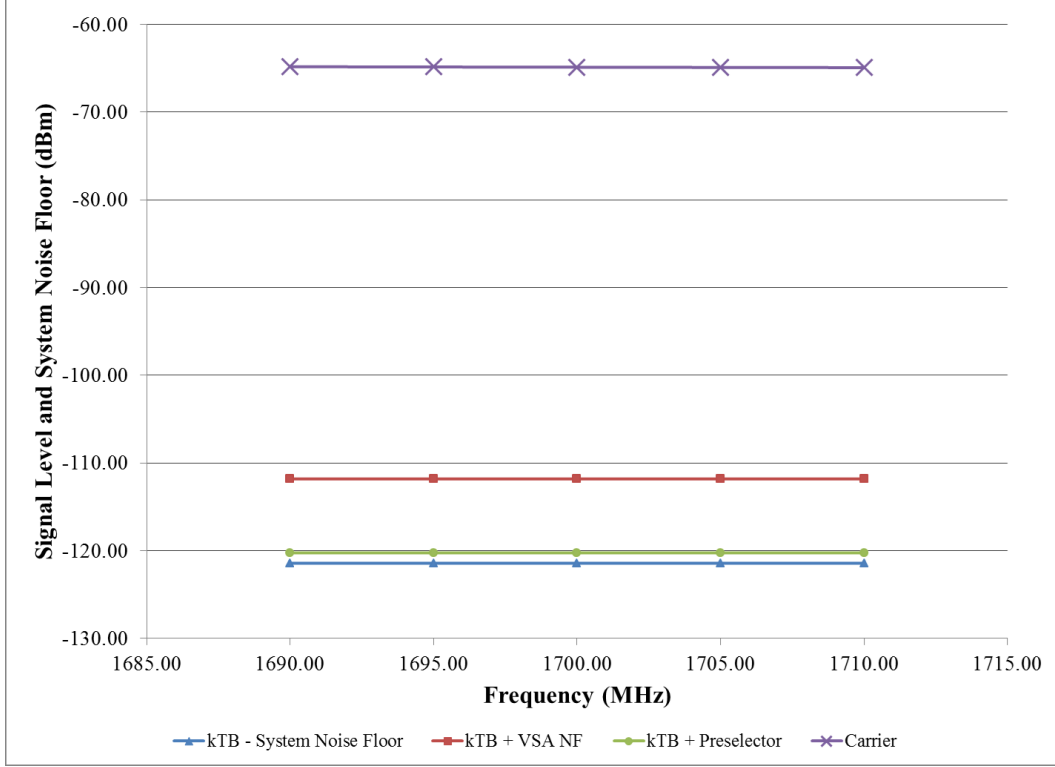


Figure 18. Carrier RSL and system noise floor (kTB) for different component configurations.

If we need to calculate the carrier-to-noise ratio for a given configuration, then we must determine system noise temperature. For a system with a preselector similar to that shown in Figure 17, the system noise temperature is a cascade of the noise temperature for each component in the chain, including the antenna noise temperature. The antenna noise temperature changes as the antenna is pointed toward the ground versus the sky. The equivalent noise temperature for each component in Table 5 can be calculated based on the following equation:

$$T_e(n) = T_n(nf - 1) \quad (4)$$

where T_n is the physical temperature of the n^{th} component and nf is the noise factor as discussed previously. The physical temperature for most components is usually taken to be ambient temperature, 290 K. For this system, the system noise temperature, T_s , is given by the following equation:

$$T_s = 10 \log_{10}[(t_{ant} \cdot g_{cf}) + (t_{cf} \cdot g_{cf}) + t_{LNA} + t_{ca} + t_{VSA}] + 30. \quad (5)$$

All lower case t 's are effective temperatures in watts and lower case g 's are gains in linear units. The variable definitions are as follows: t_{ant} is the temperature of the antenna, g_{cf} is the gain of the combination of the first cable and filter, t_{cf} is the temperature of the cable and filter, t_{LNA} is the temperature of the LNA, t_{ca} is the temperature of the cable(s) and attenuator after the preselector, and t_{VSA} is the temperature of the VSA. The last term converts from watts to dBm. The gain of the cable and filter attenuates the incoming noise from the antenna and adds its ohmic losses to the system. This is the reason it is included in both of the leading terms.

We can also compute the carrier-to-noise (C/N) ratio at the input to the receiver [14], [15]. The received signal level will depend on the gain of the transmitting antenna, the gain of the receiving antenna, distance between transmitter and receiver, and the signal bandwidth of both the transmitted signal and the received signal. The carrier-to-noise ratio is given by:

$$\frac{C}{N} = \left(\frac{p_t g_t g_r}{k t_s b_r} \cdot \frac{b_r}{b_t} \right) \left(\frac{\lambda}{4\pi d} \right)^2 \quad (6)$$

where p_t is the transmitted power, g_t is the gain of the transmitting antenna, g_r is the gain of the receiving antenna, t_s is the thermal noise of the receiving system, b_r is the signal bandwidth of the receiver, b_t is the signal bandwidth of the transmitted signal, d is the distance between the transmitting antenna and receiving antenna, and λ is the wavelength of the transmitted frequency. The equation for C/N can be written in logarithmic terms:

$$\begin{aligned} \frac{C}{N} = & P_t + G_t + G_r - 32.5 - 20 \log_{10}(d_{km}) - 20 \log_{10}(f_{MHz}) \\ & - 10 \log_{10}(k) - T_s + B_r + (B_r - B_t) \end{aligned} \quad (7)$$

The decibel sum of P_t and G_t is called the equivalent isotropically radiated power (EIRP) [16]. The free-space path loss (FSPL) is given by the terms

$$FSPL = 32.5 + 20 \log_{10}(d_{km}) + 20 \log_{10}(f_{MHz}) \quad (8)$$

and the sum of B_r and B_t is called the on-tuned rejection (OTR). We can rewrite (7) as

$$\frac{C}{N} = EIRP - FSPL - 228.6 \text{ dB} + G_r - T_s + B_r + OTR \quad (9)$$

Let's assume we have a transmitter with an EIRP of 0 dBm. The distance, d , between the transmitting and receiving antennas is 2 km and we are transmitting at a frequency of 1700 MHz. The FSPL is calculated to be 103.0 dB. The carrier arrives at the receiver with a received signal level (RSL) of -77.7 dBm. To calculate the system noise for the entire system, we sum up the noise temperature of each component, including the antenna temperature. If we assume that the antenna temperature is 290 K, then the system noise temperature is calculated to be -120.2 dB. If $B_t < B_r$ then then OTR is dominated by B_r and will contain some of the system noise floor in the measurement bandwidth. If $B_t = B_r$ then $OTR = 0$ and we are left with the receiving system's measurement bandwidth. If $B_t > B_r$ then the transmitted signal bandwidth is limited by the bandwidth of the receiving system. To achieve optimal C/N , the receiving system bandwidth should be less than or equal to the transmitted signal bandwidth. With all of the above parameters, we calculate the carrier-to-noise ratio at the input to the receiver to be 37.2 dB.

When designing a preselector, it is important to use only enough gain to overcome the losses in the system. There is a point of diminishing returns. This is illustrated in Figure 19. The graph shows that for a given preselector NF, an LNA gain greater than 25 dB results in only a small increase in C/N ratio.

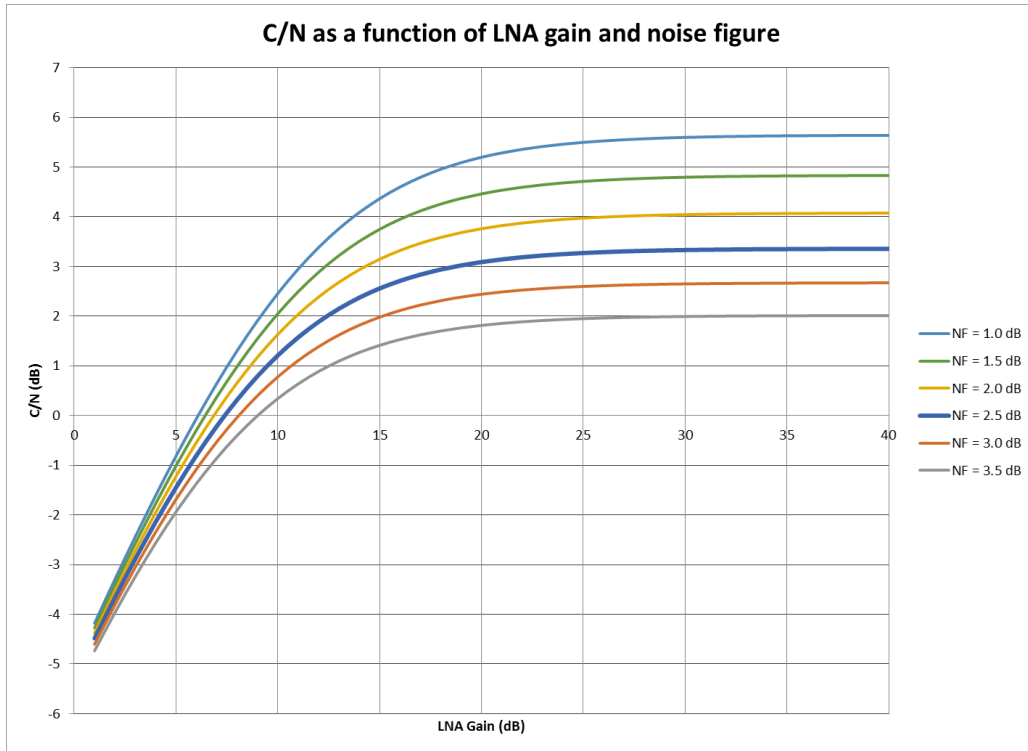


Figure 19. C/N versus LNA gain.

4.4 Bandpass Filter

As shown in Figures 20 and 21, bandpass filters are used after the PA in the transmitter to limit the emissions outside of the permitted transmission frequency range and also after the receive antenna to reduce out of band interference from extraneous signals. It is important to characterize the following two parameters associated with any bandpass filter:

- 1) Check the power rating of the bandpass filter in the transmitter and ensure that the power at the output of the directional coupler feeding the bandpass filter does not exceed this value.
- 2) Measure the insertion loss for each bandpass filter and use these values when calculating the propagation loss on the transmitter-to-receiver link.

Figure 20 shows the recommended equipment configuration for measurement of the insertion loss of a bandpass filter. Although other methods are possible (e.g., sweeping a carrier wave across), using a VNA will result in the most accurate measurements because it measures both magnitude and phase. We can see in this example that the insertion loss measured between 1746 MHz and 1782 MHz (in the passband) is approximately -0.42 ± 0.2 dB. At 1746.6 MHz we see that the attenuation for signals outside the passband is approximately 20 dB.

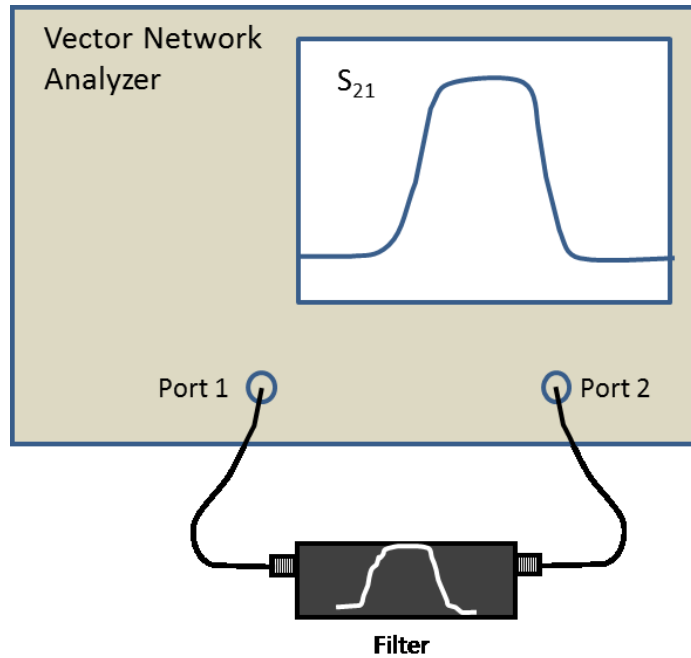


Figure 20. Equipment setup for measuring insertion loss a bandpass filter.

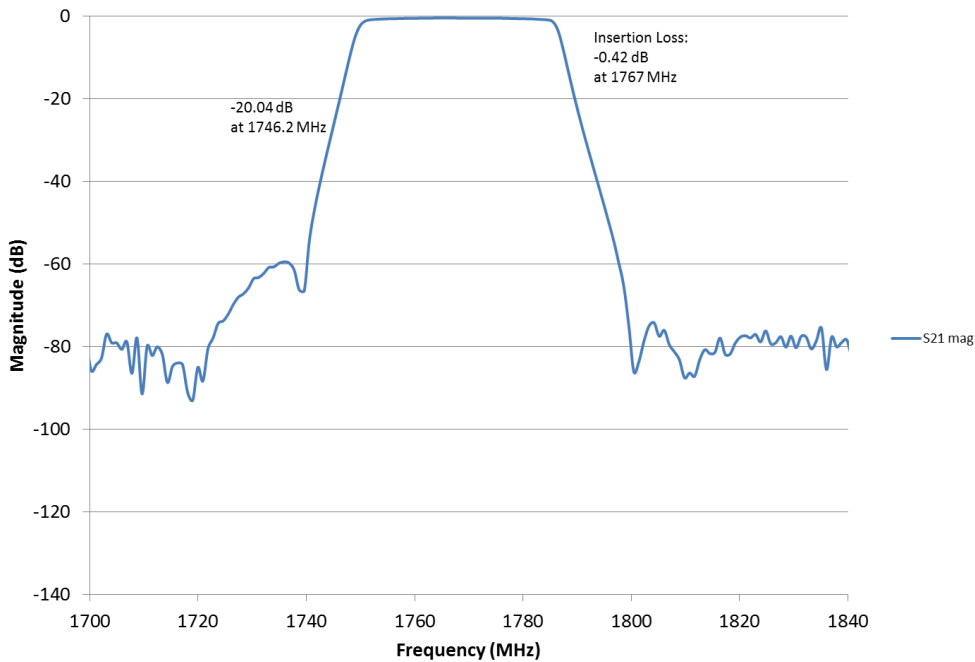


Figure 21. VNA measurement of a bandpass filter from 1755 to 1780 MHz.

4.5 Directional Couplers

Directional couplers should be used after the power amplifier to monitor the output signal level. For this reason, the coupler should be adequately rated (e.g., 250 W) for the high input power

levels associated with propagation transmitters. The coupling factor (the amount of energy coupled to the third port, e.g., -20 dB) determines the insertion loss of the coupler. The higher the coupling factor, the lower the insertion loss.

4.6 Antenna Pattern Characterization

It is important to independently measure the radiation patterns of the antennas used in any measurement system because the manufacturer's specifications are sometimes generated by a numerical analysis and not necessarily measured. Most antennas are measured in a free-field environment, in the antenna's far-field [17]–[19].

Under the typical configuration where the transmit antenna is located on a fixed mast and the receive antenna is located on the roof of a vehicle, the following measurements should be made:

- 1) Measure the 3D in-situ gain pattern of the receive antenna (i.e., pattern measurements should be made with the antenna on the van in the position it will have when used to make the measurements in the field).
- 2) Obtain the gain and 3 dB beamwidth of the transmit antenna.

If any of these parameters are available as specifications, those values can be used; however, it is preferable to measure these parameters to 1) verify the specification values, and 2) measure the modified *in situ* pattern with the antenna mounted on its vehicle.

When making measurements to characterize the antenna gain pattern, those measurements should be made in the far-field of the antenna [17]–[19], which is defined as follows:

$$d_f = \frac{2D^2}{\lambda}, \quad (10)$$

where D is the largest physical linear dimension of the antenna and λ denotes the RF wavelength. Additionally, to be in the far-field region, d_f must satisfy

$$d_f \gg D, \quad (11)$$

and

$$d_f \gg \lambda. \quad (12)$$

For example, the middle of the AWS-3 band is 1767.5 MHz, which corresponds to a wavelength of 0.17 m, and the largest dimension of the ITS transmitting antenna is 0.6 meters. The calculated far-field distance is about 4.2 m (13.8 feet). This means that any antenna gain measurements for the ITS transmitting antenna must be made at least 4.2 m from the antenna.

For the antenna on the van, the impinging field produces currents on the outside of the van and on the antenna and so it is important to measure the antenna gain pattern of the antenna and the van combined so the measured pattern incorporates both antenna and vehicle pattern effects. The Earth can also affect the antenna pattern. For low antenna heights, a surface wave will develop

and change the propagation loss [19]. The referenced report shows that the surface wave impacts the propagation loss for antenna heights less than 2 wavelengths, at distances less than 10 m, for frequencies less than 300 MHz. For frequencies greater than this, antenna heights should be more than 2 wavelengths above the ground, the effect of the surface wave due to the presence of the earth is assumed to be negligible, and the pattern of that antenna should be measured in as close to a free-field environment as possible.

Some researchers use absorbing material on the ground to emulate a free-field measurement. We chose to measure the antenna pattern including ground bounce effects to emulate what happens when the van is driving in the environment and receives signals from the ground and the surrounding environment.

If an antenna will not be attached to a vehicle, the optimal way to measure the antenna would be in an anechoic chamber. If an anechoic chamber is not a feasible option, one can measure the antenna above a surface and place absorber material on the ground where the ground bounce would occur. Finally, if absorbing material is not available, one can use a vector network analyzer with a time-domain option, measure the antenna pattern at various azimuths and then use time gating to gate out the ground bounce. Antenna measurement details are presented in Appendix B.

4.7 Antenna Directionality Considerations

For most propagation measurements, antennas should be omnidirectional at both ends of the link. Directional antennas may seem desirable because they can provide additional gain in the propagation measurement system's link budget. But accurate aiming of directional antennas is difficult in ordinary field conditions. Furthermore, verification that directional antennas have been properly aimed is highly problematic. This is due to three factors. First, proper aiming will require an accurate direction to true north, good to within a fraction of the antenna's horizontal beamwidth. This is not easy to determine at a field site. The magnetic declination of the earth's magnetic field must be included in the calculation of true north. The magnetic declination changes daily and across the United States. This is shown in Figure 22.

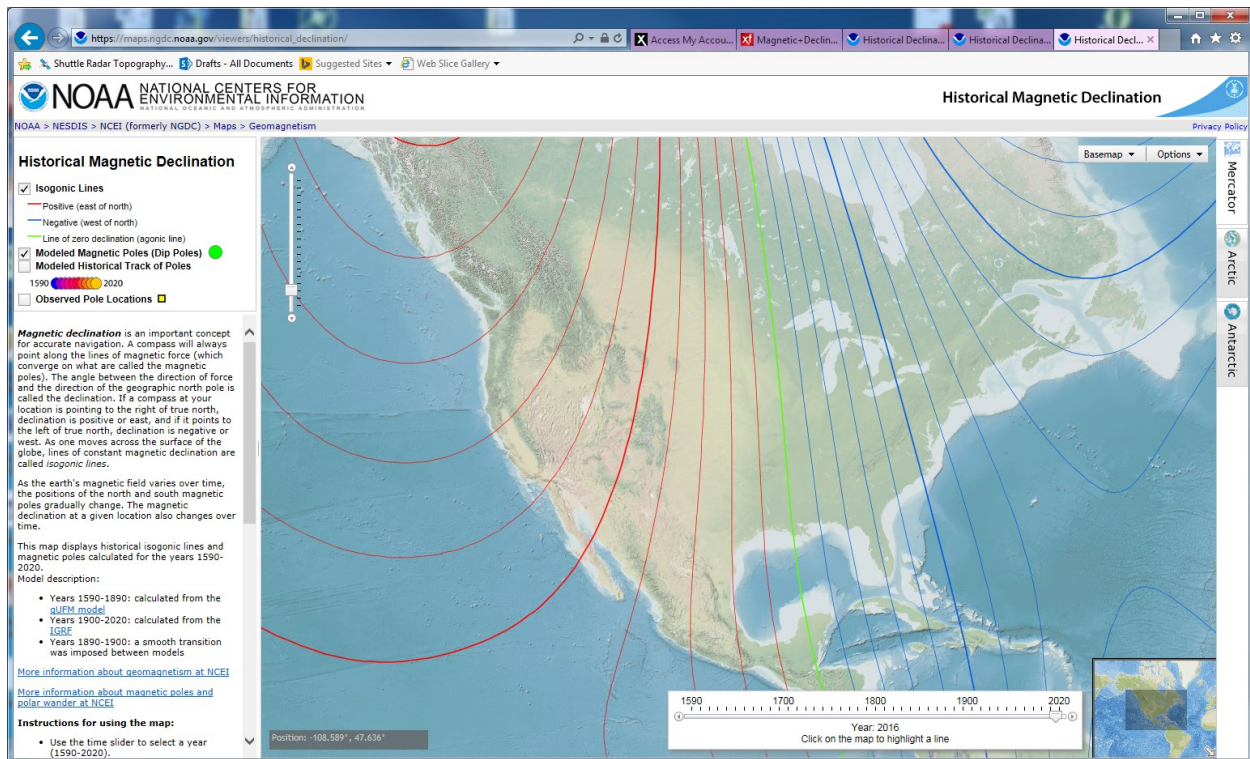


Figure 22. Magnetic declination of the earth's magnetic field in North America. See https://maps.ngdc.noaa.gov/viewers/historical_declination/index.html (accessed 8/24/2018).

Second, when at least one end of a propagation measurement system is moving, there is little time available to determine the direction of the azimuth along which a directional antenna needs to be aimed to point exactly at the (moving) other end of the link, and then to aim it. Third, a directional antenna must not simply be aimed in the direction in which maximum propagation signal is obtained on the link, as this will not necessarily be the true direction to the other end of the propagation link. That is, the highest signal power level is not necessarily coincident with the true direction between the two ends of the link. This is illustrated in Figures 23 and 24. In Figure 23, we are using a directional antenna with a highly directional pattern and we want to aim it into the Martin Acres neighborhood to make measurements. The intended boresight line is shown by the orange, dotted line. The boresight gain of this antenna is 16 dBi. In Figure 24, we make a mistake and actually are a few degrees off from the boresight line and when we make antenna gain corrections to our antenna, we think we have a gain of 16 dBi, but in reality, our gain along the boresight line is less than this value and so our measurement results are incorrect.

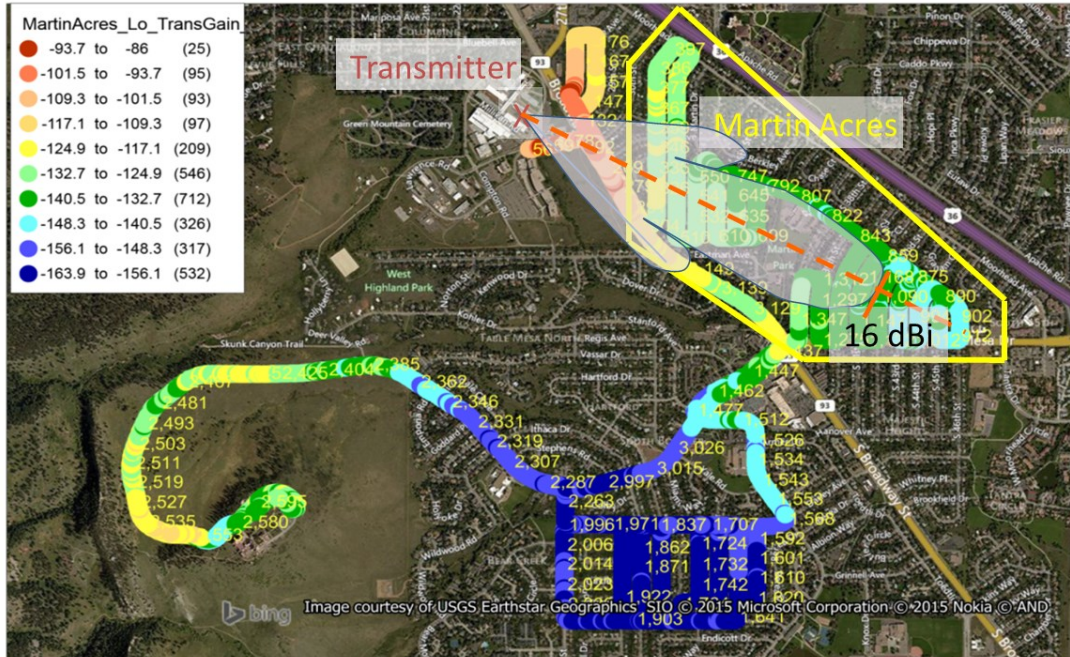


Figure 23. Using a directional antenna to make measurements in the Martin Acres neighborhood.

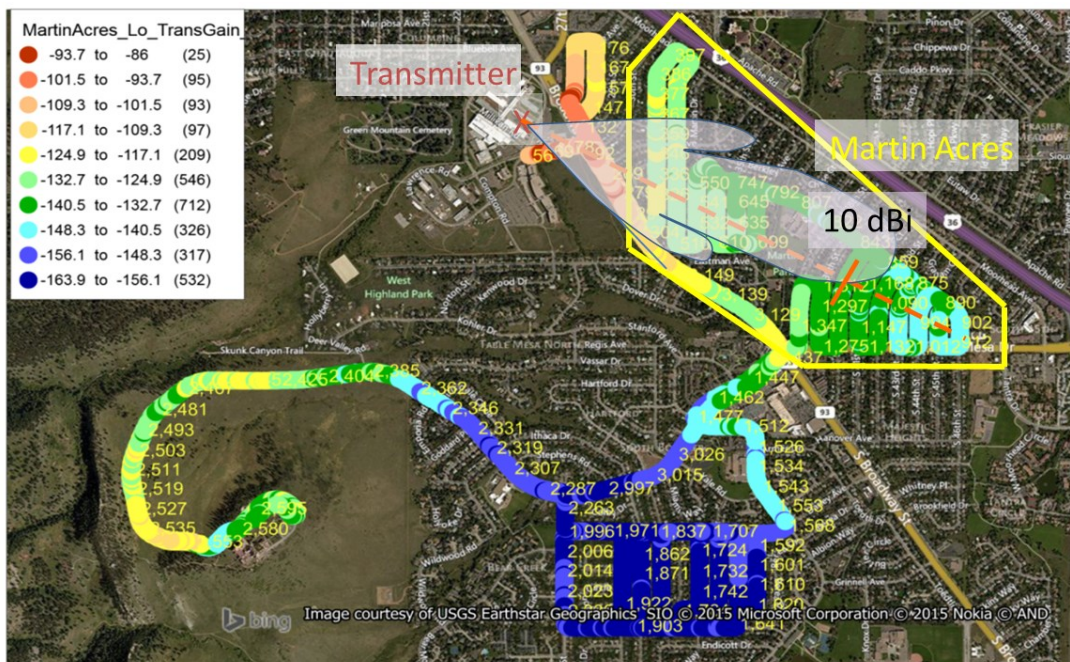


Figure 24. Misaligned directional antenna used to make measurement in the Martin Acres neighborhood.

Failure to properly aim a directional antenna during propagation measurements will result in the antenna's own directionality pattern appearing in the propagation data as if it were an azimuth-dependent variation in propagation factors. Given the seriously compromising nature of this

potential result, and the difficulty of avoiding it, directional antennas are not recommended in propagation measurements.

If higher antenna gain than the 0-dBi or 3-dBi gain found in many omni antennas is desired or needed in a propagation measurement link, the way to achieve this is to use omnidirectional antennas with relatively narrow beamwidths in the vertical dimension. Such antennas include stacked dipole designs, which may easily be found with 8 dBi or more of gain.

5. SYSTEM MEASUREMENTS

5.1 Detection Algorithms and System Noise Floor

As shown in Figure 11, a SA is a key piece of equipment used as a receiver during propagation measurements. This section discusses fundamental guidelines that should be followed when operating a SA; however, these same parameters are found in one form or another in other types of receiving systems so understanding their effects on measurements is important for most or all types of propagation measurement systems.

The first consideration is how to set an appropriate value for the resolution bandwidth (RBW)⁵ of an SA. The RBW directly affects the noise floor (but not the noise figure) of the instrument :

$$N_{sys} = -174 + 10 \log_{10}(RBW) + NF. \quad (13)$$

N_{sys} is the system noise floor, -174 is the dBm value for kT in a 1 Hz bandwidth, RBW is in units of hertz, and NF is the noise figure of the instrument. Figure 25 shows the CW signal level and the system noise level based on (13) plotted versus RBW using a peak and RMS average detection algorithms.

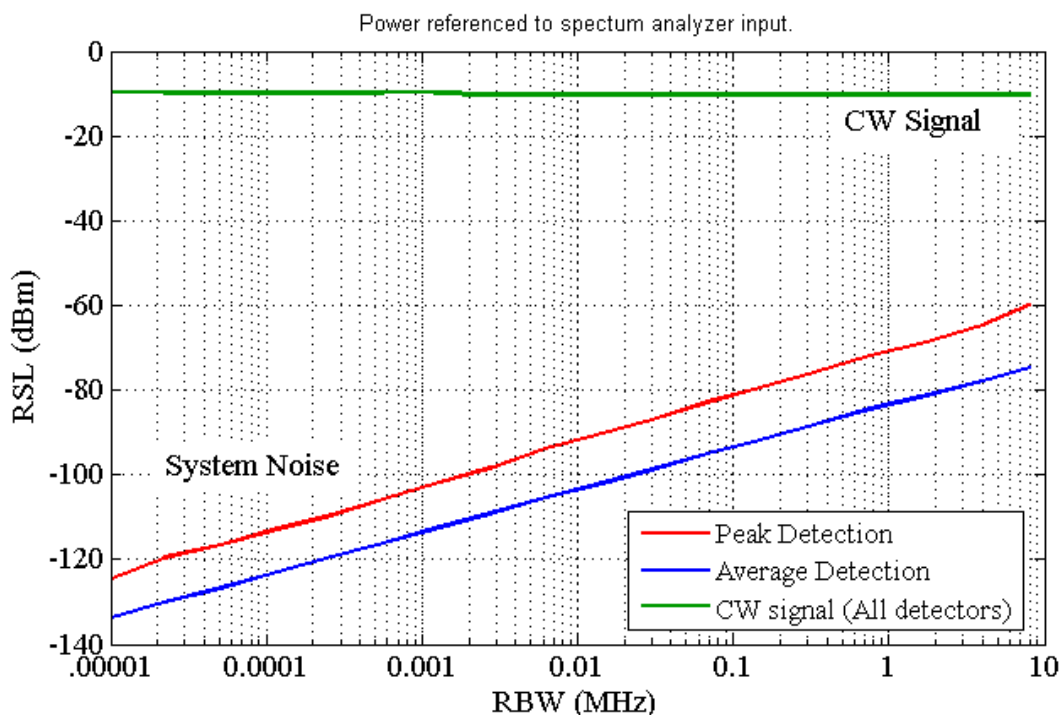


Figure 25. RBW vs. RSL for system noise and a CW signal.

These results show that as the RBW decreases, the system noise floor decreases, and the level of a CW signal does not change (as the theoretical bandwidth of a CW signal is zero hertz). Thus,

⁵ RBW is also called the intermediate frequency (IF) bandwidth of a SA or other receiver.

the signal-to-noise ratio (SNR) increases at the rate of $10\log(\text{RBW})$ as the RBW is decreased. These results show that **when viewing a CW signal, the user should set the RBW to as small a value as possible**. In practice, however, there are two factors that limit how small the RBW can be. The first factor is the SA sweep time, which increases linearly with the inverse of the RBW. Therefore, it is necessary to find a compromise between SNR and acceptable sweep time. The second factor is the spectral width of the CW signal. Although a theoretically perfect CW signal has zero bandwidth, in practice there will exist non-zero phase jitter in the signal generator. Small amounts of phase instability are essentially the same as frequency instability—thus no CW signal ever achieves truly zero bandwidth. This, along with propagation channel multipath that causes spectrum spreading and Doppler frequency shifting of the CW signal as one end of the propagation system moves, will make a received tone which is nominally CW have, in fact, a non-zero bandwidth.

If signals other than CW signals are used to make propagation measurements and non-pulsed signals with flat spectra, maximum SNR is achieved when the RBW is equal to the emission bandwidth of the signal. Wider RBW values will reduce SNR; narrower RBW values will (at best) leave the optimal SNR unchanged.⁶

Figure 26 illustrates the point that the RBW should not be set smaller than the bandwidth of a signal. This figure shows the RSL of bandpass Gaussian noise-like signal (i.e., has a flat spectrum) plotted versus RBW when the RBW is 6 kHz or wider. We see that, for the system under consideration, the SNR remains fixed at its maximum value as long as the RBW is 6 kHz or wider. In summary then:

- For non-CW signals, the RBW should be set equal to the signal's emission bandwidth.
- For CW signals, the RBW should be made as small as possible since the SNR increases with decreasing RBW; however, a practical limit occurs near 10 kHz.

⁶ For pulsed signals that are peak-detected, SNR is reduced at the rate of $10\log(\text{RBW})$ as RBW is reduced from the optimal value.

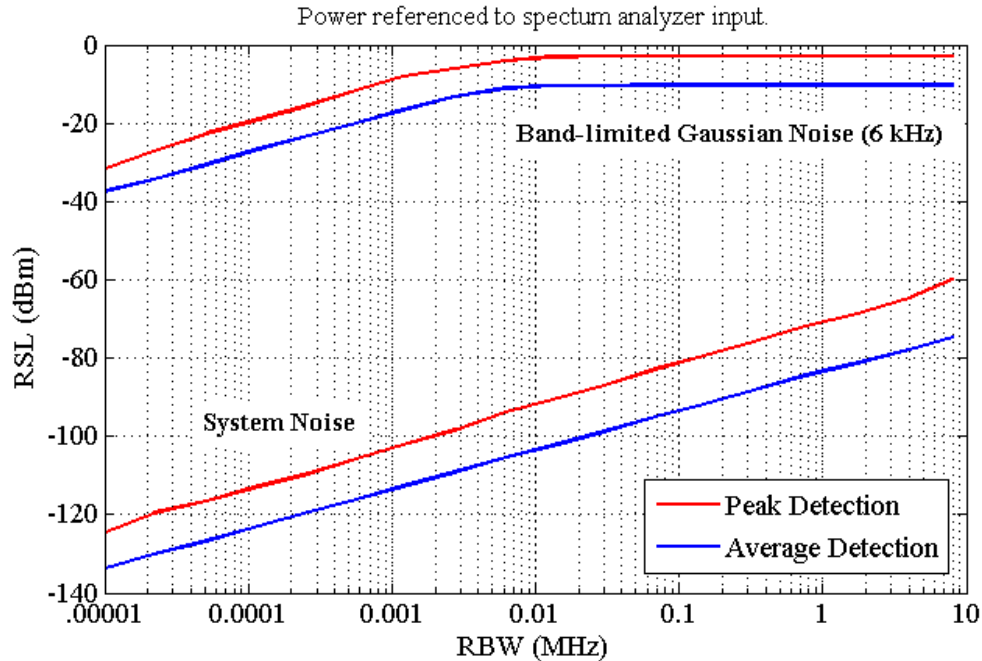


Figure 26. RBW vs. RSL for system noise and band-limited Gaussian noise with a bandwidth of 6 kHz.

The second consideration when operating an SA is the selection of an appropriate detection algorithm. SA data traces consist of screen-display points called bins. The number of data bins per trace can be as low as about 401 and can be as high as 40,000 or more. But for every single bin data point that is displayed, the SA itself may have digitized⁷ hundreds or thousands of raw data points. The process by which the plethora of raw samples are converted to a single data point per displayed screen bin is called detection. Commonly encountered detection options include: a) sample detection, which selects the first (or last, or middle, etc.) raw point out of every bin interval; b) positive peak detection, which locks to the highest-power (maximum power) raw data point within each bin interval; c) negative peak detection, which locks to the lowest-power raw data point within each bin interval; d) normal detection, which alternates between positive peak detection and negative peak detection from one bin to the next; and d) RMS averaging, which computes the root mean square power average value from all of the raw samples that have been collected during each bin interval.

Figure 27 shows examples of the spectrum of a CW signal for four different types of detection algorithms and the noise floor around that CW signal. The SNR of the signal changes based on the detector settings. For a strong CW signal, the measured power value is independent of detector mode; peak values, sampled values and RMS values all collapse to (nearly) the same single value.

SAs, however, are *power summing* devices. This means that the *sum* of the power of input signals and spectrum analyzer internal thermal noise is displayed in every SA data trace. As a

⁷ For analog SAs, the digitizer rate and output is replaced by the rate and output of independent samples, which is essentially (1/RBW).

CW signal power level comes to within about 10 dB of the SA noise floor, the contribution of the SA's internal thermal noise to the total power being measured (signal plus internal thermal noise) becomes significant. This noise contribution makes the (apparent) measured power of the CW (or any other) signal appear higher than it really is. It also makes the (apparent) measured power of the signal appear to fluctuate, not because of any fluctuation in the signal, but because the fluctuating noise in the SA becomes a significant contributor to the overall measured power level.

Detector settings should be chosen based on the type of signal that is to be measured. Peak detection should be used when searching for the maximum value of a received signal. This is especially true for signals that are highly dynamic in time, e.g., pulsed. Peak detection is typically used, for example, when measuring radar signals. RMS detection is normally used if the objective is to evaluate the mean value of a signal over time. Sample detection is typically chosen when there is a desire to reflect the variability of a received signal. System noise floors are typically measured using either RMS detection or sample detection.

A note of caution about using RMS average detection: The computed RMS average that is displayed in a SA data trace is no better than the number of raw samples that were averaged for each displayed SA trace bin. SA data traces need to be swept slowly enough in time to allow a statistically significant number of raw samples to be included in each display-bin value. Otherwise, the "average" values that are displayed can be the result of averaging just a few, or even a single, raw data value. In which case the "RMS average" that is displayed is in reality no different from a sample-detected value. In order to obtain something close to a true RMS average, the time per displayed trace bin should be at least as long as ten times the value of $(1/\text{RBW})$, and preferably more like 100 times $(1/\text{RBW})$.

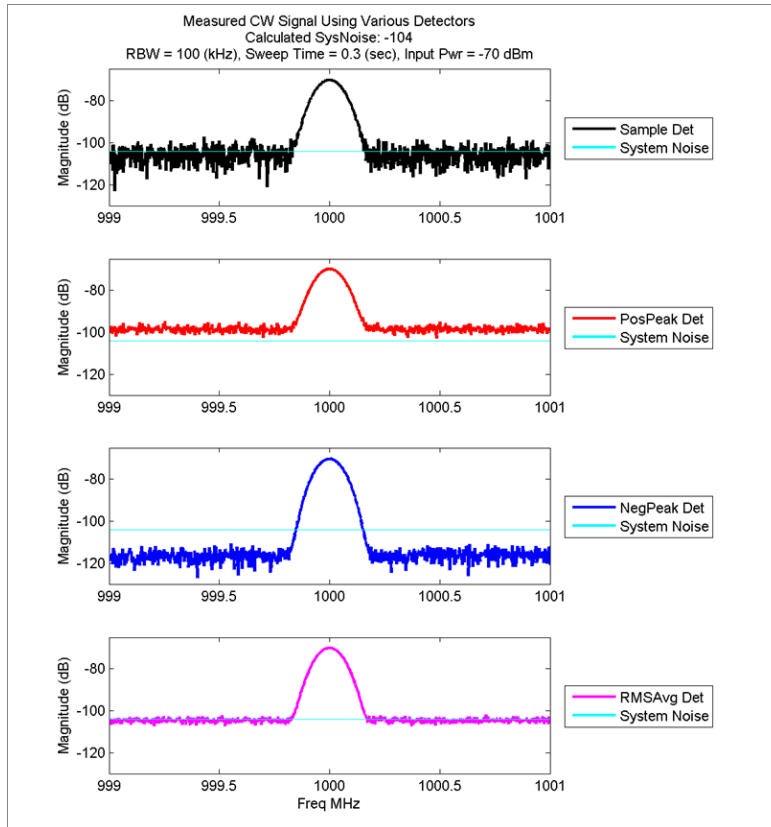


Figure 27. Measured CW signal showing the effect of various detection algorithms for a system noise floor of -104 dBm.

5.2 System Noise Floor Measurement

This section addresses how to determine the system noise floor of the propagation measurement system and the associated uncertainties as the signal level approaches the system noise floor. As discussed in Section 5.1, the noise floor level is one of two key parameters that define the dynamic range of a receiver. The dynamic range of the measurement receiver, in turn, needs to be properly matched to the propagation testing. We can simulate path loss at various distances by inserting a variable attenuator into the system. We then observe the received power of our system as we vary the attenuator settings with a signal generator output signal level equal to 0 dBm. A schematic of the test setup used by ITS to measure the noise floor of its propagation measurement system is shown in Figure 28. We use a laboratory-grade vector signal analyzer (VSA) in our measurement system. This system corresponds to the end-to-end system defined by the transmitter and receiver components shown in Figures 10 and 11 *without* the power amplifier.

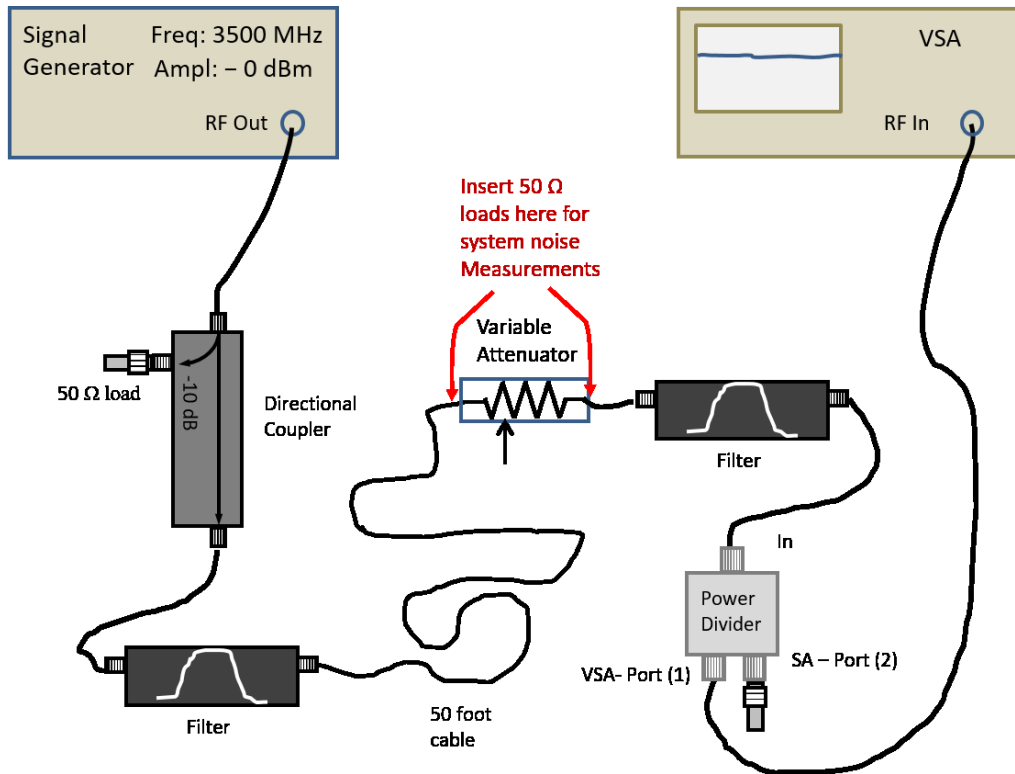


Figure 28. ITS measurement system testing with a variable attenuator.

To quantify the dynamic range of our system we increase the attenuation and observe the received signal level as we approach the system noise floor. The test procedure is as follows: Set the variable attenuator to 0 dB (which simulates no path loss), measure the received CW signal level for approximately 2 minutes using the VSA. Set the variable attenuator to 20 dB (which simulates a free-space path loss of 20 dB), measured the received signal level for approximately 2 minutes using the VSA. We continue this procedure down to a variable attenuator setting of 110 dB which is the limit of the variable attenuator.

The results of the testing at attenuator settings of 20 dB, 50 dB, 70 dB, 90 dB, and 110 dB, are shown in Figure 29. The graph shows the received signal level as a function of time. The top trace is the received signal level when the variable attenuator was set to 20 dB. Notice that the power level of this signal is not 20 dB. That is because the system losses for the measurement system are around 17 dB, which accounts for this offset. As the received signal level approaches the system noise floor, the signal level becomes more uncertain because of the contribution of the VSA's internal noise to the total measured power. As the simulated path loss approaches 110 dB, we see that we are approaching the noise floor of the VSA. The noise floor of the receive system is measured either by removing the variable attenuator and connecting 50 Ω loads at the ends of the cables (if the signal generator remains on) or by turning the signal generator off and connecting a 50 Ω load to the end of the receive cable attached to the left side of the filter in the diagram. If measurements are being made in the field, then the transmitter is turned off and a 50 Ω load is connected to the antenna cable input to the receiver.

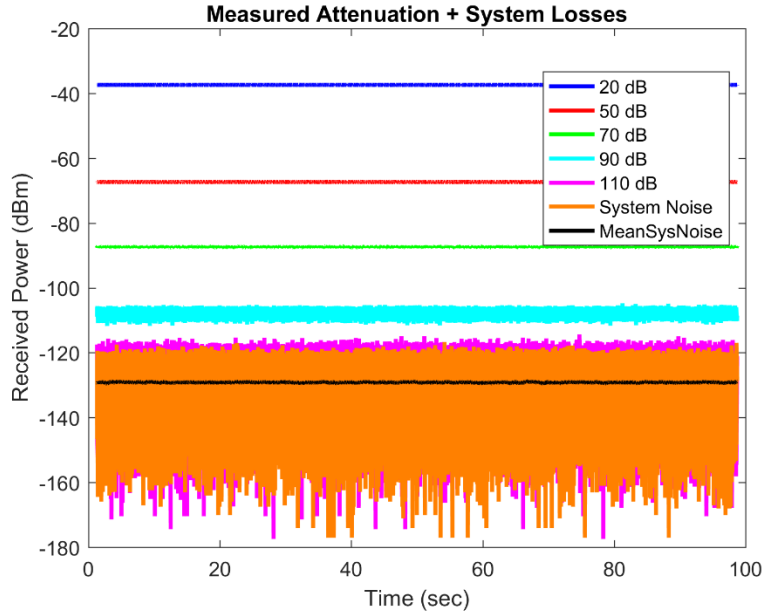


Figure 29. VSA measurement results for the ITS system as a function of attenuation.

The graph in Figure 30 shows the average received power for all measured points in a measured two-minute record as a function of the variable attenuator setting. ITS plots these points to show the linearity of the system and the system noise floor. The system linearity is given by the equation shown next to the measured points. In Figure 30(a), we include all variable attenuation settings down to -110 dB, excluding the system noise floor. The slope of the equation used to fit the data is very close to one. The y-intercept is -17.7 dB, which is the system loss that we measured. Figure 30(b) shows the linearity fit when the system noise floor is included. The equation now shows a y-intercept of -23.2 dB and the slope is less than one, so this fit is biased by the system noise floor measurement. The mean system noise floor of the VSA system is approximately -129 dBm as shown in Figure 29. It is important to know what the signal noise floor of any system is so that we know the signal-to-noise ratio for a measurement.

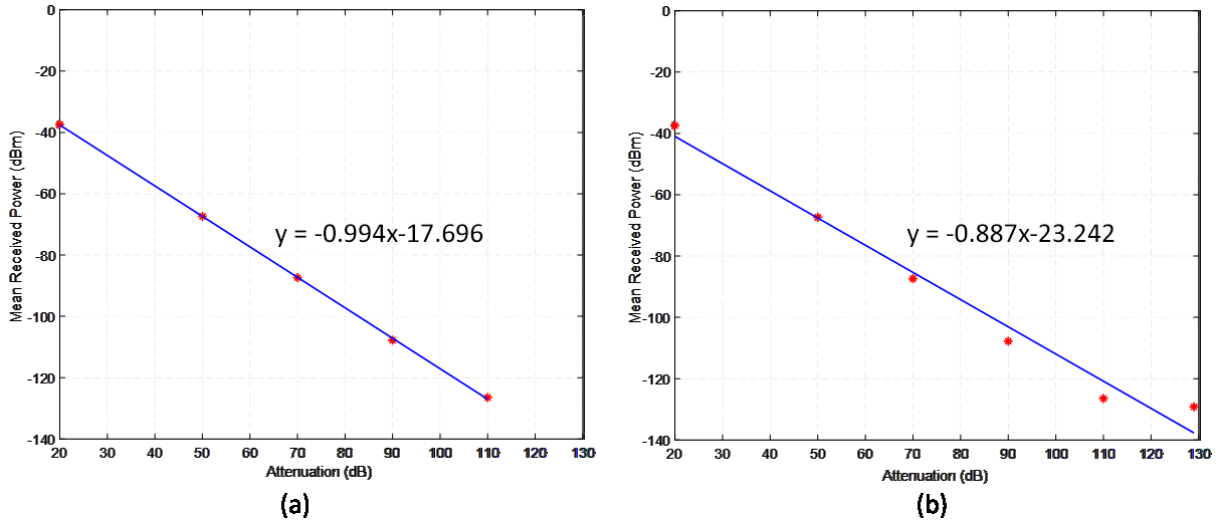


Figure 30. VSA measurement results for the ITS system as a function of attenuation both with and without the noise floor points.

5.3 System Dynamic Range

When conducting propagation measurements it is important that the dynamic range of the measurement system be matched to the types of measurements that need to be made. The dynamic range of a receiver is the difference between the receiver’s maximum input power (the saturation power or overload point) and the minimum measurable power level (approximately equal to, or a little less than, the system’s noise floor). For a measurement to be valid, input signals must be within these boundaries.

Figure 31 illustrates the concept of dynamic range and its relationship to the noise floor and saturation level of a receiver. The left side of the figure shows a generic receiver with an input signal power level equal to P_r . The receiver, which may be a spectrum analyzer or some other power measurement device, computes the power of the signal at its input, which is denoted by P_{meas} . When the input signal is below the receiver noise floor, the measured signal level does not vary linearly with the input power level; if the input signal is more than 10 dB below the receiver’s noise floor, it is nearly unmeasurable. Similarly, as the input power level approaches the saturation power of the receiver, then the measured signal power varies non-linearly with input power. If the receiver is driven into total saturation, the measured signal power will become fixed at the receiver’s maximum overload point. In order for the power measurement device (i.e., the receiver) to measure the signal linearly, the received signal level must fall between P_{min} and P_{max} . To ensure system linearity the received power should technically be between about $P_{min} + 10$ dB and $P_{max} - 10$ dB.

When making propagation measurements, it is necessary to estimate the minimum and maximum expected propagation losses, L_{min} and L_{max} anticipated to occur during testing and to make sure that the values of P_{min} , P_{max} , and the *EIRP* of the test transmitter are sufficient to measure propagation loss values that span the range defined by L_{min} and L_{max} . The values of L_{min} and L_{max}

that can be measured by a given propagation measurement system defined by P_{\min} and P_{\max} are given by the following two equations:

$$L_{\min} = EIRP + G_r - P_{\min} , \quad (14)$$

$$L_{\max} = EIRP + G_r - P_{\max} . \quad (15)$$

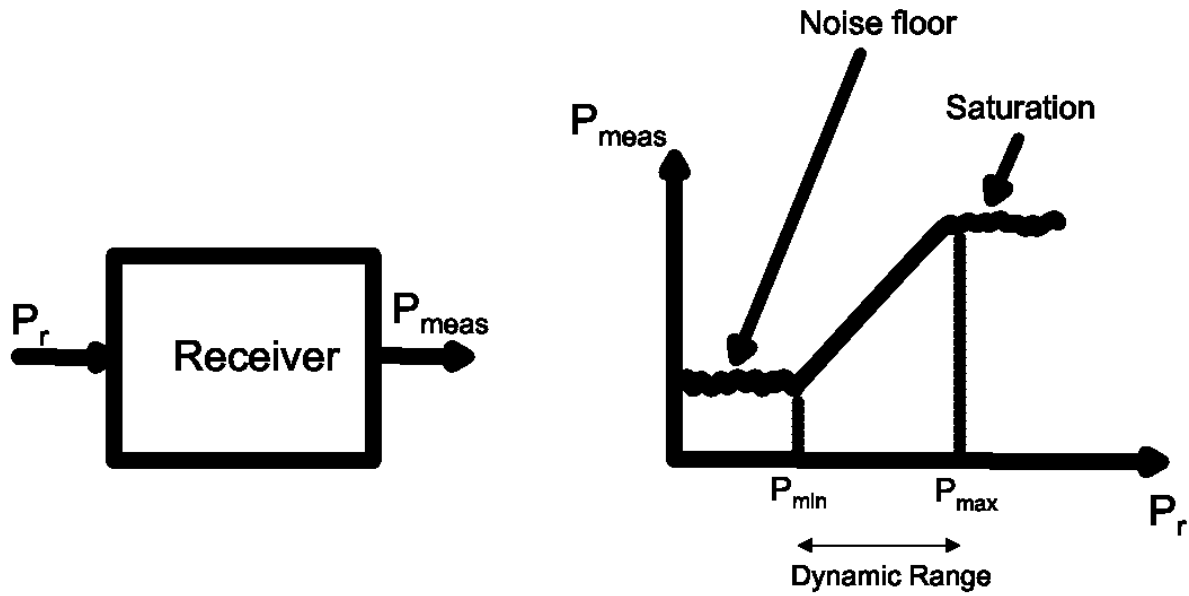


Figure 31. Illustration showing the dynamic range of a receiver and its relationship to the noise floor and saturation power.

Figure 32 shows the system dynamic range of two different types of receivers, an SA (blue trace) and a VSA (red trace). The SA has a system noise floor of approximately -120 dBm for an RBW of 3 kHz, shown in the upper graph. The system noise floor of the VSA is approximately -130 dBm as shown in the upper graph, and the VSA has a limiting upper range of -42 dBm as shown in the lower graph. The dynamic range of the VSA is approximately 88 dBm. The SA dynamic range is limited by its system noise floor, but as both instruments are currently configured, the SA measures higher received signal levels than the VSA. The VSA upper limit could be increased by changing the sensitivity range, however this only affects measurements near the transmitting antenna or distances less than ~ 100 m.

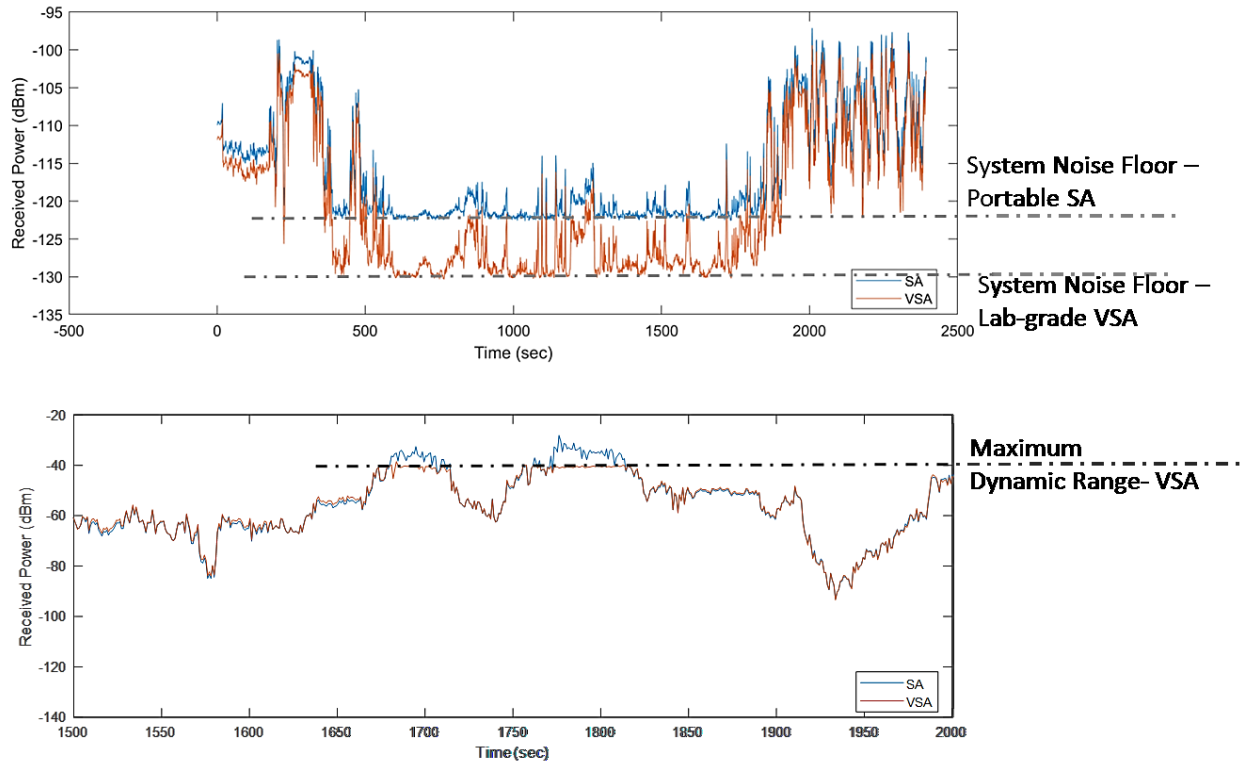


Figure 32. Dynamic range for an SA (blue trace) and a VSA (red trace).

5.4 EMI/EMC Problems

EMI and EMC issues can occur due to the radiating fields from computers, unshielded equipment, or any piece of equipment where the integrity of the shield has been compromised. Radiating fields can induce unintended currents on wires or circuit boards in pieces of equipment and can cause extraneous signals. These are some of the most difficult problems to both identify and correct. EMI/EMC issues typically arise when different pieces of equipment are placed in close proximity one to another. If unexplained signals are observed, ITS recommends either inserting metal sheets or RF absorbing material (such as absorbing material used in anechoic chambers) between the equipment to isolate the different pieces and help determine which pieces of equipment are interfering with one another.

EMI can also be caused by common electromagnetic propagation modes that reside on the outside of RF cables and can be introduced onto equipment that is not well grounded. One remedy for this is to place inductors on the outside of the cable, which will dampen the fields as they move along the cable.

Ground loops, which are caused when equipment is not connected to the same ground, are another EMI issue. One technique to minimize these ground loops is to place computers on one circuit and all other equipment on another circuit. Some pieces of equipment have grounding cables and these should be tied to the equipment chassis.

Power supplies and power generators can also be a significant source of EMI, particularly if the wiring is electrically long relative to the frequency being measured. For alternating current (AC) power, generators and extension cords are typically utilized for field measurements when utility power is not available. Automobile inverters are another choice to power instruments installed in a vehicle. Unless specifically designed for the purpose, however, these devices can produce significant voltage spikes and surges in response to step changes in load (e.g., an air conditioning unit cycling on and off). In addition, long extension cords can easily couple in strong low-frequency electromagnetic energy (e.g., amplitude modulation (AM) radio) that can disrupt measurements of weak or sensitive signals. For this reason, ITS recommends utilizing an uninterruptible power supply (UPS), preferably with EMI filtering and sine wave output, placed as close as possible to the instruments being powered. Ideally, transient loads should be connected to a separate source of power—either a separate generator or secondary alternator in a vehicle.

A vivid example of common mode, radiation, and ground loops was demonstrated in the laboratory. We combined a CW signal and a PN sequence signal into a power amplifier. The receiving equipment was in close proximity to the power amplifier and the two systems were on different ground circuits. We were injecting the power amplifier with high signal levels. The resultant waveform as measured by a VSA is shown in Figure 33.

The PN sequence signal is shown in the center of the graph. The transmitting CW signal is shown on the right side of the graph, and the 2nd harmonic of the CW signal is shown on the left side of the graph.

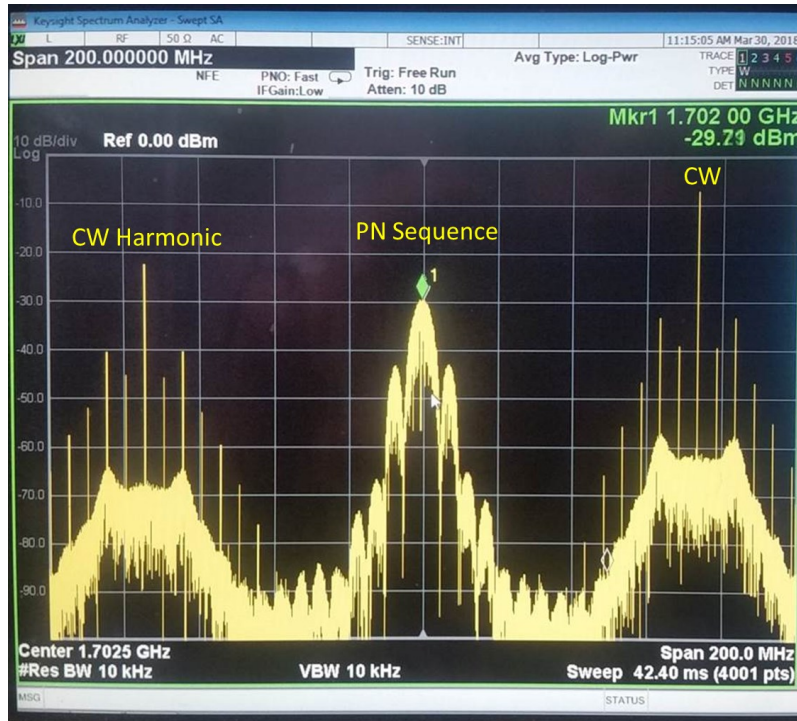


Figure 33. EMI problems—two signals through power amplifier.

We moved the power amplifier to a Faraday cage [20], and made sure the systems were on the same ground. The result is shown in Figure 34.

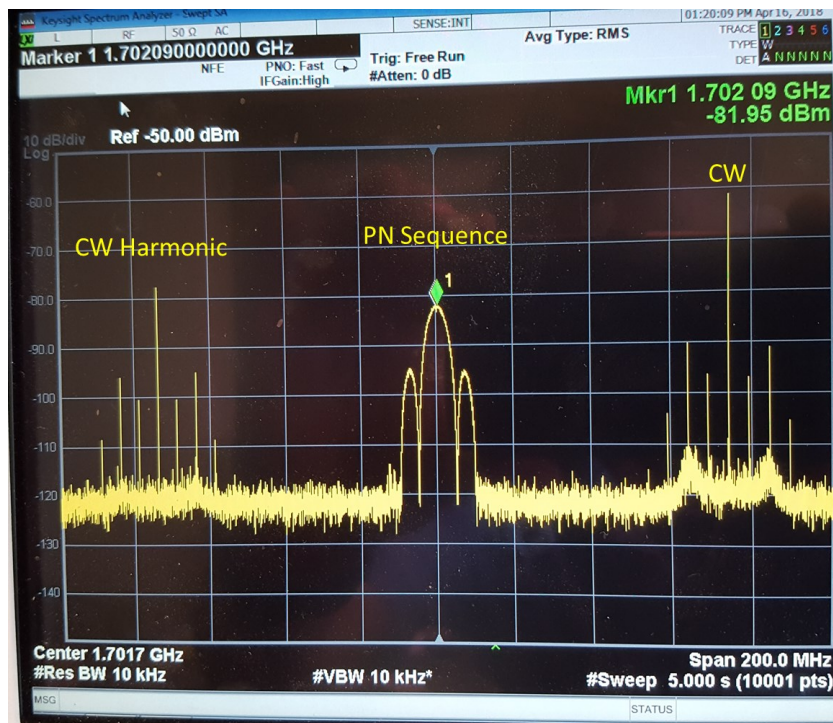


Figure 34. EMI problems—power amplifier in Faraday cage, and common ground circuit.

The power amplifier without the Faraday cage was allowing common modes to flow on the cables and also radiate into the environment which resulted in the spectral regrowth on both signals and the raised noise floor. This clearly demonstrates that combining two signals into a single power amplifier can be hazardous to the measurement and is why we fully test systems before deploying them into the field.

Back in Section 4.2, we tested the CW signal through the power amplifier and saw that there was no spectral regrowth and that the harmonics were at acceptable levels. Once we combined the two high power signals into the power amplifier, the power amplifier saturated and added non-linear effects to the desired signals.

Similar EMI effects can be experienced with electrically long direct current (DC) power leads. DC power leads should be twisted-pair, with suitable bypass capacitors installed as close to the terminals of the device being powered as possible. Improperly shielded control cables, such as those carrying RS-232 or other single-ended signals, can also radiate and disrupt measurements of sensitive signals.

Electronic circuit boards are another prime source of EMI. Many in-house constructed measurement systems may make use of custom-designed and built electronic circuit boards for a variety of functions (signal generation, instrument control, signal distribution, etc.). These boards, even if procured commercially, may not meet the most rigorous EMI/EMC requirements for use in sensitive instrumentation. Researchers at ITS have observed that many of these boards

can radiate energy significant enough to disrupt over-the-air signals in a variety of frequency bands. Thus, additional shielding or dedicated metal enclosures are highly recommended.

Cell phones and Wi-Fi hotspots are another source of EMI. Many measurement campaigns are carried out in remote locations where cellular signals may be weak or nonexistent. As a result, these devices will generate higher-power transmissions to overcome the severe path loss. If the sources of these signals are close to the measurement system, they can easily couple into the measurement system, overwhelming shielding and filters designed to block them. ITS recommends establishing and maintaining a minimum stand-off distance between cell phones, Wi-Fi (IEEE 802.11x standard) access points and hotspots, and the measurement system.

Most EMI problems appear as extra, unwanted signals when bench testing a system. They can also be seen as a greater than expected noise floor, or as unknown signals that wander through the current spectrum span. Also, signals that appear and disappear when moving cables, or components are signs of either broken equipment or radiation that is getting into the system. Ground loops appear as shifting signal levels in the system level.

6. BENCHTOP TESTING

Having an in-depth understanding of a measurement system is imperative to making good propagation measurements. If the system has been well-characterized on a laboratory benchtop prior to deployment, then measurement personnel can more quickly and effectively identify system failures at field locations. The purpose of performing propagation simulations on the benchtop is to understand a propagation channel in a conducted environment before adding antennas to the system. During benchtop testing, measurements are performed on the characteristics of, and variations in, RF connections, system losses and gains, received signals for various instrument settings, the system noise floor, and the system dynamic range. Possible EMI/EMC issues that may be encountered in the field need to be anticipated in this phase of work. Use of a fading simulator is recommended in this work phase, to examine the measurement system's performance in various fading environments that may be encountered in the field. End-to-end testing of the measurement system is recommended, including its data-collection and data-processing algorithms.

6.1 Link Budget

Benchtop testing also allows us to understand the details of a measurement system and the data post-processing algorithms used to calculate the basic transmission loss/gain (BTL/BTG) of the propagation channel as depicted in Figure 35. The propagation channel is the path between the output of the transmitting antenna and the input of the receiving antenna. To accurately measure the propagation channel, we have to understand the losses and contributions from each of the components. This is why we took great care in measuring each component and the assembled system in the previous sections. We use these values in the following equation:

$$BTL = P_t - P_r + (G_t - L_t) + (G_r - L_r), \quad (16)$$

where BTL is the basic transmission loss in dB; P_r is the received power in dBm; P_t is the transmitted power in dBm, G_t (dBi) and L_t (dB) are the transmitting antenna gain and losses on the transmitting side of the system, respectively; and G_r (dBi) and L_r (dB) are the receiving antenna gain and losses on the receiving side of the system, respectively. BTL is multiplied by minus one to obtain BTG .

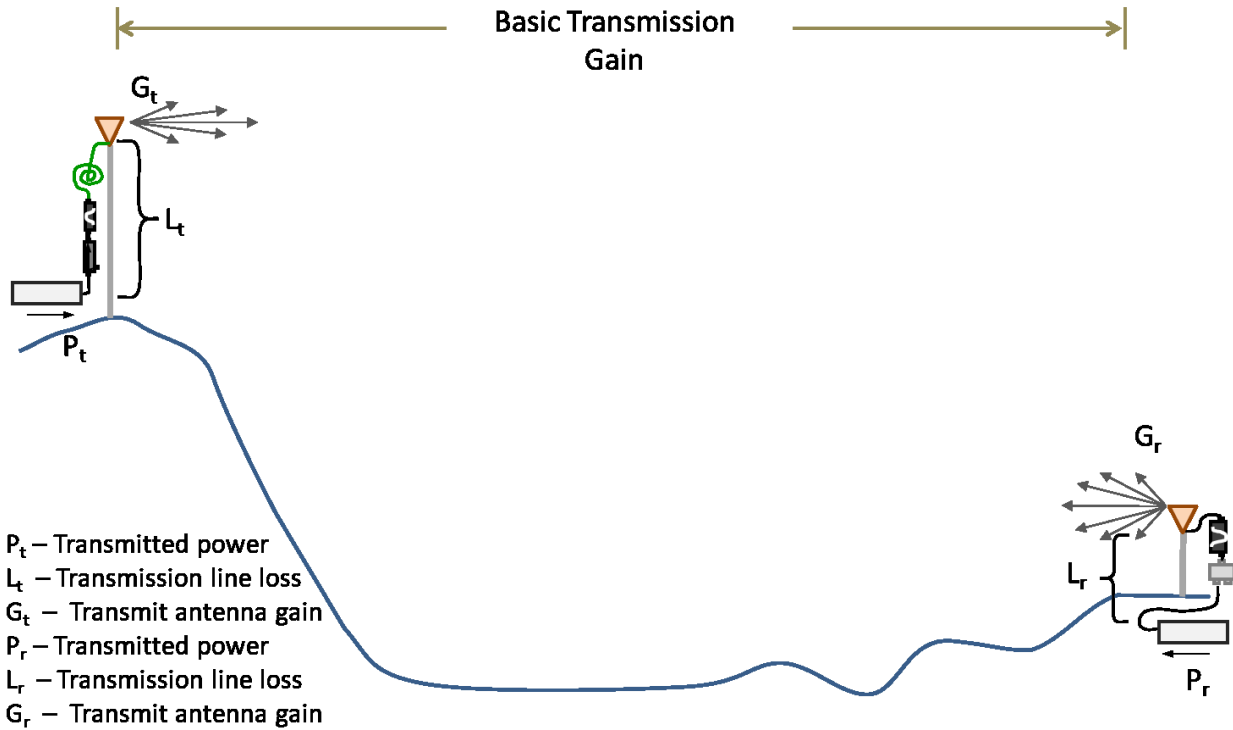


Figure 35. Link budget parameters.

In Section 6.2, we introduce a single power level into the system to simulate a simple propagation loss measurement to understand the data processing algorithms, and to make sure the measured component losses and the transmitting power levels used in the link budget have been accounted for correctly. In Section 6.3, we simulate various types of fading channels into the system and look at the variability of the received power, and the statistics of these well-known channels. By simulating these environments on the benchtop, will ensure that the system will operate correctly for the in-situ, radiated measurements performed in real-world environments (see Section 7.)

6.2 Benchtop Testing – Single Power Level

When antennas are added to the system and the propagation channel is in either an indoor or outdoor environment, the propagation channel becomes highly variable. For this reason, it is useful to begin with simple benchtop measurements, without antennas and the power amplifier, and then add more complexity to the system on the bench prior to conducting outdoor measurements with the entire system.

To begin our system testing, we return to Section 5.2, where we inserted a variable attenuator into the system. The variable attenuator simulates a simple propagation channel. Since the test configuration in Figure 35 does not include antennas, the link equation that corresponds to this test setup is the same as that shown in (16) but with the transmitting and receiving antenna gains set to 0 dBi. Our goal is to measure the measurement system’s variability by measuring the received signal power at the VSA as a function of time. Since the propagation channel

(attenuator) does not include any time-varying behavior in this test, any time-variability is due to the measurement system itself.

The test transmits a CW signal using several attenuator settings. We choose attenuator settings to look at the dynamic range of the system. These attenuator settings could be something like 0 dB, 45 dB, and 90 dB. We then record the received signal power for 120 seconds. For these tests, we typically transmit a power, P_t , equal to 0 dBm. In Figure 36, the repeatability of the received signal power is shown for a 20 dB attenuator setting and a 90 dB attenuator setting. The system losses are approximately 15.0 dB for this test. The mean value for the received power (P_r) for the top trace is -35.6 dBm with a standard deviation of 0.01 dBm, and the mean value for the received power for the bottom trace is -105.4 dBm with a standard deviation of 0.12 dBm. The uncertainty for the measurement is greater as the signal approaches the system noise floor (see Section 5.2.) Using (16), we can compute the propagation channel loss (i.e., the attenuator) using the system losses ($L_t + L_r = 15$ dB), the transmitted power ($P_t = 0$ dBm), and the antenna gains ($G_t = G_r = 0$ dBi). For the first attenuator setting, we calculate a channel loss of 20.8 dB and for the second attenuator setting we calculate a channel loss of 89.87 dB. The attenuator has about 0.5 dB of loss in itself, so we see that the difference between the measured and actual value of the attenuator setting is between 0.2 and 0.4 dB. This is the first test showing that our data processing algorithms and measured system losses are being correctly applied.

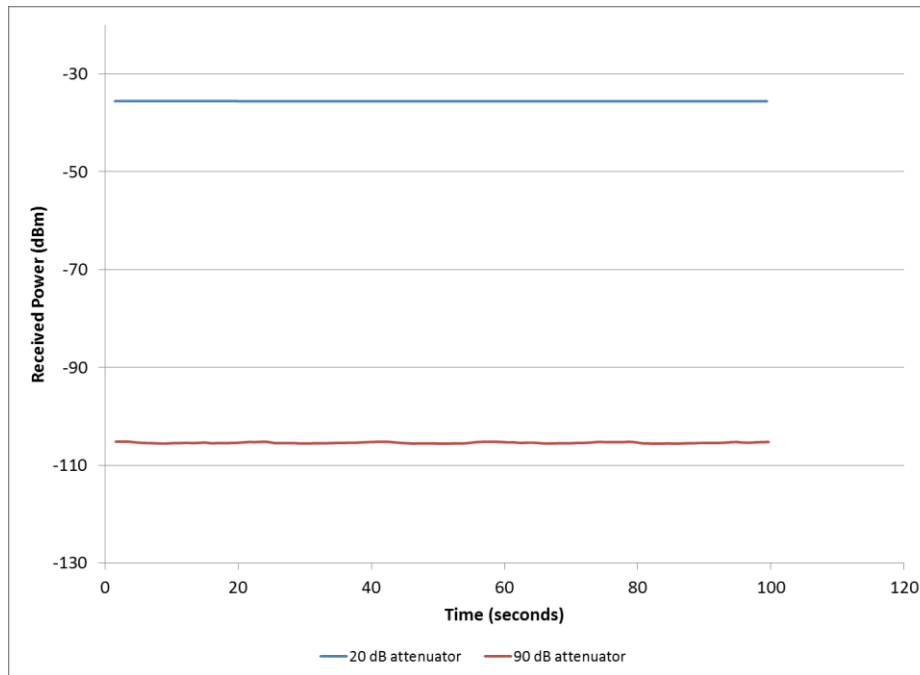


Figure 36. Received signal power in dB for a simulated 20 dB path loss and 90 dB path loss.

6.3 Benchtop Testing – Simulated Fading Environments

The actual mobile channel can exhibit a high degree of variability. Therefore, it is important to understand the mobile channel and how the data is going to be processed in the laboratory before conducting the actual measurements in an indoor or outdoor environment.

ITS uses the built-in fading simulator in a signal generator to simulate Rayleigh and Rician fading channels as would be seen in the outdoor environment. A Rayleigh fading channel is found in a non-line-of-sight (NLOS) condition where signals are converging on the receiver from all directions. In this type of channel there is no direct propagation path between the transmitting and receiving antennas [4]. A Rician fading channel is indicative of a channel where there is a direct signal component from the source and indirect signal components from the surrounding environment. The fading simulator allows one to change various parameters for Rayleigh and Rician fading channels; one can change the vehicle speed, the amount of the direct component present in a Rician channel, and whether the Doppler shift is up-shifted, down-shifted, or in the center of the fading distribution. We can also change the variable attenuator to simulate various amounts of path loss in these types of signal environments.

A time-domain measurement of a Rayleigh fading channel [4], [7], [8], is shown in Figure 37. The top plot is the linear signal envelope (blue trace), averaged over a 1 second sliding window average (red trace). The bottom plot is the signal envelope using a dB scale. Notice the large signal excursions in the bottom plot. These excursions can easily be 30 to 40 dB. These are deep signal fades due to multipath found in Rayleigh-fading environments.

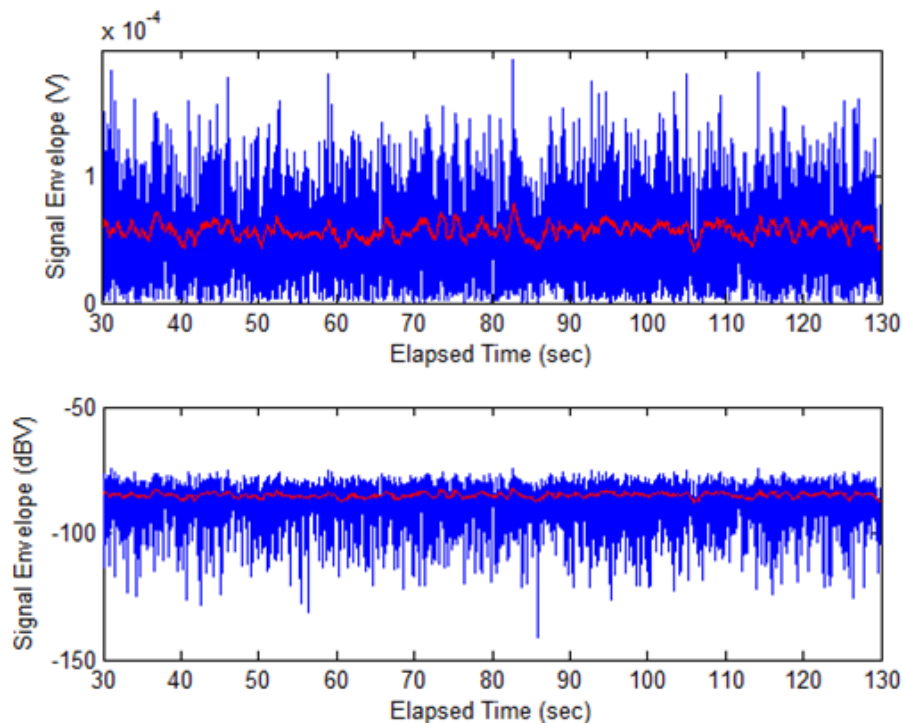


Figure 37. Simulated Rayleigh fading channel measured with a VSA. The fast-fading data (blue trace) and the slow-fading data (red trace) calculated using a 1 second moving average.

To understand a measured Rayleigh fading channel, we can begin by looking at the probability distribution function (PDF) for the channel to ensure that the measured channel exhibits Rayleigh characteristics. The fading simulator was set up to generate a Rayleigh-fading channel with a vehicle speed of 8.9 meters per second (m/s) (20 miles per hour (mph)). The PDF is obtained by normalizing the fast-fading data (blue trace) by the slow-fading data (red trace) and

binning the data to display the PDF distribution. Normalization is the process of dividing the fast-fading data by the slow-fading data in the linear domain. The normalized fast-fading data and the PDF are shown in Figure 38. The measured data does exhibit a Rayleigh-like distribution.

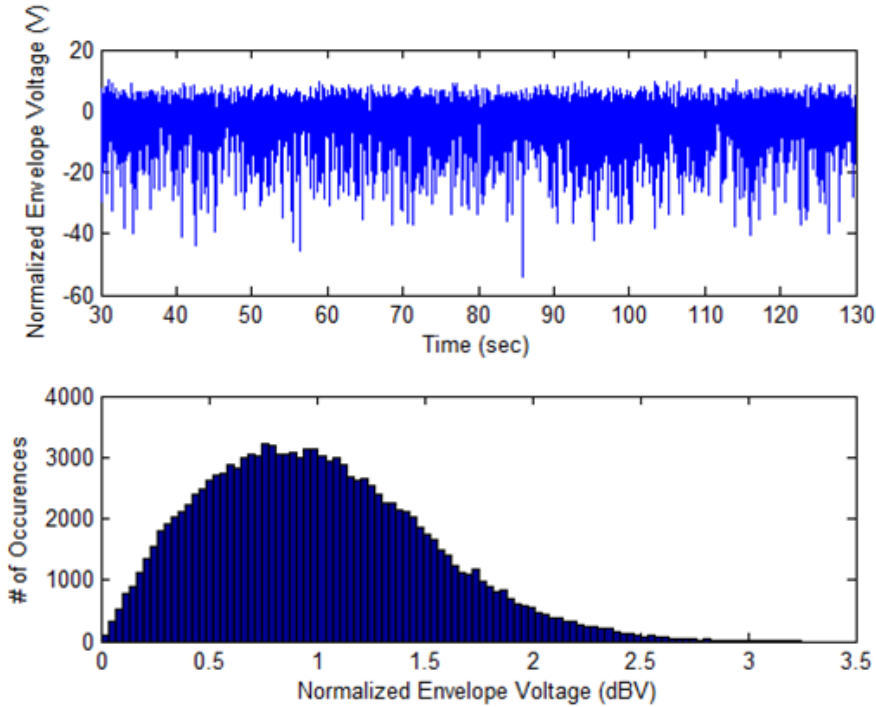


Figure 38. Normalized Rayleigh fading channel and the PDF for the simulated channel.

The Doppler frequency is another measured parameter that can be used to verify the validity of the simulated measured signal. The Doppler frequency is calculated from the following equation:

$$f_d = f_c \frac{v}{c} \cos \theta, \quad (17)$$

where f_d is the Doppler frequency, f_c is the carrier frequency, v is the speed in meters per second (m/s), c is the speed of light in m/s, and θ is the angle between the source and the receiver. For this simulated measurement, θ is set to zero, v is 8.94 m/s, and f_c is 430 MHz. This gives us a Doppler frequency of 12.8 Hz. The power spectrum for the Rayleigh channel in Figure 38 is shown in Figure 39. We can see that the dominant peak is located at the maximum Doppler frequency of 12.8 Hz and there are several other components between 0 and 12.8 Hz. These components are due to the received signals arriving from different directions, which is indicative of propagation in a Rayleigh fading channel.

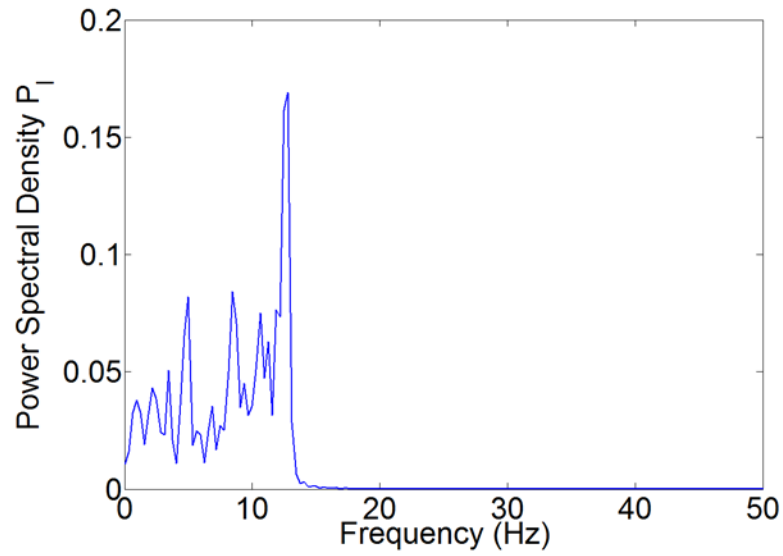


Figure 39. Simulated power spectrum for a Rayleigh channel.

During this phase of the testing, we would also simulate a Rician-fading channel and process the data to understand the statistics of the channel and our data post-processing algorithms [7], [8].

7. IN-SITU (RADIATED SIGNAL) SYSTEM TESTING

After benchtop testing, the entire measurement system, including the power amplifier and the transmitting and receiving antennas, should be assembled in an area where over-the-air testing can be performed, either in an indoor environment or an outdoor environment. End-to-end testing should include the following:

- Check transmit signal for proper spectral characteristics and power levels.
- Perform an initial sanity check by transmitting and receiving over a line-of-sight path where free-space loss conditions exist. Check that the measurement system properly calculates free-space path loss.
- Check that all software scripts and real-time displays are working properly.
- If measurement equipment is installed in a vehicle, check for EMI/EMC problems as described in Section 5.4. The vehicle will provide some shielding from the outside environment; however, it also allows reverberant fields and grounding problems to exist, so making sure that EMI problems are revisited is important.

The routes driven in this section are in the middle of a residential neighborhood with mostly one-story homes and large, mature trees. Signal propagation depends on the environments surrounding the receiving and transmitting antennas. For these measurements, the transmitting antenna is placed on the roof of the laboratory in a free-space environment. The receiving antenna will be placed in two different environments. We will show a measurement and the analysis of both a Rayleigh-fading environment (NLOS) and a Rician-fading environment (LOS).

7.1 NLOS Drive Route—Rayleigh Fading

Analyzing data from a real-world measurement can tell us a lot about signal propagation. In this data set, we can analyze areas along the drive route that exhibited a Rayleigh-fading environment and a place where high signal levels existed due to the presence of a wave-guiding street. Figure 40 shows the location of the transmitter atop the laboratory building (red plus sign) and the analyzed drive path for a NLOS path as shown by the blue line. The first thing we notice in Figure 41, at about 702 seconds, is a rise in the signal level. This rise in signal level corresponds to a street (shown by the yellow arrow) that provides a wave-guiding channel for the transmitted signal, even though the rest of the drive route is in an area where there are many houses and trees.

The linear signal envelope for this drive path is shown in the top graph in Figure 41 and the dB signal envelope is shown in the bottom plot. Most of the drive path exhibits large signal excursions similar to those simulated in the bottom plot in Figure 37. To see if this is a Rayleigh channel, we apply the same analysis as those developed in Section 6.3. We begin by looking at the NLOS statistics and Doppler frequency for the data from 659 to 671 seconds. Figure 42 shows the linear signal envelope (top plot) and the dB signal envelope (bottom plot) for the signal from 659 to 671 seconds as well as the slow-fading signal (red trace). Again we notice the

large signal fades which are indicative of a Rayleigh-fading environment. The slow-fading signal envelope and Doppler frequency spectrum for this section of the run is shown in Figure 43. The Doppler frequency spectrum tells us that we were driving at a constant velocity through the channel with a Doppler shift of about 15 Hz. We can also look at the PDF to see if it displays a Rayleigh distribution, similar to the analysis performed in Section 6.3. The PDF for the signal from 659 to 671 seconds is shown in Figure 44. The red trace is a numerically-generated Rayleigh PDF chosen to provide a best fit to the data. The close agreement between the measured distribution and a best-fit Rayleigh distribution strongly suggests this portion of the data was in a Rayleigh-fading environment or a NLOS region of the drive run. This PDF looks similar to the simulated PDF shown in Figure 38.

Finally, as part of this analysis, we can look at the power spectrum. The full power spectrum associated with the signal from 659 to 671 seconds is shown in Figure 45. The transmitted frequency is 3500 MHz. The Doppler frequency spectrum is shown between approximately ± 104 Hz. The negative Doppler shifts are down-Doppler and tells us that the receiving vehicle was moving away from the transmitting antenna, the positive Doppler shifts correspond and are called up-Doppler and tells us that the receiving vehicle was approaching the transmitting antenna. A Doppler shift of 0 dB tells us that the receiving vehicle was perpendicular to the transmitting antenna. The maximum Doppler shift of ± 104 Hz corresponds to a velocity of approximately 8.94 m/s (20 mph) for the given transmitting frequency. There are a large number of signals arriving at our receiving antenna from different angles as calculated using (16). This tells us that we are in a Rayleigh-faded environment where there are no strong LOS paths for the given time interval. Notice also that the maximum signal in the Doppler spectrum would correspond to the location of the wave-guiding street.



Figure 40. NLOS drive path in Martin Acres next to the Boulder Laboratories. The transmitter is shown by the red + and the street chosen for analysis is shown by the blue line. The yellow arrow is the location of a wave-guiding street.

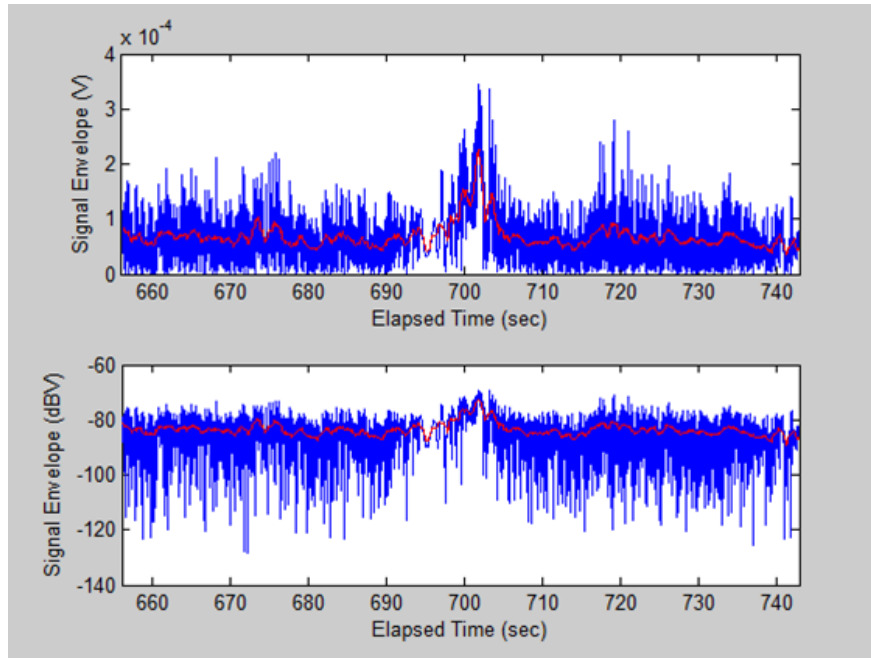


Figure 41. NLOS environment in the Martin Acres neighborhood. The blue trace is the fast-fading data and the red trace is the slow-fading data which is a 1 second windowed average.

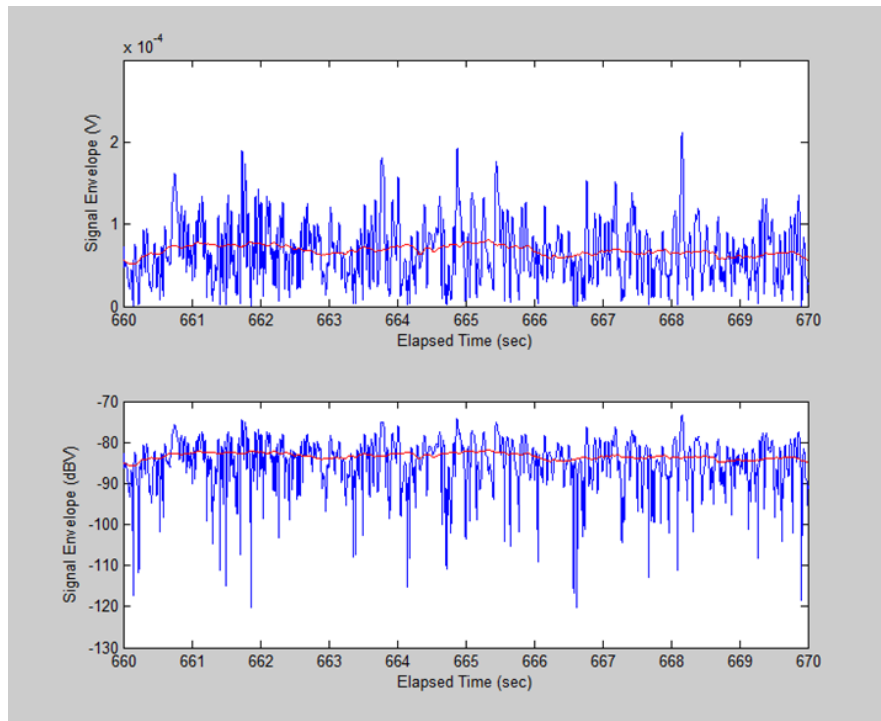


Figure 42. Linear signal envelope and dB signal envelope for the run from 659 to 671 seconds.

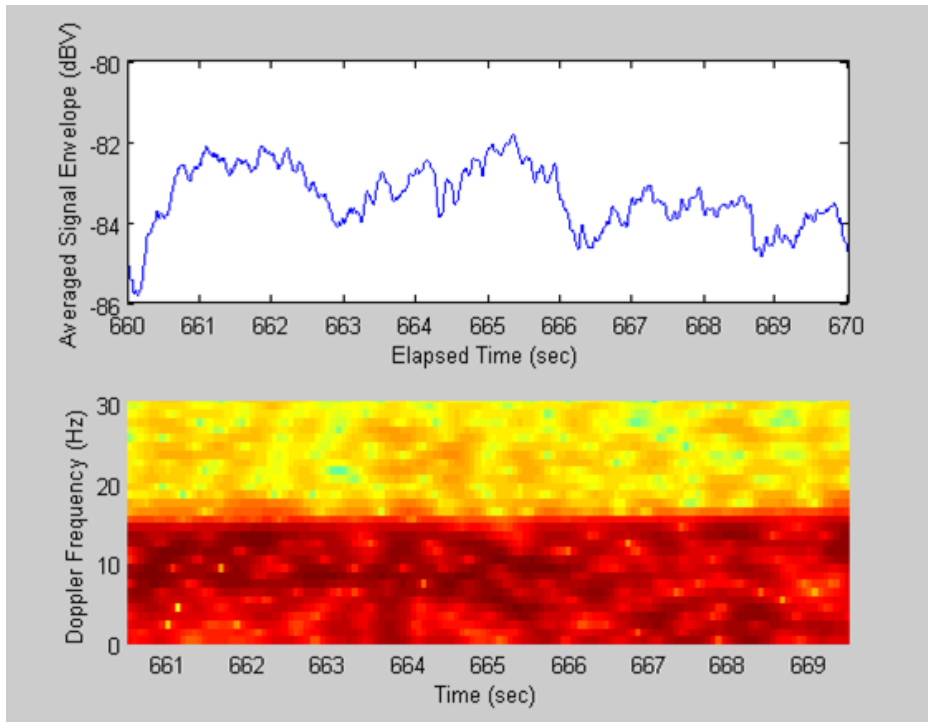


Figure 43. Slow-fading dB signal envelope and the Doppler frequency spectrum from 659 to 671 seconds.

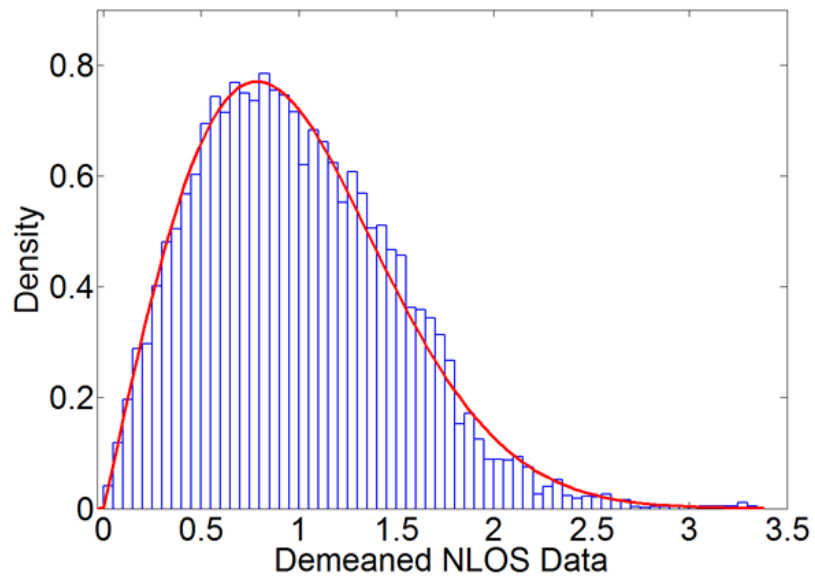


Figure 44. PDF for the NLOS drive run in Martin Acres from 659 to 671 seconds.

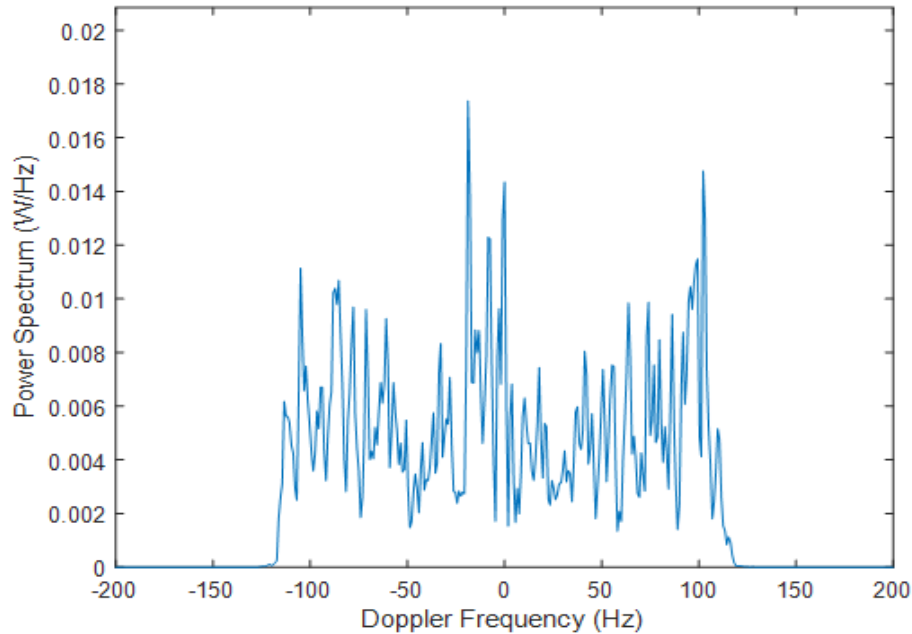


Figure 45. Power spectrum for a NLOS drive test showing a Doppler frequency spectrum from approximately -104 Hz to $+104$ Hz.

7.2 LOS drive route—Rician fading

To look at the propagation characteristics of a LOS drive route, we can make measurements along a street in the Martin Acres neighborhood that will exhibit Rician-fading statistics. This street is shown in Figure 46 by the blue line. The transmitting antenna was in the same location as for the previous Rayleigh-fading drive route. The linear signal envelope and the dB signal envelope for the LOS portion of the run is shown in Figure 47. We will look at various time intervals for this run and apply a similar analysis to understand the measurement as we did for the NLOS example given above.

From approximately 465 seconds to 488 seconds, we notice that the fluctuations in the signal envelope are much smaller for this time interval than for any other interval for this drive route. This signal behavior is indicative of a vehicle that is stopped. This can be seen in Figure 48 in the bottom plot that shows the Doppler spectrum. We see that the Doppler frequency has dropped for this interval to near zero which implies that the vehicle velocity is also near zero. Small movements in the surrounding environment, such as a passing vehicle, can contribute to a non-zero Doppler shift.

To analyze an interval of the drive route that contains a Rician-fading distribution, for a LOS case, we process the data from 505 to 515 seconds. The linear signal envelope and the dB signal envelope from 505 to 515 seconds is shown in Figure 49. The fast-fading data is shown by the blue trace and the slow-fading data is shown by the red, one-second, moving-averaged data. There is an oscillatory nature to the slow-fading data. This oscillation is indicative of a direct LOS signal component from the source. The isolated, slow-fading data and the Doppler spectrum for this time interval is shown in Figure 50. The Doppler spectrum tells us that we were driving

at a constant velocity during this time interval. The PDF for the data from 505 to 515 seconds is shown in Figure 51. The PDF tends toward a Gaussian distribution, which is indicative of a strong line-of-sight (LOS) component in the received signal [4].



Figure 46. LOS drive path in Martin Acres next to the Boulder Laboratories. The transmitter is shown by the red + and the street chosen for analysis is shown by the blue line.

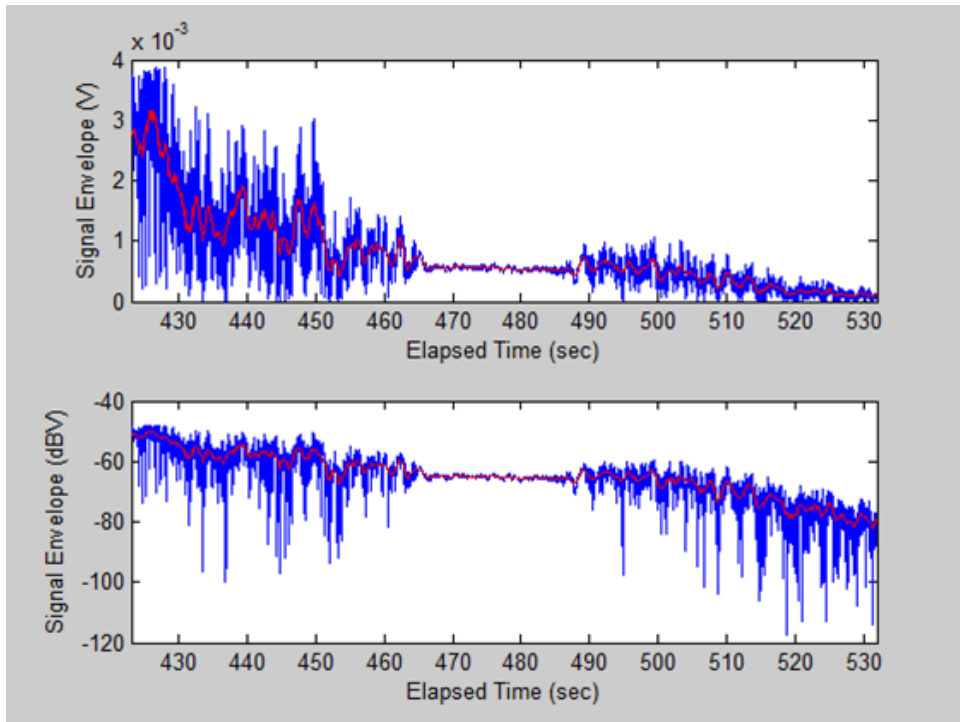


Figure 47. LOS environment in the Martin Acres neighborhood. The blue trace is the fast-fading data and the slow-fading data which is shown by the red trace using a 1 second windowed average.

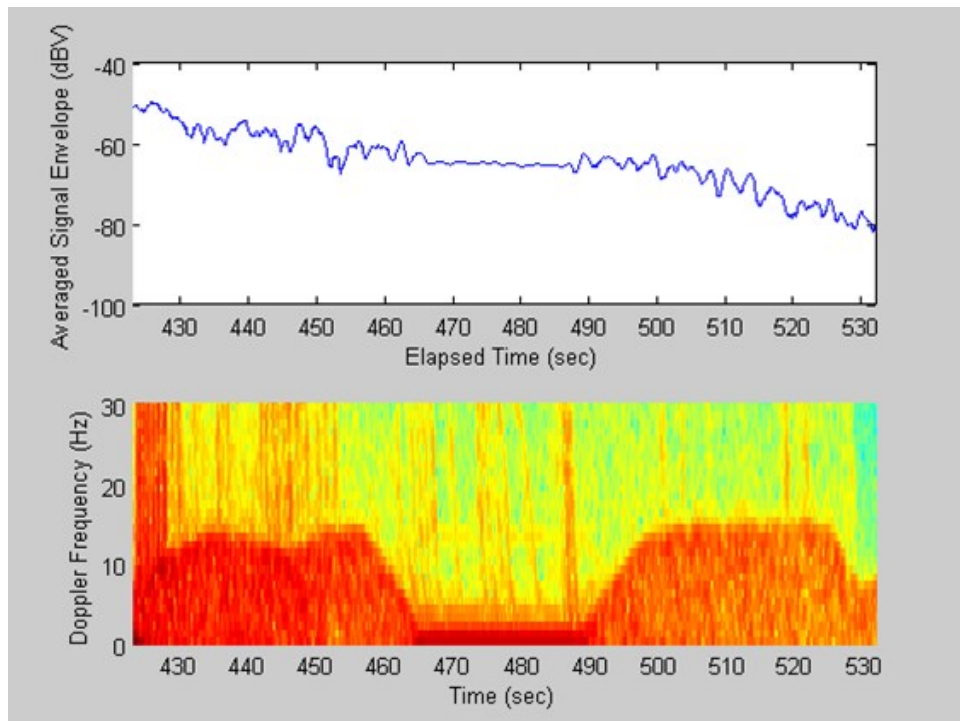


Figure 48. Slow-fading dB signal envelope and the Doppler frequency spectrum for the LOS condition on Lashley Lane in Martin Acres.

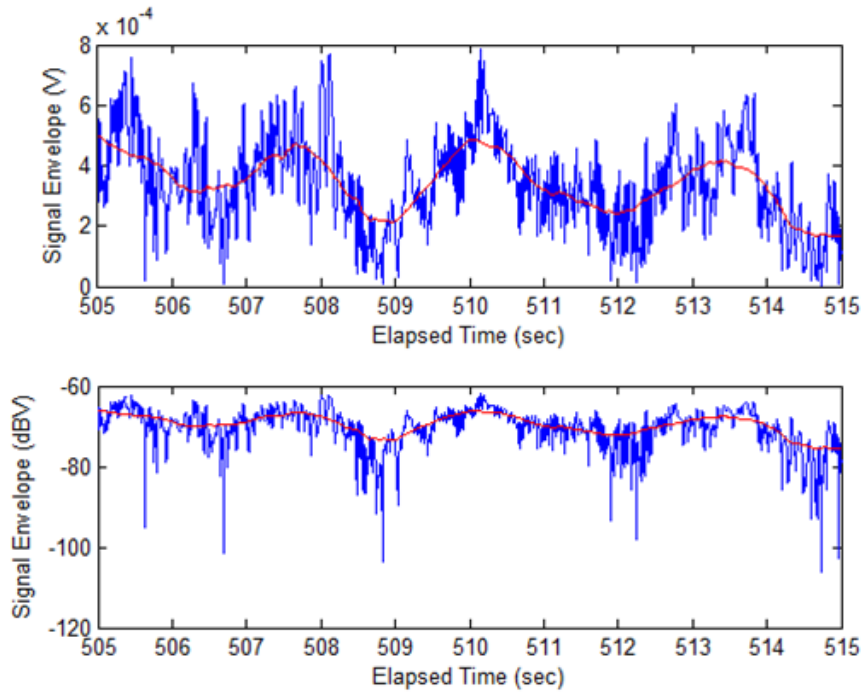


Figure 49. Linear signal envelope and dB signal envelope for the run from 505 to 515 seconds for the LOS condition on Lashley Lane.

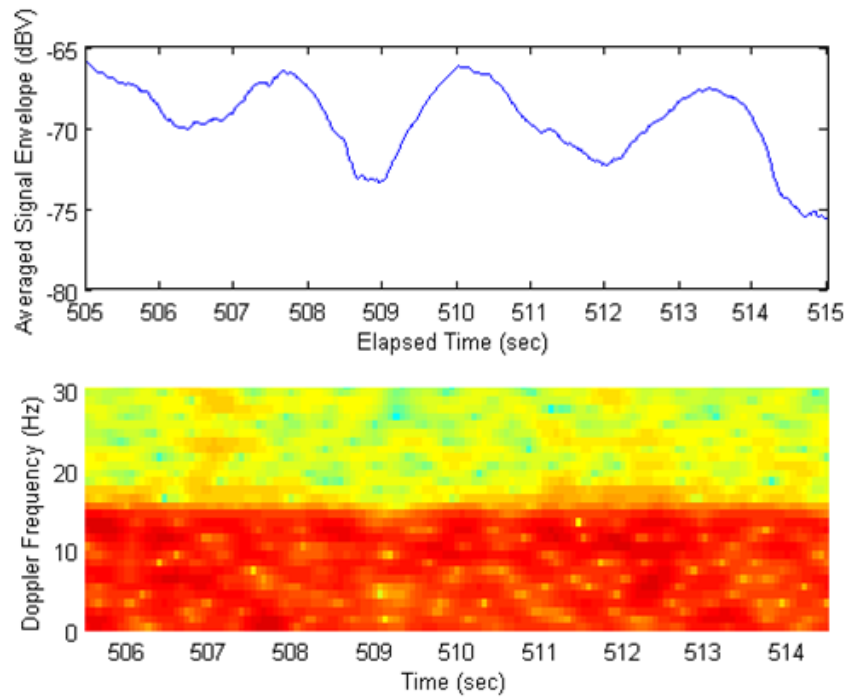


Figure 50. Slow-fading dB signal envelope and the Doppler frequency spectrum from 505 to 515 seconds for the LOS condition on Lashley Lane.

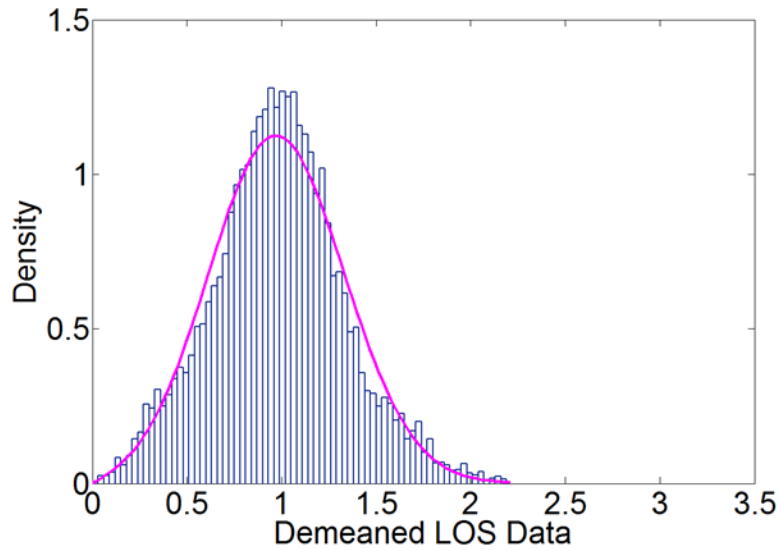


Figure 51. PDF for the LOS drive route in Martin Acres from 505 to 515 seconds.

7.3 Measurement System Repeatability Measurements

It can also be very informative to understand measurement repeatability over the same drive route and what parameters in the environment contribute to the repeatability for a given system. We completed an extensive set of measurements before our measurement system deployed. We conducted drive route repeatability and static positions repeatability tests at our Table Mountain Research facility [38]. This location is optimal for repeatability testing because there are very few buildings and low-profile vegetation. We drove a route on Table Mountain a total of four times and looked at the measurement variability. We also looked at static position repeatability for three locations at Table Mountain. The results of this analysis have been provided in Appendix C, Sections C.1 and C.2.

We also completed a sensitivity analysis using a screening experiment to understand which environmental/system parameters would contribute to measurement variability. A summary of the experiment and the results are given in Appendix C, Section C.3.

8. SUMMARY OF BEST PRACTICES

When deploying a verified system to real world measurements, there are some procedural considerations for successful measurement campaigns. The following list summarizes important procedures used by ITS during its long history of conducting measurement expeditions to characterize outdoor RF propagation characteristics. See also Appendix C.

- Use the same components and equipment for both the verification and the actual measurement campaigns. Specifically, if any of the components break, it is very important that the losses for the replaced components be re-measured even if they are the same model number. Also, if the system is disassembled between measurements, it is important that all components and losses be re-characterized and verified before measurements.
- During outdoor testing, long cables should be secured to either the mast or other stable platforms to prevent connector damage and provide phase stability during measurements. Cables should not be dragged along the ground or bent in a tighter radius than suggested by the manufacturer. Connectors should be protected by rubber caps and all connectors should be cleaned before measurements.
- All equipment should be warmed up for 30 minutes to 1 hour before testing. The longer the power amplifier has to warm up, the more stable the output power will be. Also, the calibrations and stability of receiving equipment will give better measurement results.
- It is important to bring copies of permits, copies of the test plan, copies of equipment setup procedures, and a notebook or paper for making notes during a measurement. Measurements can be stressful and if standard procedures are available in a notebook, then a checklist can be marked off, and the testing proceeds much more smoothly.
- Once the measurement is completed, it is important to quickly review the collected data to ensure data integrity and to make sure that the GPS positions have been properly recorded. Sometimes measurements have to be repeated so it is important to allow at least an extra day in the test plan to make up any measurements. The GPS location of the transmitter should also be recorded and the height of the transmitting antenna above the ground.
- No measurement effort is without complications and so a list of lessons learned should be compiled at the end of each testing campaign.

9. REFERENCES

- [1] Federal Communications Commission, “Amendment of the Commission’s Rules with Regard to Commercial Operations in the 1695-1710 MHz, 1755-1780 MHz, and 2155-2180 MHz Bands,” Report and Order, DA/FCC: FCC-14-31, Adopted March 31, 2014, https://apps.fcc.gov/edocs_public/attachmatch/FCC-14-31A1_Rcd.pdf, accessed May 17, 2016.
- [2] Commerce Spectrum Management Advisory Committee, “1755-1850 MHz Airborne Operations: Air Combat Training System Sub-Working Group Final Report,” March 2014, https://www.ntia.doc.gov/files/ntia/publications/acts_swg_final_report_posted_03042014.pdf.
- [3] U.S. Department of Commerce, Institute for Telecommunication Sciences, National Institute of Standards and Technology, “Channel Sounder Measurement Comparison: Conducted Tests,” ITS/NIST Technical Report, U.S. Department of Commerce, forthcoming, 2018.
- [4] A. Molisch, *Wireless Communications – 2nd edition*, J. Wiley & Sons, Ltd., November, 2010.
- [5] C. R. Anderson, “Design and Implementation of an Ultrabroadband Millimeter-Wavelength Vector Sliding Correlator Channel Sounder and In-Building Multipath Measurements at 2.5 & 60 GHz,” Master’s Thesis, Virginia Polytechnic Institute and State University, May 6, 2002, <http://theses.lib.vt.edu/theses/available/etd-05092002-101656/unrestricted/AndersonThesisETD.pdf>, accessed February, 2017.
- [6] R. T. Johnk, P. Papazian, P. McKenna, N. DeMinco, G. Sanders, H. Ottke, “A Mobile Propagation Measurement System,” *2009 IEEE International Symposium on EMC*, pp. 103-118, 2009, <https://www.its.bldrdoc.gov/publications/3210.aspx>
- [7] R. T. Johnk, C. A. Hammerschmidt, M. A. McFarland, J. J. Lemmon, “A Fast-Fading Mobile Channel Measurement System,” *2012 IEEE International Symposium on EMC*, pp. 584-589, 2012, <https://www.its.bldrdoc.gov/publications/2686.aspx>
- [8] R. T. Johnk, C. A. Hammerschmidt, Irena Stange, “A High-Performance CW Mobile Channel Sounder,” *2017 IEEE International Symposium on EMC/CSI*, pp. 698-703, 2017, <https://www.its.bldrdoc.gov/publications/3186.aspx>
- [9] C. A. Hammerschmidt, H. E. Ottke, J. R. Hoffman, “Broadband Spectrum Survey in the Denver Area,” NTIA Technical Report TR-13-496, U.S. Department of Commerce, August 2013. <https://www.its.bldrdoc.gov/publications/2735.aspx>.
- [10] C. Drentea, *Radio Communications Receivers*, Blue Ridge Summit, PA: TAB Books, 1982.
- [11] R. Ulrich, J. Whitaker, *Communications Receivers: DSP, Software Radios, and Design*, New York: McGraw-Hill Companies, 2001.

- [12] R. Pettai, *Noise in Receiving Systems*, New York: John Wiley & Sons, 1984.
- [13] “Noise Figure,” *Microwave Encyclopedia*, IEEE, 2018, <https://www.microwaves101.com/encyclopedias/noise-figure>, accessed April 25, 2018.
- [14] T. Pratt, C. Bostian, J. Allnutt, *Satellite Communications*, New York: John Wiley & Sons, 2nd ed., 2003.
- [15] F. Sanders, “Antenna Selection for Monitoring of Airborne Radio Systems,” NTIA Technical Memorandum TM-13-492, U.S. Department of Commerce, November 2012, <https://www.its.bldrdoc.gov/publications/2691.aspx>.
- [16] F. Sanders, “Derivations of Relationships among Field Strength, Power in Transmitter–Receiver Circuits and Radiation Hazard Limits,” NTIA Technical Memorandum TM-10-469, U.S. Department of Commerce, June 2010, <https://www.its.bldrdoc.gov/publications/2507.aspx>.
- [17] Capps, C., “Near-field or Far-field,” *EDN Magazine*, August 2016, pp. 95-102.
- [18] R. Bansal, “The Far-field: How Far is Far Enough,” *Applied Microwave and Wireless*, November, 1999.
- [19] N. DeMinco, “Propagation Loss Prediction Consideration for Close-In Distances and Low-Antenna Height Applications,” U.S. Department of Commerce,, NTIA Report, TR-07-449, July 2007, <https://www.its.bldrdoc.gov/publications/2486.aspx>.
- [20] “Faraday cage,” *Merriam Webster Dictionary* (online), <https://www.merriam-webster.com/dictionary/Faraday%20cage>, accessed April 30, 2018.
- [21] Agilent Technologies, “Agilent E4419B Power Meter-User’s Guide,” April 5, 2013.
- [22] Agilent Technologies, “N9030A PXA X-Series Signal Analyzer-Data Sheet,” <http://cp.literature.agilent.com/litweb/pdf/5990-3952EN.pdf>, accessed January, 2017.
- [23] Stanford Research Systems, “FS725 Benchtop rubidium frequency standard,” www.thinkSRS.com, accessed January, 2017.
- [24] Ophir RF, Approved Test Report, personal communication, March, 2015.
- [25] A. Castro, “RF/ μ W Measurement Uncertainty: Calculate, Characterize, Minimize,” *Agilent Aerospace and Defense Symposium*, 2013.
- [26] C. L. Grachanen, “Mismatch Uncertainty Calculator: A Microwave Freeware Software Tool,” *Cal Lab*, March/April, 1998.
- [27] Joint Committee for Guides in Metrology (JCGM/WG1), “Evaluation of measurement data – Guide to the expression of uncertainty in measurement,” Bur. Intl. Poids et Mesures (BIPM), September, 2008.

- [28] J. D. Splett, H. K. Iyer, C.-M. Wang, C. N. McCowan, “Computing Uncertainty for Charpy Impact Machine Test Results-NIST Recommended Practice Guide,” NIST Special Publication 960-18, October, 2008.
- [29] L. A. Muth, D. M. Diamond, J. A. Lelis, “Uncertainty Analysis of Radar Cross Section Calibrations at Etcheron Valley Range,” NIST Technical Note 1534, September, 2004.
- [30] C. Grosvenor, D. Camell, G. Koepke, D. Novotny, R. T. Johnk, “Electromagnetic Airframe Penetration Measurements of a Beechcraft Premier 1A,” NIST Technical Note 1548, August, 2008.
- [31] D. A. Hill, M. Kanda, E B. Larsen, G. H. Koepke, R. D. Orr, “Generating Standard Reference Electromagnetic Fields in the NIST Anechoic Chamber, 0.2 to 40 GHz,” NIST Technical Note TN-1335, February, 1990.
- [32] H. Kobayashi, Y. Yamaguchi, Y. Cui, “Simple Near-Field to Far-Field Transformation Method Using Antenna Array Factor,” *Journal of Wireless Networking and Communications*, Vol. 2, pg. 43-48, 2012.
- [33] S. Eser and L. Sevgi, “Open-Area Test Site (OATS) Calibration”, *IEEE Antennas and Prop. Magazine*, Vol. 52, No. 3, June 2010.
- [34] D. Camell, R. T. Johnk, D. Novotny, C. Grosvenor, “Free-Space Antenna Factors through the Use of Time-Domain Signal Processing,” *IEEE Intl. Symp. Electromag. Compat.*, 2007.
- [35] R. Johnk, “High-resolution Time-Domain Site Attenuation Measurements using Conventional EMC Test Antennas — A Numerical Study,” *IEEE International Symposium on EMC*, 18 to 22 August 2008, pp. 1 to 6.
- [36] R. T. Johnk, J. D. Ewan, N. DeMinco, R. L. Carey, P. McKenna, C. J. Behm, T. J. Riley, S. Carroll, M. A. McFarland, J. W. Leslie, “High-Resolution Propagation Measurements using Biconical Antennas and Signal Processing,” *IEEE International Symposium on EMC*, July 2010.
- [37] Agilent Technologies, “Agilent Time-Domain Analysis Using a Network Analyzer,” Agilent Application Note 1287-12, 2007.
- [38] Table Mountain Field Site, <https://www.its.bldrdoc.gov/resources/table-mountain/tm-home.aspx>, accessed Jan. 11, 2017.
- [39] K. Karlsson, J. Carlsson, T. Andersson, M. Olback, L. Strandberg, M. Hellgren, “Distance Dependent Radiation Patterns in Vehicle-to-Vehicle Communications,” Science Partner Technical Research Institute of Sweden, SP Report 20145:07.
- [40] R. Jesch, “Measured Vehicular Antenna Performance,” *IEEE Trans. Vehicular Technol.*, Vol. VT-34, No. 2, May, 1985.

- [41] A-H systems, <http://www.ahsystems.com/catalog/log-periodic-antennas.php>, accessed January, 2017.
- [42] WIPL-D, Inc., <http://www.wipl-d.com/applications/lpda.htm>, accessed January, 2017.
- [43] International Centre for Theoretical Physics – Wireless, *Radio Laboratory Handbook - Vol I*, <http://wireless.ictp.it/handbook/download.html>, Chapter 6, accessed January, 2017.
- [44] R. E. Kirk, *Experimental Design*, 4th ed. Thousand Oaks, CA: Sage Publications Inc., 2013.
- [45] G. E. P. Box, J. S. Hunter, and W. G. Hunter, *Statistics for Experimenters*, 2nd ed., Hoboken, New Jersey: John Wiley & Sons, Inc., 2005.
- [46] D. J. Sheskin, *Handbook of Parametric and Nonparametric Statistical Procedures*, 5th ed. CRC Press, 2011.
- [47] H. S. Gitlow, A. J. Oppenheim, R. Oppenheim, and D. M. Levine, *Quality Management*, 3rd ed. New York, NY: McGraw-Hill/Irwin, 1995.
- [48] G. K. Griffith, *Statistical Process Control Methods for Long and Short Runs*, 2nd ed. Milwaukee, WI: ASQC Quality Press, 1996.
- [49] D. J. Wheeler and D. S. Chambers, *Understanding Statistical Process Control*, 2nd ed. Knoxville, TN: SPC Press, 1992.

ACKNOWLEDGEMENTS

This document was initially prepared for the Spectrum Sharing Test and Demonstration (SST&D) program. We thank the Defense Spectrum Organization, Defense Information Systems Agency for allowing us to distribute this to a wider audience. We also thank them for funding the field measurements used to collect RF propagation data.

We also thank Irena Stange and Frank Sanders for their helpful and constructive reviews. We thank Mark McFarland for the uncertainty analysis presented in Appendix C.

APPENDIX A—MEASUREMENT SYSTEM UNCERTAINTIES

ITS used its recent system verification with NIST [3] to understand the uncertainty analysis presented in this document. The list of uncertainty terms given in Table A-1 is a compilation of uncertainty sources that contribute to the end-to-end uncertainty of a measurement system.

Table A-1. Typical uncertainty sources and their values for the ITS measurement system.

| Uncertainty Term | Uncertainty (dB) |
|-------------------------------------|------------------|
| Power Meter, manufacturer | 0.04 |
| Coupling Coefficient | 0.50 |
| Power Amplifier stability, measured | 0.08 |
| VSA, manufacturer | 0.35 |
| Γ_{PA} , manufacturer | 0.17 |
| Γ_{PM} , manufacturer | 0.03 |
| Γ_{VSA} , manufacturer | 0.02 |
| $\Gamma_{coupler}$, measured | 0.02 |
| Γ_{ch} , measured | 0.02 |
| Rb frequency stability | neg. |
| Antenna Gain, measured | 3.00 |
| Antenna Mismatch, manufacturer | 0.35 |
| Measurement System (Type A) | 0.06 |
| Measurement Repeatability (Type B) | 0.70 |
| Component Losses | 0.50 |
| Combined Uncertainty | 3.21 |

This is a list of the main contributions to uncertainties in the ITS system. Each measurement system has its own list of major contributions to uncertainty and uncertainty analysis should be performed on each system individually. A brief description of each uncertainty term, the origin of the uncertainty, and references are presented in this section. Additional uncertainty terms include uncertainties due to the model, the terrain database, and the computed geographical parameters such as antenna height above ground and elevation angle calculations. In this section, we focus on the uncertainties in the end-to-end measurement system only. The largest source of uncertainty will be from the propagation channel. This channel uncertainty can be gleaned from the repeatability measurements discussed in Appendix C, Sections C.1 and C.2. A schematic showing the location of reflection coefficients that contribute to the uncertainty in the ITS system is shown in Figure A-1.

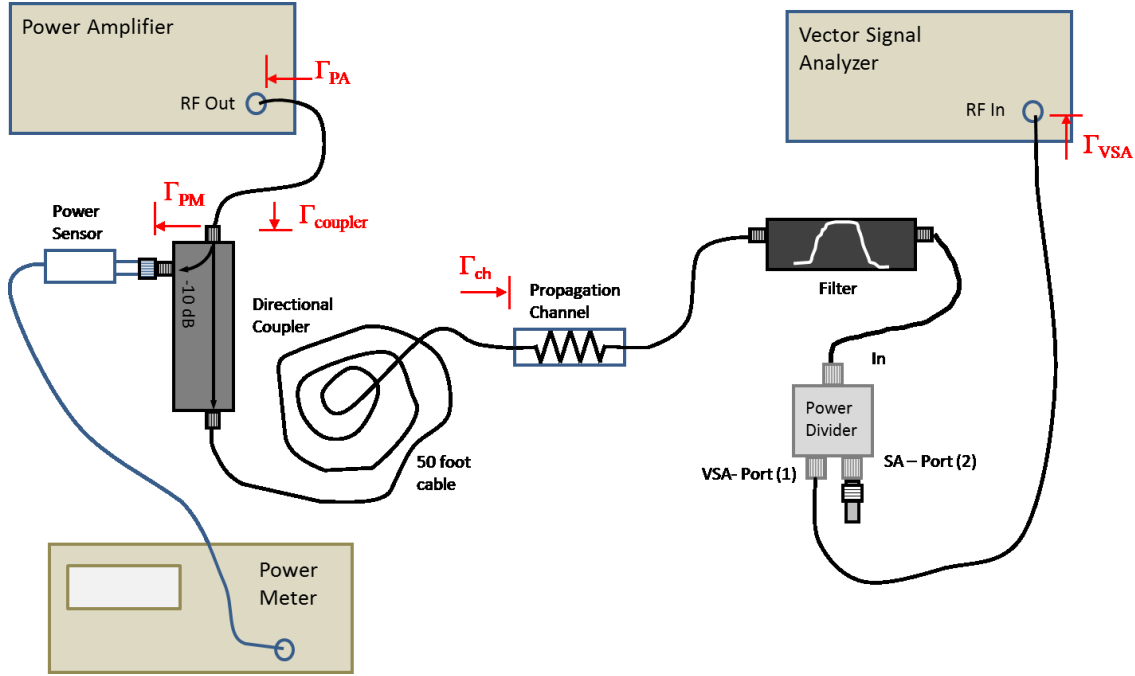


Figure A-1. Reflection coefficient definitions for uncertainty terms.

Several of the uncertainty terms are obtained from the manufacturer. These include the uncertainty of the power meter, the VSA, the uncertainty of the rubidium oscillator, the uncertainty of the antenna mismatch, and the reflection coefficients for the power amplifier, Γ_{PA} , the power meter, Γ_{PM} , and the VSA, Γ_{VSA} , [21]–[24]. The uncertainties for the coupling coefficient and the component losses are based on the uncertainty for repeated measurements, such as those that were described in Section 4.1.

The reflection coefficients for the coupler, $\Gamma_{coupler}$, and the channel, Γ_{ch} , were taken from measured values. When measuring components using the VNA, we typically set up the instrument to measure all four S-parameters (S_{11} , S_{21} , S_{12} , S_{22}). We can convert S_{11} to a reflection coefficient using the formula [25], [26],

$$\Gamma_{coupler} = \frac{S_{11(coupler)} - 1}{S_{11(coupler)} + 1} \tag{18}$$

The uncertainty in the antenna gain was determined by calculating the uncertainty of the measurements that were made at Table Mountain as discussed in Section B.5.

Type A measurement uncertainties of the measurement system were determined during a series of repeated measurements over a period of 10 days in a collaboration with NIST. These measurements were performed using three different attenuator settings in a conducted channel. We measured these three different attenuator settings using two different input power levels into the measurement channel, 0 dBm and 30 dBm. The maximum measured uncertainty of all tests was entered into the uncertainty table.

Type B measurement uncertainties were calculated by comparing the measured basic transmission gain for three different measurement runs using the same drive route. We used the data from run 1 as the reference and then looked at the basic transmission gain for the closest neighbor locations in runs 2 and 3. At these locations, we looked at the maximum difference in basic transmission gain to determine the uncertainties.

The combined uncertainty is obtained by taking the root sum of squares (RSS) of all uncertainty terms as defined in the following equation:

$$\epsilon_{combined} = \sqrt{\sum \epsilon_i^2} . \quad (19)$$

In this equation, $\epsilon_{combined}$ denotes the combined error (see entry at bottom of Table A-1) and the epsilon values in the sum on the right side of the equation denote the individual non-decibel uncertainties (those values listed in the table above the last row). Uncertainty analyses for other systems have been completed in different ways [27]–[30].

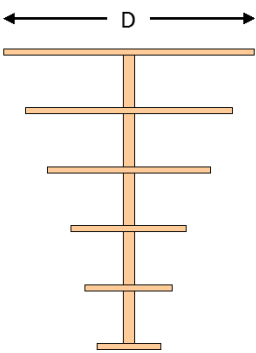
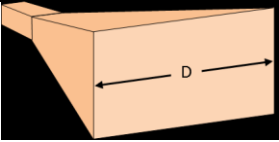
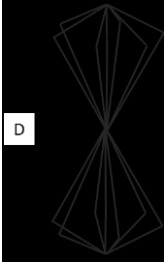
APPENDIX B—ANTENNA CHARACTERIZATION

The first section in this appendix will show the far-field characteristics for different types of antennas. The next four sections will discuss various methods of measuring the antenna gain pattern of an antenna. We will discuss the most accurate method first and then conclude with a very general way to measure the antenna gain pattern if no other resource is available.

B.1 Far-field Characteristics of Some Common Antennas

Antenna far-field distance is defined in [17]–[19]. The usual criterion is the distance from the antenna at which radiated wave front shapes (technically always spherical) approach flatness (become planar) to within a pre-defined percentage. Usually this distance is the Fraunhofer limit of about D^2/λ or $2D^2/\lambda$, where D is the antenna diameter or other physical aperture size and λ is the radiation wavelength. The largest dimensions of various types of antennas are shown in Table B-1 along with examples of the far-field distances at representative RF frequencies.

Table B-1. Various antennas, their largest aperture dimension, and the far-field distance for their lowest and highest frequencies.

| Antenna Type | Largest dimension, D (m) | Far-field distance (m) (f_1 [MHz]) | Far-field distance (m) (f_2 [MHz]) |
|---|----------------------------|--|---|
|  Log-periodic antenna | 0.51 | $R_{\text{far-field}} = 0.51$ $(f_1 = 290)$ | $R_{\text{far-field}} = 12.36$ $(f_2 = 7000)$ |
|  Dual-Ridged Guided (DRG) antenna | 0.24 | $R_{\text{far-field}} = 0.27$ $(f_1 = 700)$ | $R_{\text{far-field}} = 6.99$ $(f_2 = 18,000)$ |
|  Biconical antenna | 1.02 | $R_{\text{far-field}} = 0.14$ $(f_1 = 20)$ | $R_{\text{far-field}} = 2.27$ $(f_2 = 330)$ |

B.2 Anechoic Chamber Measurements

The most accurate way to measure the free-field antenna pattern of an antenna is to use an anechoic chamber. Figure B-1 shows a schematic of the measurement of an antenna in an anechoic chamber [31]. An anechoic chamber has RF absorbing material (such as carbon-loaded foam) on the walls, floor, and ceiling and is designed to cover a specific frequency range. Typically these facilities have a moveable platform where the antenna under test can be mounted. The platform can typically operate in three dimensions so that a complete radiation pattern can be obtained. Typically, the facility should measure the antenna gain in the far-field of the antenna; therefore, larger antennas require larger facilities; however, there are facilities that can measure near-field antenna patterns and transform them to the far-field [32]. One can also find chambers that will fit a vehicle and can therefore be used to measure the antenna pattern on a vehicle. The benefits of such a facility is that it simulates a free-field environment; however, these chambers are typically very busy, so there may be a long lead time before a measurement can be made. The cost to rent the facility for testing may also be a consideration.

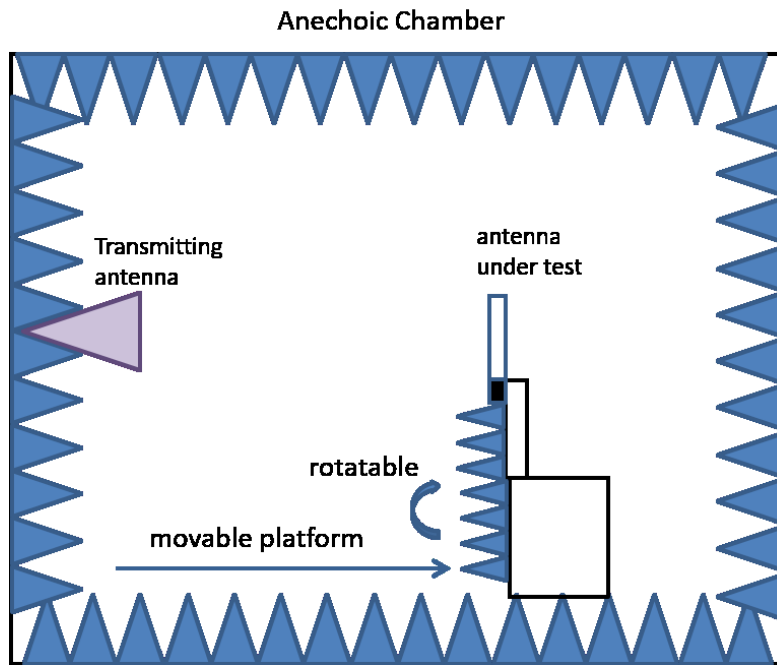


Figure B-1. Schematic showing a measurement of an antenna in an anechoic chamber.

B.3 Open Area Test Site (OATS)

Another method used to measure the radiation patterns of antennas is to use an open area test site (OATS) facility [33]. These facilities are outdoor facilities and usually have a metallic ground plane or a metallic mesh on which antenna stands are placed to make measurements. A picture of the National Institute of Standards and Technology (NIST) OATS facility at the Department of Commerce (DOC) Boulder Laboratories is shown in Figure B-2.



Figure B-2. Photo of an antenna measurement at the NIST OATS facility at the Boulder Laboratories.

In the experiment shown in the photograph, the antennas were mounted on custom-built towers and placed close enough together to minimize the contribution from the ground bounce to the received signal. OATS facilities are typically used for EMC/EMI measurements. The advantage to using an OATS facility to measure antennas is that the reflection coefficient of the ground plane is constant and can be modelled accurately. The disadvantage is that these types of facilities are costly. OATS facilities that can be used for a fee are scarce, expensive, and require long-lead times to get scheduled.

B.4 Free-Field Antenna Measurements

If an anechoic chamber or OATS facility is not available, free-field antenna measurements can be made on a flat surface using microwave absorbers to minimize the ground bounce and simulate a free-field environment. There are also time-domain techniques used to remove the ground bounce from the measurement and simulate a free-field antenna. One method is to place an absorber at the point of reflection as shown in Figure B-3.

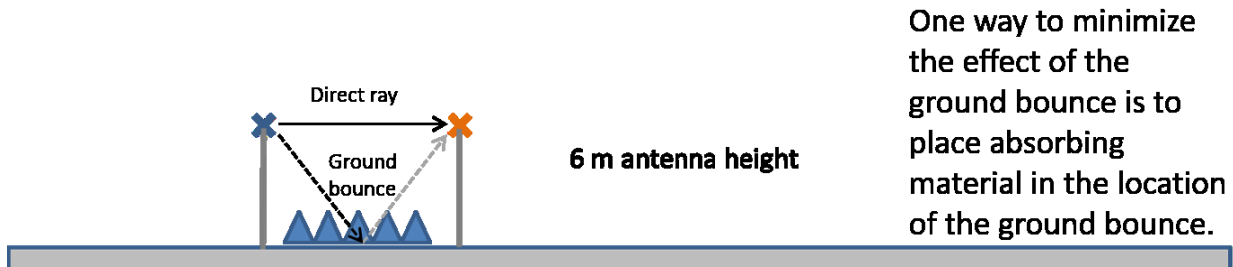


Figure B-3. Microwave absorber placement to minimize reflection into receiving antenna.

Using a VNA, we can remove the ground bounce from the final antenna measurement by time-gating the measured waveform. The direct-coupling wavelet and the associated ground reflection wavelet (or ground bounce) are shown in Figure B-4. Time-gating can be used to isolate the ground bounce and minimize it using techniques described in [34]–[37].

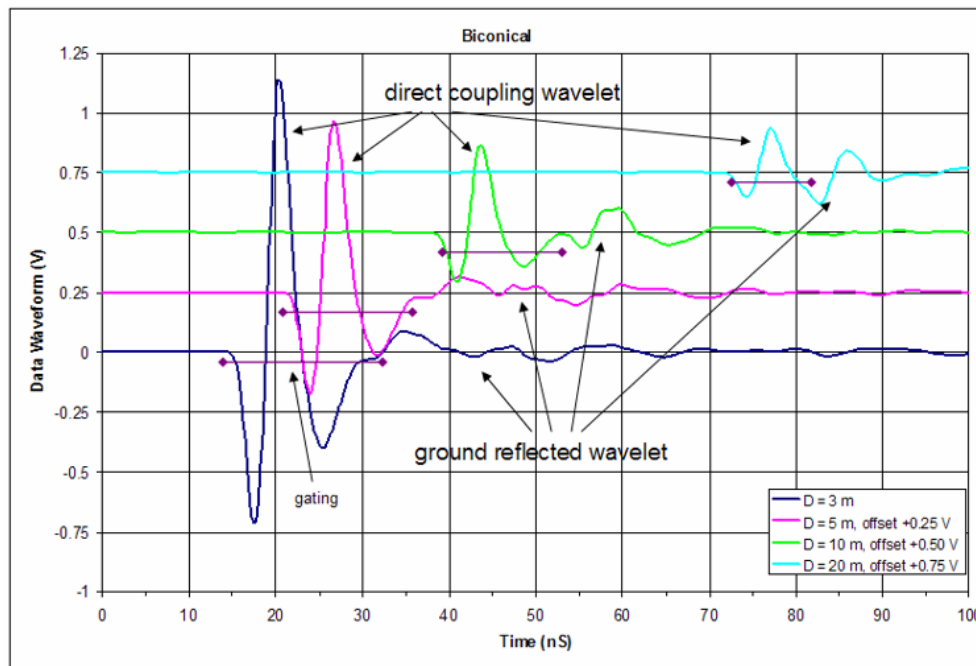


Figure B-4. Time-domain responses for antenna measurements on an OATS facility at various distances.

B.5 Turntable Measurements at Table Mountain

Measurements of the pattern of an antenna mounted on a vehicle can also be performed on a turntable. ITS, for example, sometimes measures a reference antenna, a transmitting antenna, and an antenna/van combination on the turntable at the Table Mountain Field Site [38]. The advantage to these measurements is that the test facility is outfitted to do these types of measurements, the test enables *in-situ* measurements, and the *in-situ* azimuthal pattern is obtained by spinning the vehicle on the turntable [38]–[40].

We cite, by way of example, two antennas used in an ITS propagation measurement system. The transmitting antenna is omnidirectional and has a nominal gain of 8 dBi and a length of 0.6 m; the receiving antenna is also omnidirectional with a nominal gain of 2 dBi and a length of 0.3 m. As calculated above, the far-field distance for the transmitting antenna is approximately 4.5 m and the far-field distance for the 0.3 m antenna is approximately 1.1 m.⁸

To ensure that the measurement was made in the far-field of the antennas, antennas were separated by as great a distance as was feasible. A vector network analyzer was used for the measurement. The VNA is a very accurate measurement instrument, but has a higher system noise floor than other methods may have. So the antenna-to-antenna distances were limited to where the cable losses would not adversely impact the signal-to-noise ratio. Also, there were vehicles, buildings, and miscellaneous antenna stands at the measurement site; it was necessary to minimize the impact of these in our measurements by moving the antenna away from these reflection sources.

The radiation pattern and gain of a calibrated antenna was measured as shown in Figure B-5. This is the reference measurement for all other radiation pattern measurements that follow. A log-periodic dipole antenna (LPDA) or log-periodic antenna (LPA) was chosen as the reference antenna both because it has a very distinctive antenna pattern and because it has been calibrated by the manufacturer.

⁸ There is a misconception that the far-field distance for an antenna-vehicle configuration is determined by the largest dimension of the antenna-plus-vehicle combination. It is true that currents may be induced on the vehicle due to the antenna's radiated electric field, and these currents can change the radiation pattern of the antenna. But if the antenna and vehicle are not electrically connected then they do not act as a combined antenna; the antenna can be treated in isolation from the vehicle, albeit with a somewhat disturbed radiation pattern.

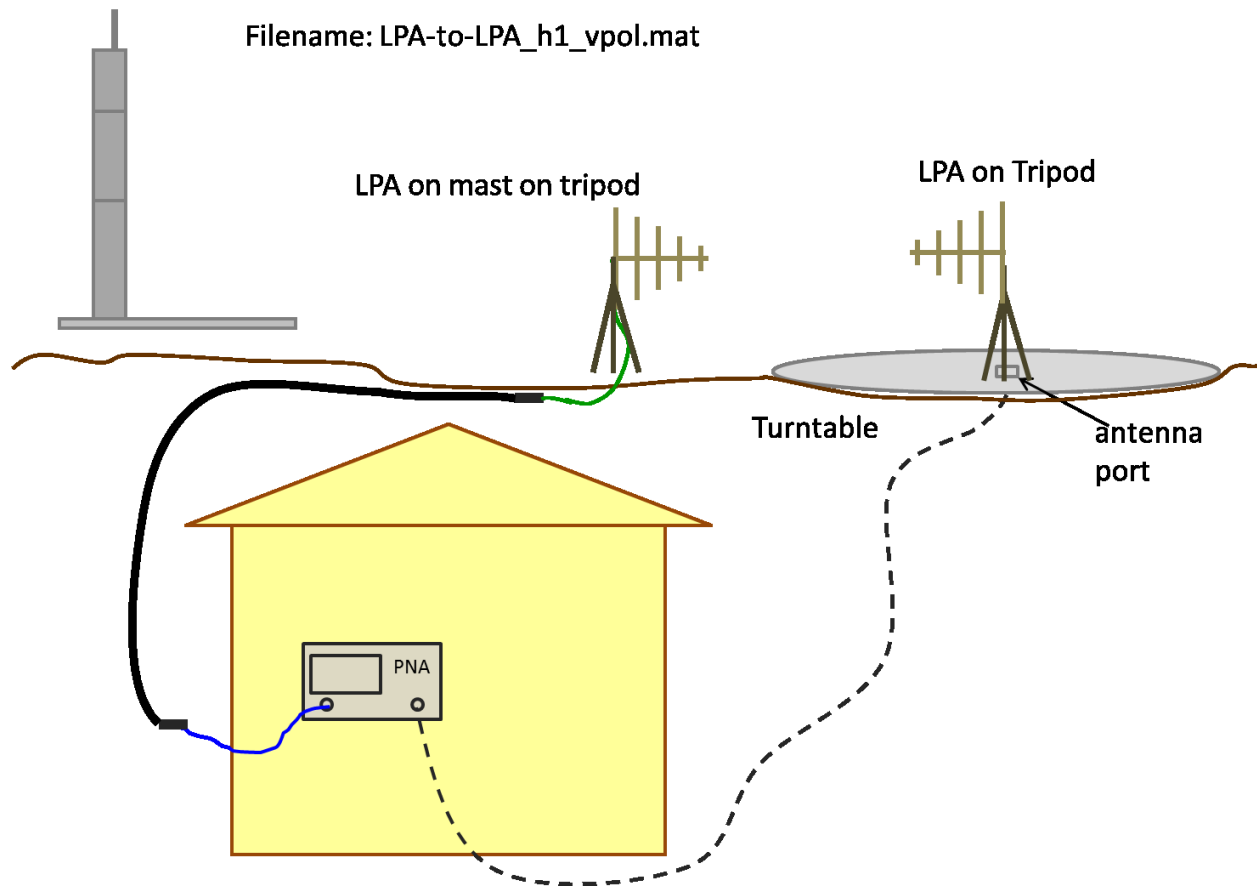


Figure B-5. LPDA reference measurement.

To verify that the van had a minimal influence on the radiation pattern of the antenna, the antenna was measured with and without the van. Figure B-6 shows a photo of the set-up for measuring the LPA antenna. The transmitting antenna was located on the cellular-on-wheels (COW) and the LPA antenna was placed on the roof of the van on a tripod so that its height was equal to the transmitting antenna height.

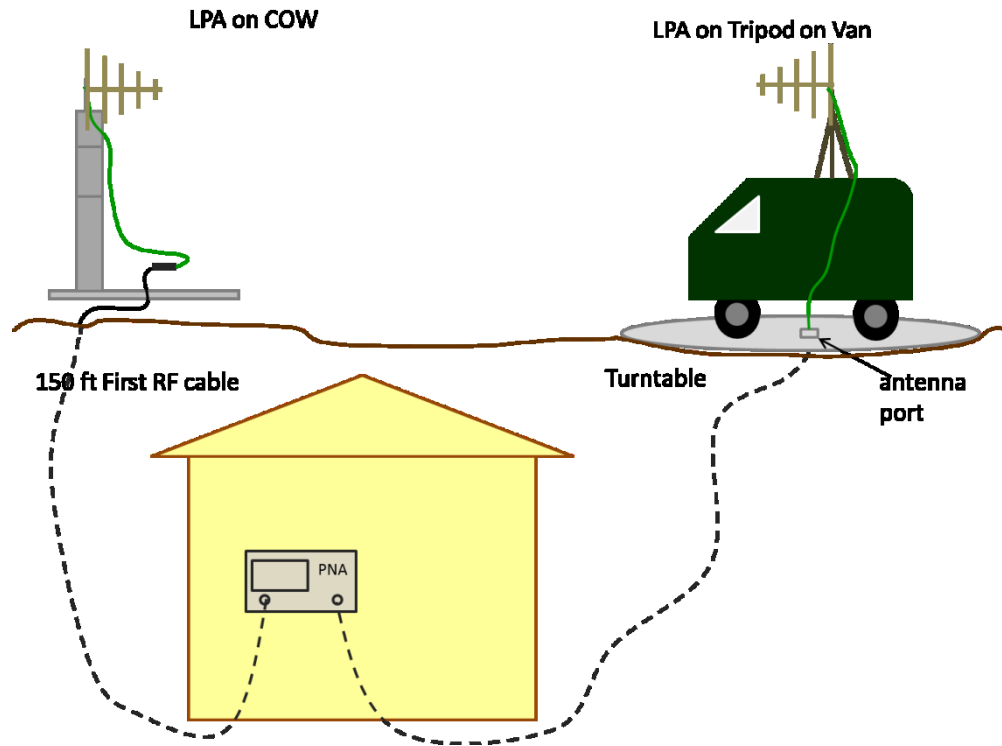


Figure B-6. Measurement of a log-periodic antenna on top of the van.

The turntable was rotated and initial measurements at two different angular resolutions were made to ensure that the angular resolution and speed did not impact the measurement of the antenna pattern. The manufacturer's antenna pattern is shown in Figure B-7(a) and the measured antenna pattern for the antenna and van combination at the Table Mountain facility is shown in Figure B-7(b). The green trace is the manufacturer's data for the antenna pattern at 1 GHz. The green and brown traces are manufacturer's data at other frequencies. ITS measurement results were compared to radiation patterns on the manufacturer's website for this type of antenna [41]. Also a numerical result is shown in [42] at 1 GHz. There is a slight impact on the antenna pattern, compared to the manufacturer's data, due to the presence of the van.

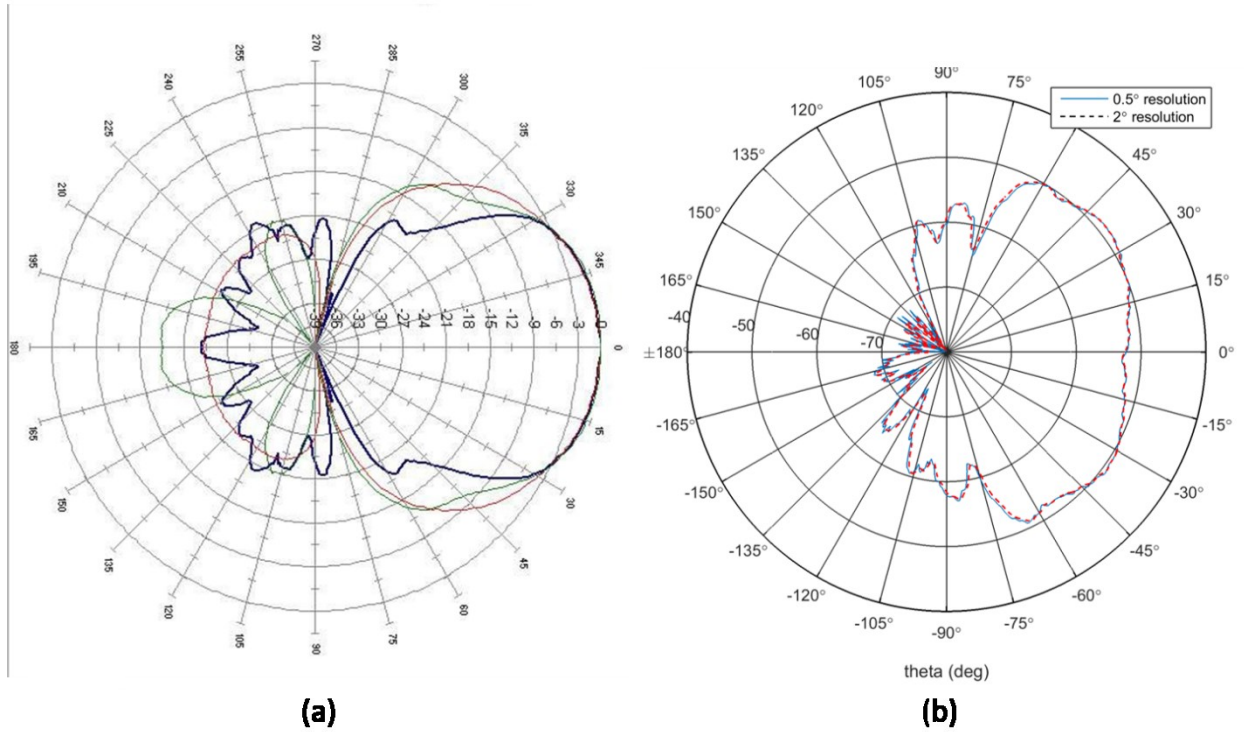


Figure B-7. (a) Manufacturer’s antenna radiation pattern at three different frequencies, (b) measured antenna radiation pattern at the Table Mountain facility.

The gain of the LPA antenna at 1760 MHz is approximately 7.2 dBi as given by the manufacturer which will be used as our reference antenna gain, G_{ref} . The conversion from S-parameter values, measured with the VNA, to gain is given by [43]:

$$G_{ant} (dBi) = G_{ref} + (S_{21(ant)} - S_{21(ref)}). \quad (20)$$

In this equation, G_{ant} , is the gain of the unknown antenna, G_{ref} , is the gain of the reference antenna, $S_{21(ant)}$, is the measured insertion loss for the unknown antenna, and $S_{21(ref)}$, is the measured insertion loss of the reference antenna.

The antenna gain for the antenna on the van, both with the antenna in the center of the vehicle’s rooftop and mounted on a vehicular mast, was between one and three dBi. There were perturbations in the pattern due to the presence of the van at various heights.

B.6 General Test Procedure for Other Situations

Many researchers may not have access to either an anechoic chamber or a facility like Table Mountain to perform this type of antenna gain pattern measurements and so the following are recommended steps to ensure good data.

- 1) Choose a pair of reference antennas whose gains and patterns are known

- 2) Make a free-field reference measurement in one of the following ways:
 - a) In an anechoic chamber (see Section B.2)
 - b) With microwave absorbers at ground bounce location to get free-field (see Section B.3)
 - c) Using a numerical technique to remove ground bounce (see Section B.4)
 - d) Verifying that the measured pattern and gain are nearly theoretical ($\pm 1-2$ dB)
- 3) Mount transmitting/receiving antenna on vehicle
- 4) Ensure that both antennas are in the far-field of the other antenna using formulas given in Section 4.6
- 5) Use a turntable or a rotating joint, or move around the vehicle at one- to five-degree angular resolutions with the transmitting antenna boresighted to the antenna on the vehicle as illustrated in Figure B-8.

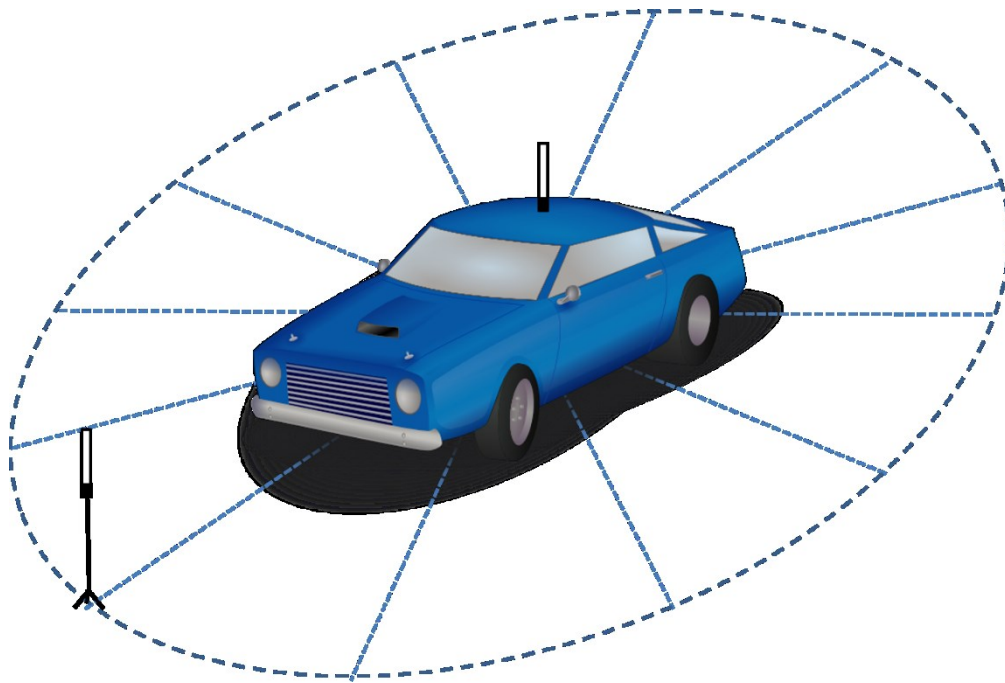


Figure B-8. Measurement of vehicle antenna.

APPENDIX C—MEASUREMENT SYSTEM REPEATABILITY

Measurement repeatability tests were conducted at our Table Mountain Research Facility [38]. (Note: this could be done at any location for any measurement system. This is an example of how ITS conducted these measurements.) This location is optimal for repeatability testing because there are few buildings and only low-profile vegetation. We drove the same route a total of four times and also measured a static channel at three locations within the same drive route. The drive route is shown in Figure C-1 along with the three static measurement locations shown by the numbered yellow dots. Most of the drive route was on top of Table Mountain, but we also drove over the edge (shown by orange line) and down to a lower area along the path where static position 3 is located.

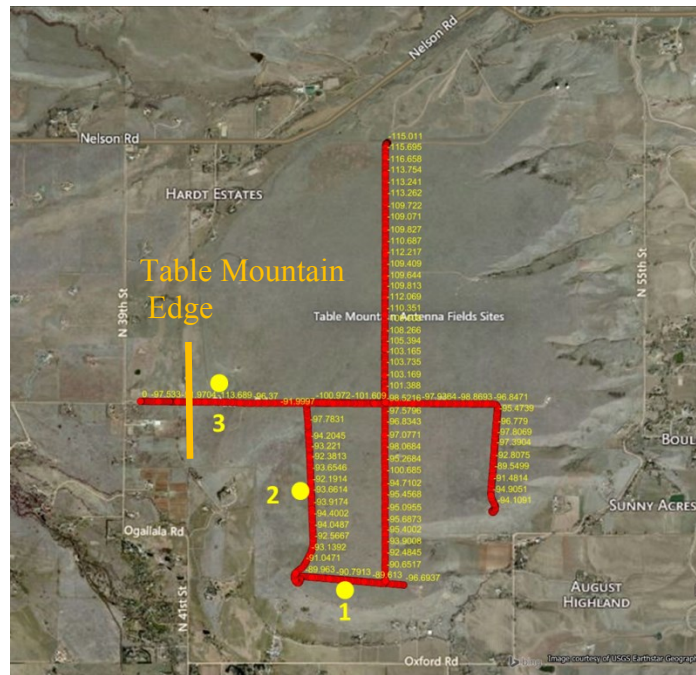


Figure C-1. Table Mountain drive route for repeatability studies and static measurement locations.

C.1 Mobile Measurement Repeatability Analysis

We measured received power along all four routes and processed the data as discussed in [6]–[8] to obtain plots of received power as shown in Figure C-2. Points of highest received power are shown by the white dots and points of lowest received power are shown by the red and purple dots. The transmitting antenna was on a 24.3 m tower at Green Mountain, which is approximately 15 km from Table Mountain toward the southwest.

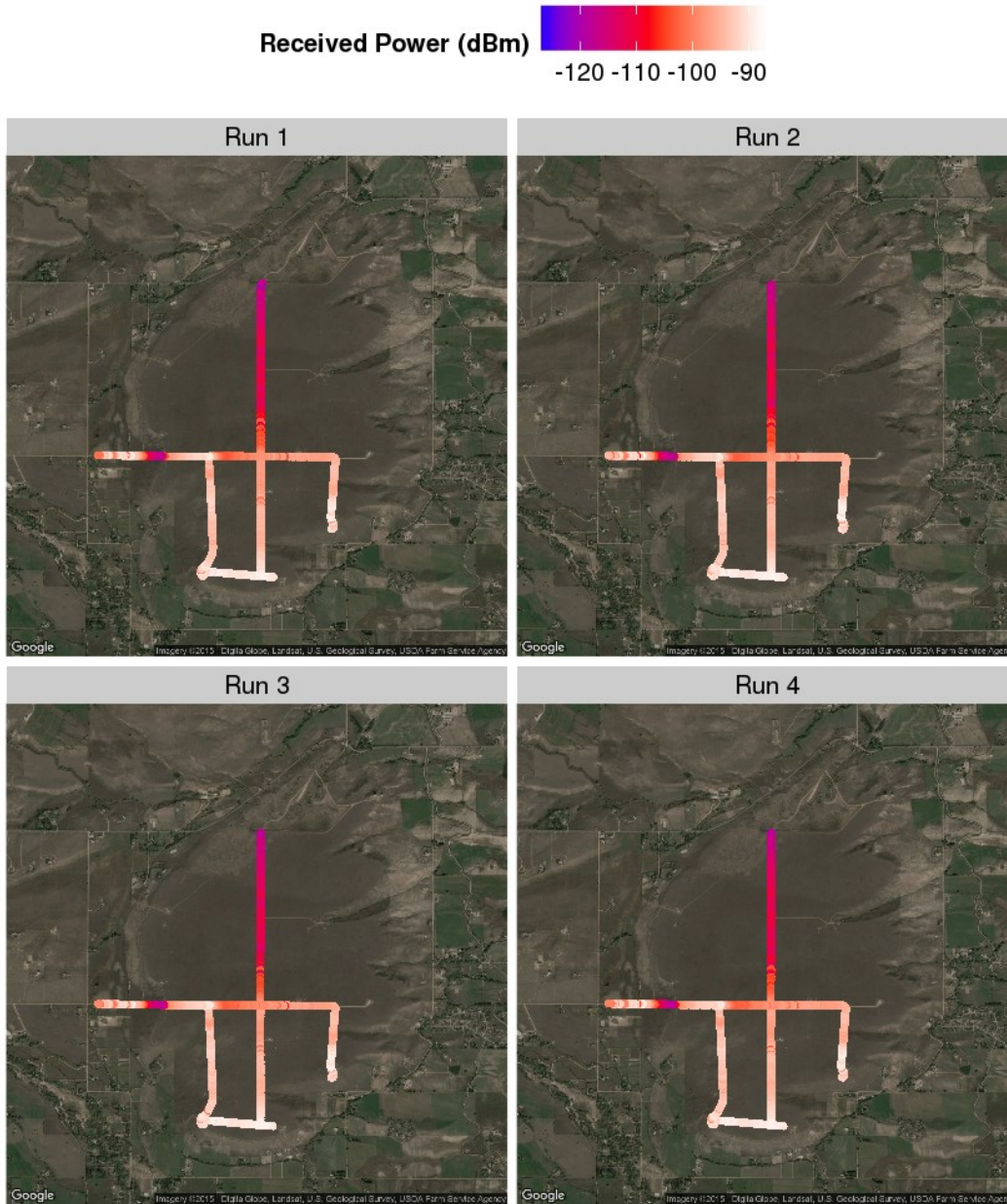


Figure C-2. Received power for all four runs at Table Mountain.

We analyzed the data in several ways to perform an uncertainty analysis for the measurements on Table Mountain. In the first analysis, the Haversine distance was computed from each observation in run 1 (1190 observations) to every other observation in runs 2, 3, and 4. Each observation is geolocated using a GPS receiver. There is no guarantee that each observation will occur at the same geolocated coordinate and so we compare observations within a defined radius. The standard deviation and the coefficient of variation of the received power was computed for all observations within the following radii of each observation in run 1: 5, 10, 25, and 50 meters. The coefficient of variation is the ratio of the standard deviation to the mean. It provides a consistent measure of dispersion variation.

For this analysis, we broke down exactly how many samples were used at each location for each radius. These sample sizes are shown in Figure C-3 and are summarized in Table C-1.

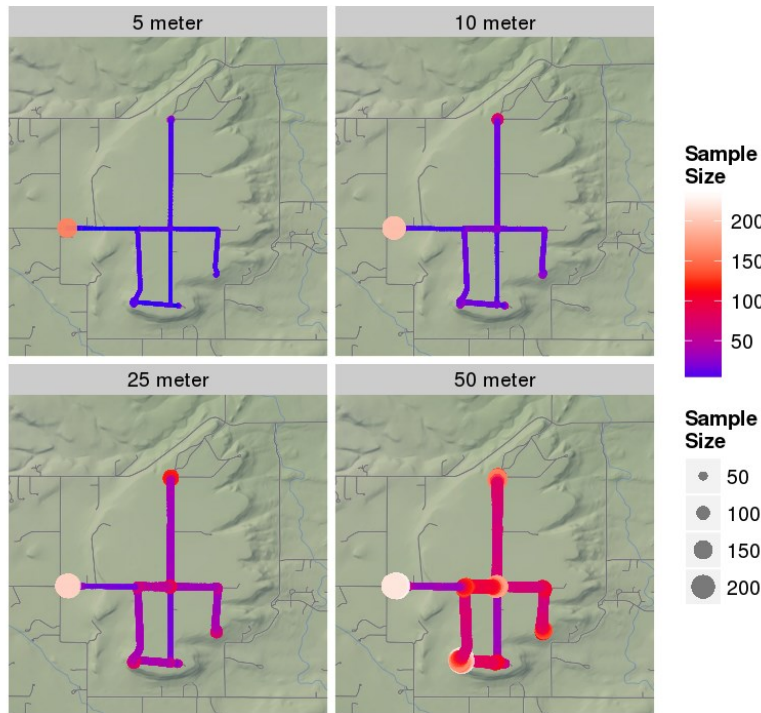


Figure C-3. Sample sizes of received power at each point for different size radius bins.

In Figure C-3, both light colors and large dots indicate large sample sizes and dark colors and small dots indicate smaller sample sizes. The only place in the 5 meter radius where sample sizes in excess of 200 sample point exist is at the end of the run where we sat until the measurement was finished. Most regions where small sample sizes exist is where the route was driven only once.

Table C-1. Summary of sample sizes by radius bin size.

| Run # | Bin size | min | max | median | s | \bar{x} |
|-------|----------|-----|-----|--------|-------|-----------|
| 1 | 5 meter | 2 | 162 | 6 | 9.38 | 6.78 |
| 2 | 10 meter | 3 | 199 | 14 | 14.57 | 16.13 |
| 3 | 25 meter | 14 | 214 | 36 | 23.05 | 41.31 |
| 4 | 50 meter | 29 | 233 | 72 | 36.33 | 82.36 |

The first set of data was analyzed using the received power values (dBm). The graphs showing how the standard deviation of the received power in dBm varies on Table Mountain are shown in Figure C-4 and statistically summarized in Table C-2.

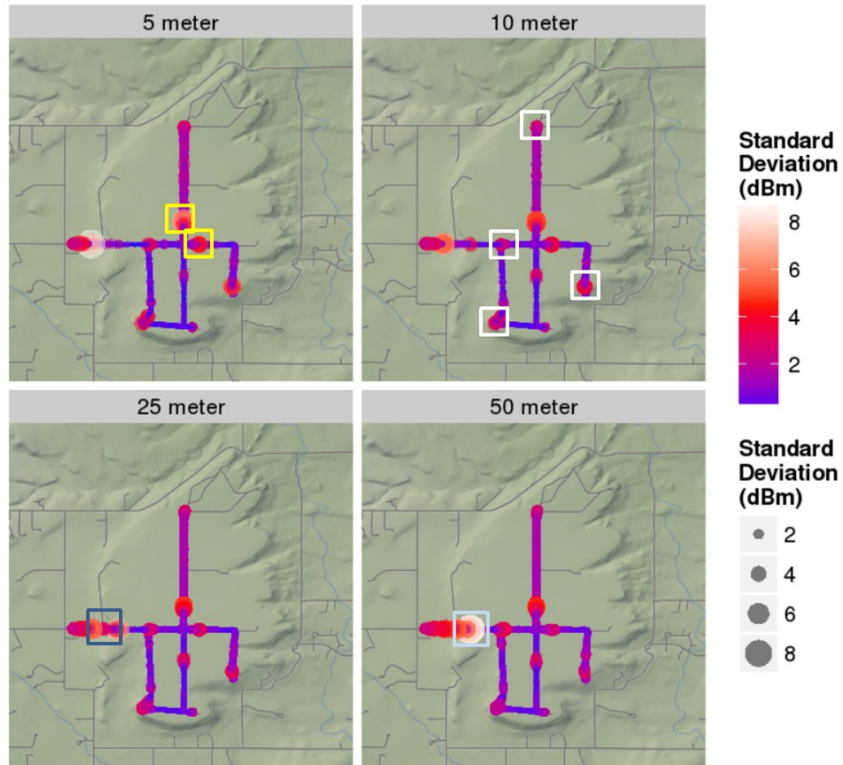


Figure C-4. Standard deviation of received power at each point for different size radius bins.

In this figure we see that there are certain points where larger standard deviations exist for all four radius sizes. These are typically where we turn from one road to another or where we turn in a small radius (white squares). Larger standard deviations also exist at places where there is no discernable terrain obstruction (yellow squares), and places where there is a terrain obstruction (blue squares). Figure C-5 shows the same data using boxplots.

Table C-2. Summary statistics of received power standard deviations by radius bin size.

| Run # | Bin Size | min | max | median | mean | Std. dev. |
|-------|-----------|------|------|--------|------|-----------|
| 1 | 5 meters | 0.00 | 8.71 | 0.68 | 0.95 | 0.89 |
| 2 | 10 meters | 0.02 | 6.45 | 0.81 | 1.06 | 0.85 |
| 3 | 25 meters | 0.25 | 6.98 | 1.02 | 1.25 | 0.91 |
| 4 | 50 meters | 0.29 | 8.79 | 1.34 | 1.48 | 1.03 |

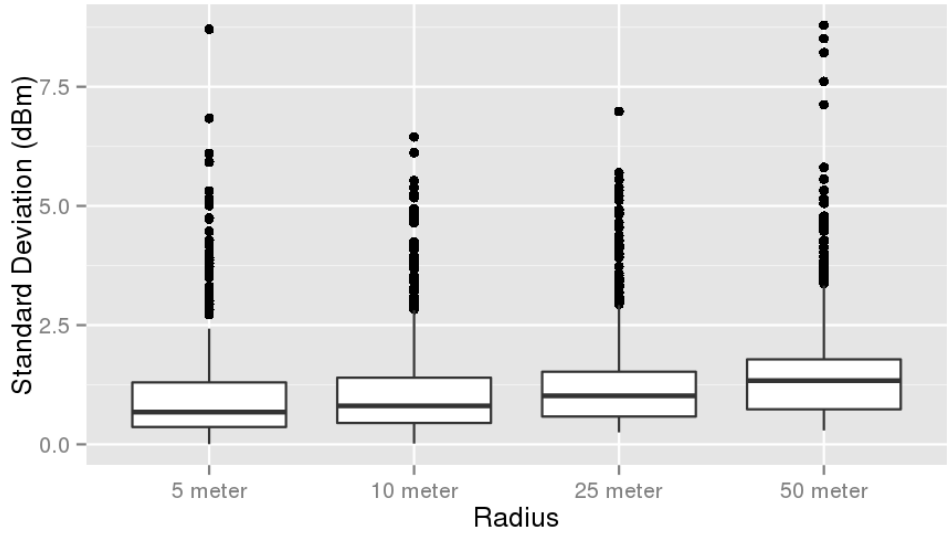


Figure C-5. Boxplots of standard deviation of received power (dBm) by radius (all samples).

Another statistic of interest is the coefficient of variation, which uses the linear received power units (mW). Figure C-6 shows the coefficient of variation of the received powers at each point for the four radius bins. Figure C-7 shows box plots of the coefficient of variation by radius and Table C-3 summarizes the analysis in a table.

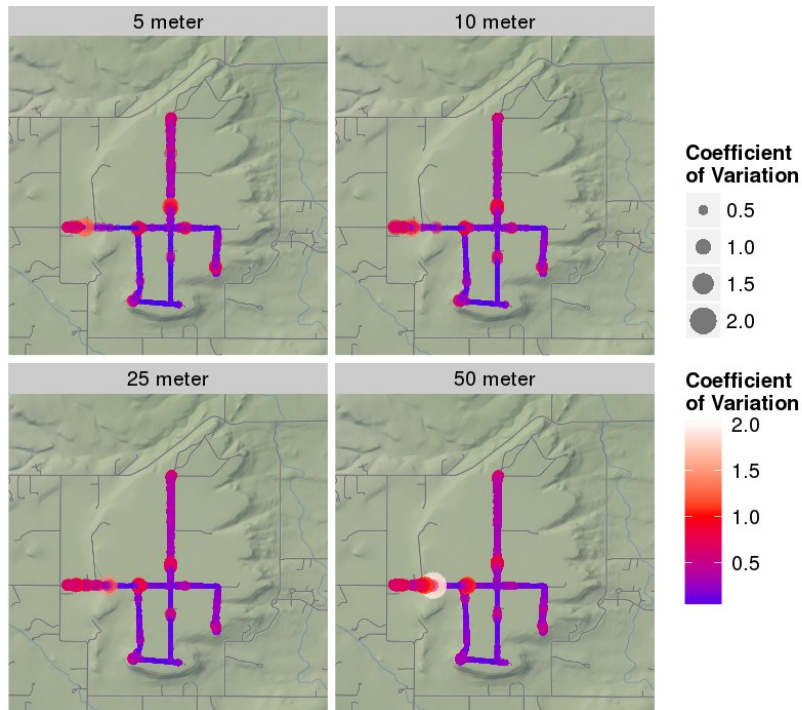


Figure C-6. Coefficient of variation of received power at each point for different size radius bins.

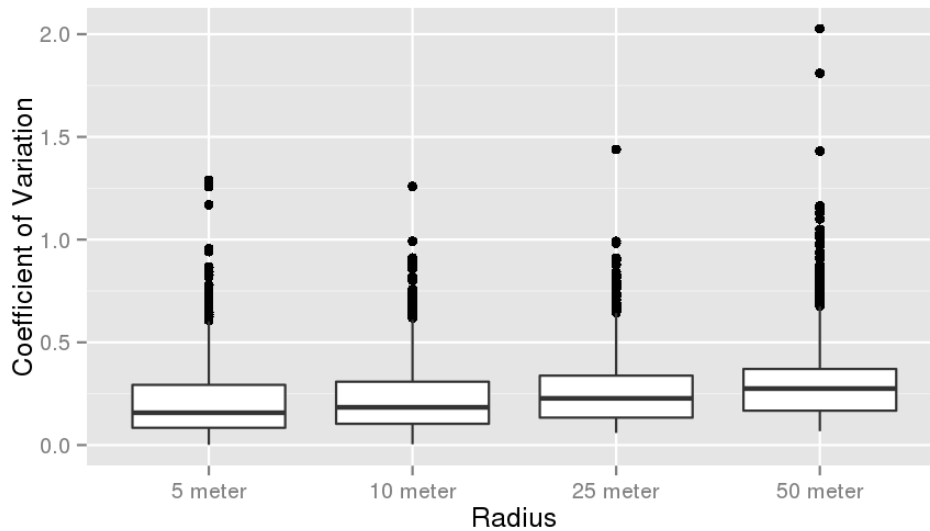


Figure C-7. Coefficient of variation of received power (mW) at each point for different size radius bins.

Table C-3. Summary of received power coefficient of variation by radius bin size.

| Run # | Bin Size | min | max | median | mean | Std. dev. |
|-------|-----------|------|------|--------|------|-----------|
| 1 | 5 meters | 0.00 | 1.29 | 0.16 | 0.21 | 0.18 |
| 2 | 10 meters | 0.00 | 1.26 | 0.18 | 0.23 | 0.17 |
| 3 | 25 meters | 0.06 | 1.44 | 0.23 | 0.27 | 0.18 |
| 4 | 50 meters | 0.07 | 2.03 | 0.28 | 0.31 | 0.21 |

In order to relate some of this data to an actual understanding of measurement positions on Table Mountain, we looked at the standard deviation of three positions along the drive path, shown in Figure C-8. We want to understand why these points give us high variability. We chose a point from run 1 and looked at the variability of the signal for the nearest neighbors from other runs within a 5 meter radius. The first point is located at the left-most intersection in (yellow square) and is shown in detail in Figure C-9.

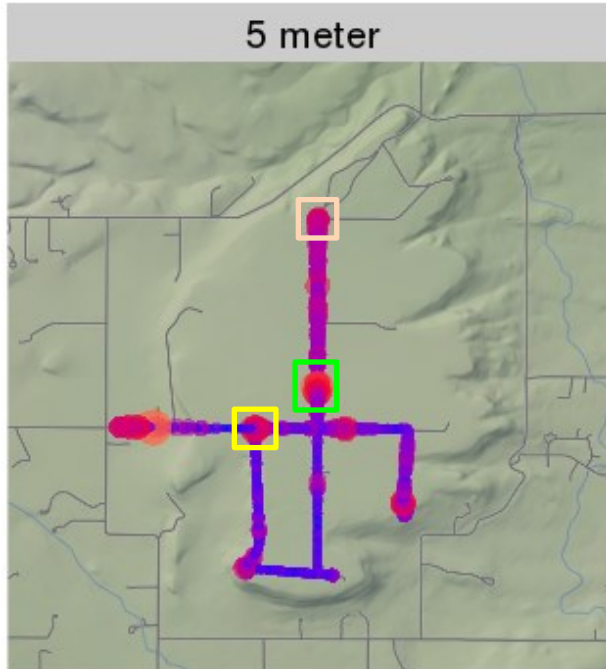


Figure C-8. Figure showing three locations of high standard deviation.

We measure the distance between the three measurement points and show the measured basic transmission loss (dB) at each of these points to determine the variability. This information is given in Table C-4.



Figure C-9. Figure showing the location of three measurement points at the left-most intersection on Table Mountain (see yellow square in Figure C-8). Google Earth ® image, 2015.

Table C-4. Summary of basic transmission loss (dB) and distance difference (m) of three measurement files for the nearest neighbor.

| Measurement File | Basic transmission loss (dB) | Δd between measurement points |
|---------------------------------------|------------------------------|---------------------------------------|
| 1 | 130.5 | 5 m (1,2), 5.4 m (1,3) |
| 2 | 137.0 | 5 m (2,1), 4.5 m (2,3) |
| 3 | 135.9 | 4.5 m (3,2), 5.4 m (3,1) |
| basic transmission loss range: 6.5 dB | | |

The differences in distance (Δd) between the measurement points are shown in the last column. The first distance in row 1 is the difference between measurement point 1 and measurement point 2 and the second distance is the difference between measurement point 1 and measurement point 3. This convention is repeated in the other two rows. The maximum distance between any of these points is 5.4 m. Since these points are close to one another, we would expect that the received power would have similar values. The actual terrain between the transmitter and receiving points does not vary, so we wouldn't expect different basic transmission loss due to terrain diffraction. We can see that the actual basic transmission loss range for all three points is 6.5 dB.

The second point is located at the northern most side of Table Mountain where there is terrain diffraction which leads to larger standard deviations. This location is shown by the orange square in Figure C-8. A close-up view of this location is shown in Figure C-10.



Figure C-10. Northern-most location on Table Mountain where large standard deviations exits.

The measured basic transmission loss and distance difference between these three measurement locations is shown in Table C-5.

Table C-5. Summary of basic transmission loss (dB) and distance difference (m) of three measurement files for the closest mutual location.

| Measurement File | Basic transmission loss (dB) | Δd between measurement points |
|--|------------------------------|---------------------------------------|
| 1 | 155.4 | 5.8 m (1,2), 1.7 m (1,3) |
| 2 | 160.4 | 5.8 m (2,1), 4.6 m (2,3) |
| 3 | 167.2 | 4.6 m (3,2), 1.7 m (3,1) |
| Basic transmission gain range: 11.4 dB | | |

The differences in distance (Δd) between the measurement points are shown in the last column. The maximum distance between any of these points is 5.8 m. Since these points are close to one another, we would expect that the received power would have similar values. The actual basic transmission loss range for all three points is 11.4 dB, which is larger than for the first set of points.

In summary, we looked at the standard deviations of received power for different sized radii for each point on Table Mountain both for a dB scale and for the coefficient of variation. For mobile measurements, we cannot force the GPS to record its position at the exact same location, so we look at the variability at points that are close to one another. We found that the means of the standard deviations varied from 0.95 to 1.48 dB with a standard deviation around this mean from 0.85 to 1.03 dB, so that we can expect a maximal mean deviation of 2 to 4 dB. We can also expect maximum deviations of approximately 9 dB. For the coefficient of variation we see the means of the standard deviations varied from 0.21 to 0.31 and the standard deviations around this mean varied from 0.17 to 0.21. We then looked at two points on the drive route where the standard deviations were higher. We looked at the difference in distance and received power levels at one point from run 1 and the two closest points from runs 2 and 3. We found at the first point, that the maximum distance between points was 5.4 m and the range of basic transmission loss was 6.5 dB. At the second point, there is terrain diffraction loss that increases the standard deviation for the basic transmission loss to 11.4 dB. The maximal distance between these points is 5.8 m.

C.2 Static Measurement Repeatability Analysis

The static measurement positions were used to understand both the measurement repeatability at one location and the drift of the GPS receiving system. If we look again at Figure C-1 we can see the positions of the static measurement locations. Static location 1 is shown in the lower center of the figure and is closest to the transmitter on Green Mountain. Measurements were collected for a total of 15 minutes at each location. Measured smoothed received power as a function of time is shown in Figure C-11. The measured received power is $90 \text{ dB} \pm 0.3 \text{ dB}$.

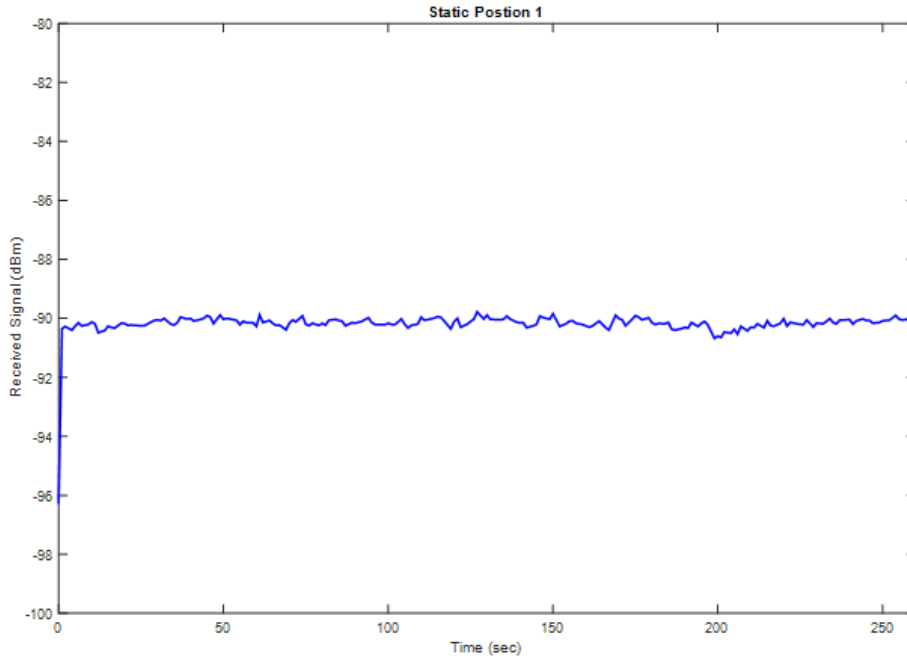


Figure C-11. Measured smoothed received power as a function of time for static position 1 on Table Mountain.

The measured smoothed received power for static position 2 is shown in Figure C-12 and has a value of -96.1 ± 0.5 dB.

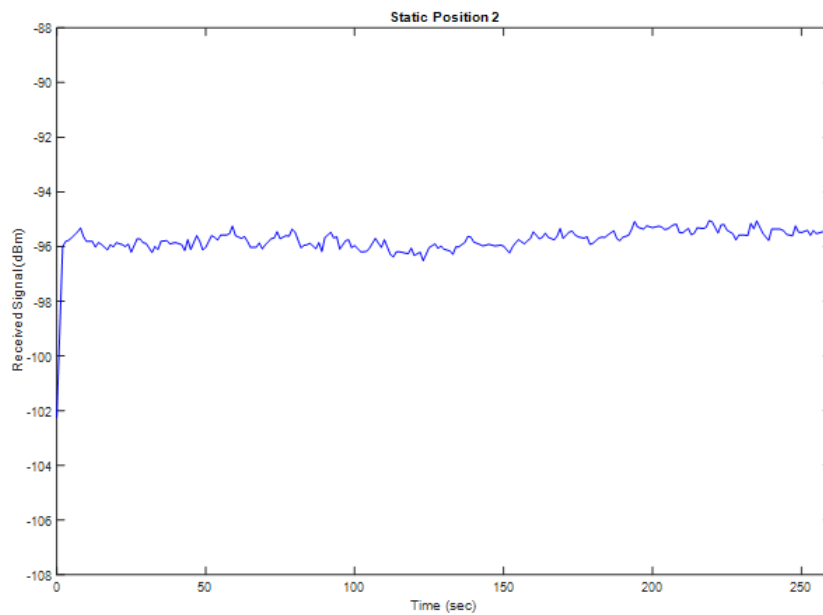


Figure C-12. Received power as a function of time for static position 2 on Table Mountain.

C.3 Parameter Dependencies on Propagation Measurements

A screening experiment is designed to determine which environmental variables influence measurements [44]–[46]. The following paragraphs will discuss a screening experiment designed for the ITS CW channel sounder followed by an initial set of results.

To design a screening experiment, the researcher must ask the question, “Which variables do I expect will have an impact on my propagation measurements?” Based on previous experiments, we chose the following six independent screening variables:

- Transmitter power
- Transmitter height (elevation angle)
- Frequency
- Receiving vehicle speed
- Amount of traffic
- Line-of-sight (LOS) vs. non-line-of-sight (NLOS)

The dependent variables for this study are received power, coefficient of variation, and K-factor assessed on an individual basis. The screening variables were studied at two levels. Table C-6 provides a summary of the screening variables.

Table C-6. Summary of screening variables.

| Variable | Low Setting | High Setting |
|-------------------------|---------------------------------|---------------------|
| Transmitter power level | 37 dBm | 47 dBm |
| Transmitter height | Building 1 – DOC Boulder campus | Green Mountain Mesa |
| Frequency | 1755 MHz | 3500 MHz |
| Receiving vehicle speed | 20 mph | 30 mph |
| Amount of traffic | Off peak | Rush hour |
| LOS vs. NLOS | Lashley Ln. | Moorhead Ave. |

The experiment has six variables or main effects. There are 15 two-way interactions which determine the number of experimental runs and how the factors will appear together in the run chart. The run chart for this experiment is shown in Table C-7.

Table C-7. Run chart for screening experiment.

| Run No. | Tx Height. | Rx Loc. | Freq (MHz) | Traffic | Tx Power (dBm) | Speed (mph) |
|---------|-------------|---------------|------------|-----------|----------------|-------------|
| 1 | ITS-Bldg. 1 | Lashley Lane | 3500 | rush hour | 47 | 20 |
| 2 | ITS-Bldg. 1 | Lashley Lane | 3500 | rush hour | 37 | 20 |
| 3 | ITS-Bldg. 1 | Moorhead Ave. | 3500 | rush hour | 37 | 30 |
| 4 | ITS-Bldg. 1 | Moorhead Ave. | 3500 | rush hour | 47 | 30 |
| 5 | ITS-Bldg. 1 | Moorhead Ave. | 3500 | off peak | 47 | 20 |
| 6 | ITS-Bldg. 1 | Moorhead Ave. | 3500 | off peak | 37 | 20 |

| Run No. | Tx Height. | Rx Loc. | Freq (MHz) | Traffic | Tx Power (dBm) | Speed (mph) |
|---------|-------------|---------------|------------|-----------|----------------|-------------|
| 7 | ITS-Bldg. 1 | Lashley Lane | 3500 | off peak | 37 | 30 |
| 8 | ITS-Bldg. 1 | Lashley Lane | 3500 | off peak | 47 | 30 |
| 9 | ITS-Bldg. 1 | Lashley Lane | 1755 | off peak | 47 | 20 |
| 10 | ITS-Bldg. 1 | Lashley Lane | 1755 | off peak | 37 | 20 |
| 11 | ITS-Bldg. 1 | Moorhead Ave. | 1755 | off peak | 37 | 30 |
| 12 | ITS-Bldg. 1 | Moorhead Ave. | 1755 | off peak | 47 | 30 |
| 13 | ITS-Bldg. 1 | Moorhead Ave. | 1755 | rush hour | 47 | 20 |
| 14 | ITS-Bldg. 1 | Moorhead Ave. | 1755 | rush hour | 37 | 20 |
| 15 | ITS-Bldg. 1 | Lashley Lane | 1755 | rush hour | 37 | 30 |
| 16 | ITS-Bldg. 1 | Lashley Lane | 1755 | rush hour | 47 | 30 |
| 17 | Green Mtn. | Lashley Lane | 1755 | rush hour | 47 | 20 |
| 18 | Green Mtn. | Lashley Lane | 1755 | rush hour | 37 | 20 |
| 19 | Green Mtn. | Moorhead Ave. | 1755 | rush hour | 37 | 30 |
| 20 | Green Mtn. | Moorhead Ave. | 1755 | rush hour | 47 | 30 |
| 21 | Green Mtn. | Moorhead Ave. | 1755 | off peak | 47 | 20 |
| 22 | Green Mtn. | Moorhead Ave. | 1755 | off peak | 37 | 20 |
| 23 | Green Mtn. | Lashley Lane | 1755 | off peak | 37 | 30 |
| 24 | Green Mtn. | Lashley Lane | 1755 | off peak | 47 | 30 |
| 25 | Green Mtn. | Lashley Lane | 3500 | off peak | 47 | 20 |
| 26 | Green Mtn. | Lashley Lane | 3500 | off peak | 37 | 20 |
| 27 | Green Mtn. | Moorhead Ave. | 3500 | off peak | 37 | 30 |
| 28 | Green Mtn. | Moorhead Ave. | 3500 | off peak | 47 | 30 |
| 29 | Green Mtn. | Moorhead Ave. | 3500 | rush hour | 47 | 20 |
| 30 | Green Mtn. | Moorhead Ave. | 3500 | rush hour | 37 | 20 |
| 31 | Green Mtn. | Lashley Lane | 3500 | rush hour | 37 | 30 |
| 32 | Green Mtn. | Lashley Lane | 3500 | rush hour | 47 | 30 |

The entire drive route is shown by the yellow dots in Figure C-13, although only the data on Lashley Lane and Moorhead Ave. (shown by the green outlines) was analyzed.

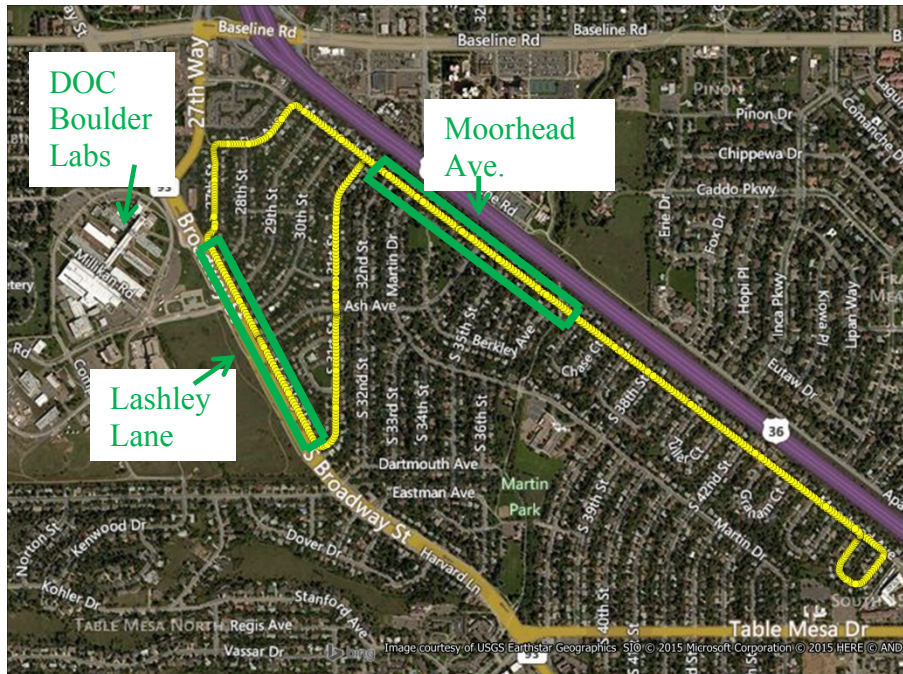


Figure C-13. Screening measurement drive route. Sections for analysis are shown by the green outlined regions.

Although measurements were made at two different frequencies, we chose not to run the analysis on this variable due to time constraints. Therefore the following analysis includes only five main effects. The received power level for all runs is shown in Figure C-14.

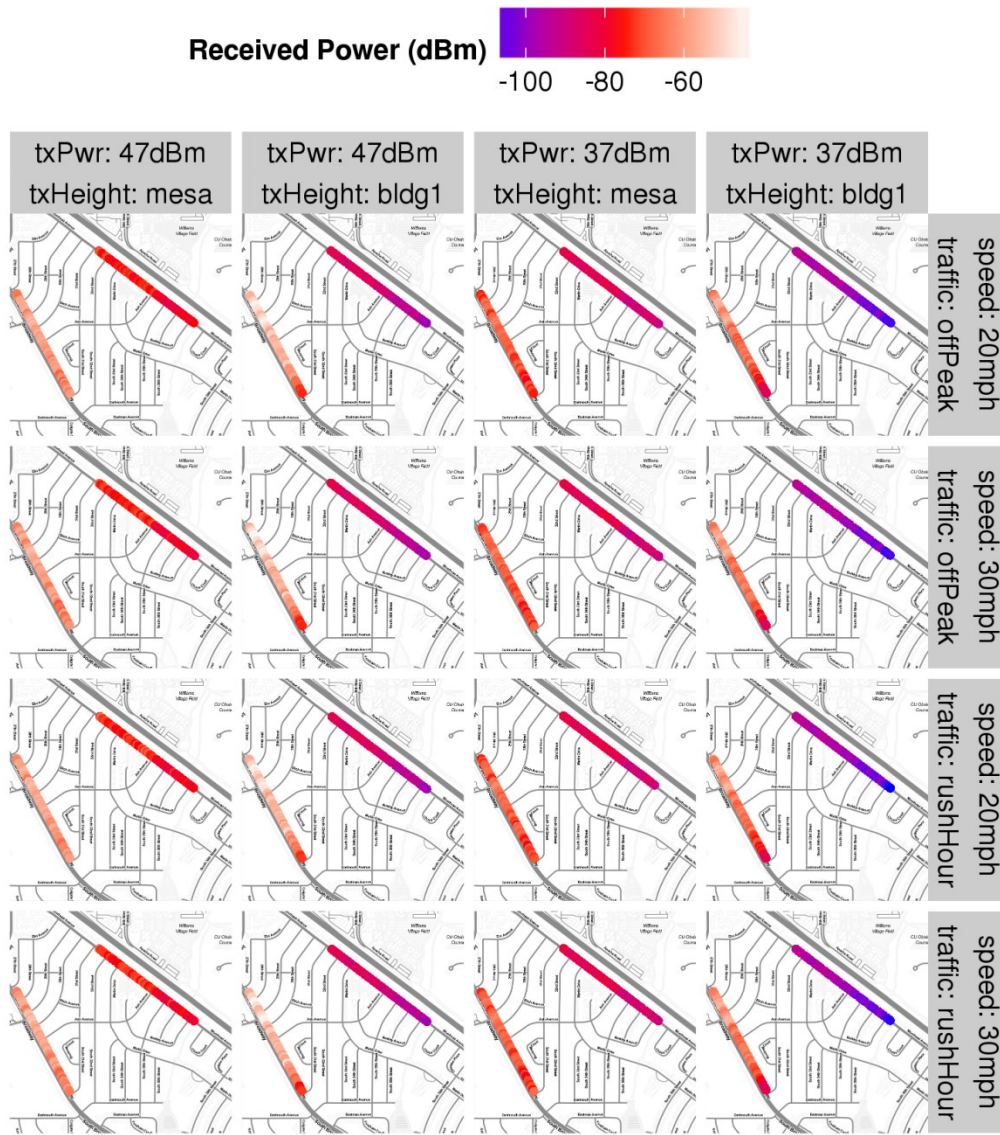


Figure C-14. Received power levels for all screening measurement runs along Lashley Lane and Moorhead Ave.

Received power levels were checked for normality and less than half of the runs were found to be normally distributed. Boxplots of received power are shown in Figure C-15. These boxplots show the received power as a function of the screening variables. We found that received power levels were greater on Lashley Lane (LOS) than on Moorehead Ave. (NLOS). We found that traffic patterns (off peak vs. rush hour) did not have a significant effect on the received power level. The transmit power influenced the received power level. The transmitting height also seemed to influence the received power level. The speed of the receiving vehicle didn't seem to have an influence on the received power level.

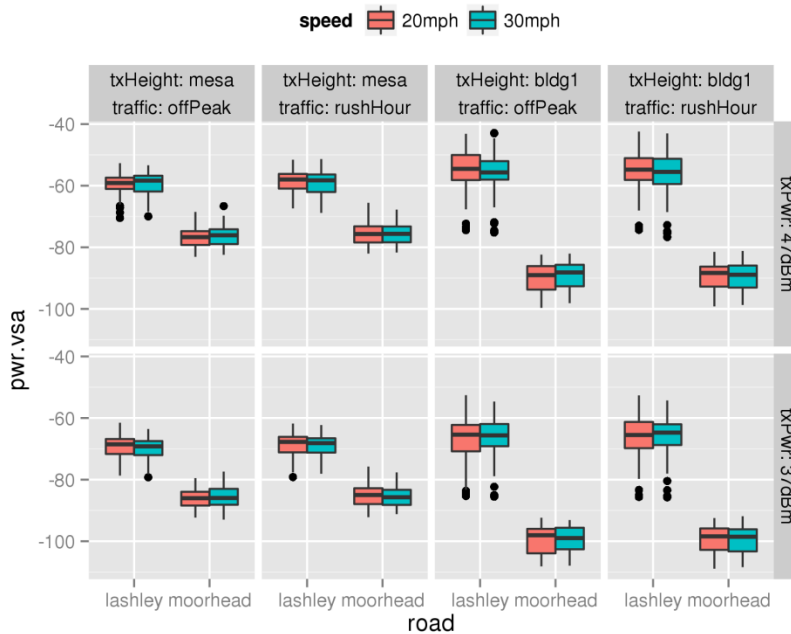


Figure C-15. Boxplots of received power as a function of the screening variables.

We expected runs along Lashley Lane to be correlated to one another and the same for Moorhead Ave. However, we found that this was difficult to demonstrate in practice due to the varying statistical sample sizes. The mean received power level for every run was calculated. The data was processed in this way because traffic patterns and speed are not consistent along the road even though we tried our best to control these effects. An analysis of variance (ANOVA) was used to determine the effect of the five screening variables and all two-way interactions among those variables on the dependent variable, received power level. From the ANOVA analysis, we used the mean squared error to develop a Pareto chart [47]–[49]. A Pareto chart is a diagram used to identify the few variables that have a large contribution to the variability of the dependent variable, the received power level. It is also used to identify the variables that have very little influence on the dependent variable.

The plot of the main effects or factors for the dependent variable, received power level, is shown in Figure C-16. The x-axis shows the screening factors and the y-axis shows the mean of the received power. This chart tells us that the largest difference for the mean of the received power is due to the road, i.e., whether we were on Lashley Lane or Moorehead Ave. (LOS vs. NLOS). The second largest effect is due to the transmitter power (txPwr), and the third largest effect is due to the transmitter height (txHeight, or elevation angle). The speed of the receiving vehicle and traffic conditions do not influence the mean of the received power level.

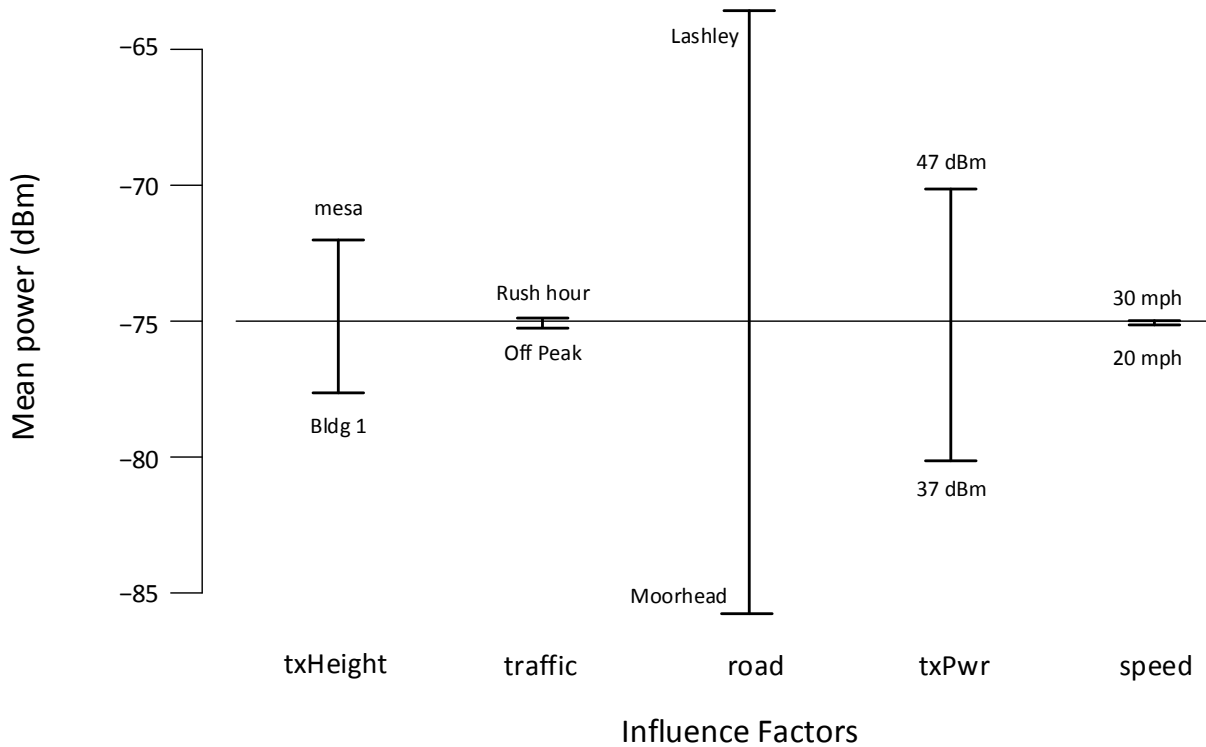


Figure C-16. Plot of main screening effects (influence factors) as a function of the mean value of the received power level in dBm.

Finally, we can develop a Pareto chart which shows how much each effect appears to influence the mean received power level. This is shown in Figure C-17. The road (LOS vs NLOS) appears to explain 75% of the data, the transmitting power explains approximately 13% of the data for a cumulative effect due to these two factors of about 88%. The combination of the transmitter height (elevation angle) with the road explains another 10% of the data, for a cumulative effect due to these three factors of approximately 98%. All other effects explain only 2% of the data.

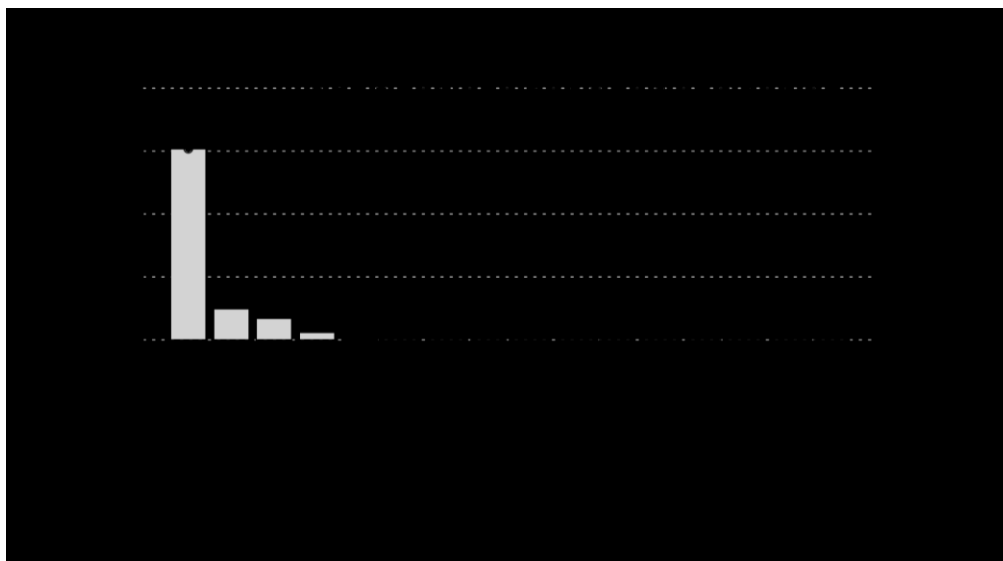


Figure C-17. Pareto chart showing the percentage influence of each main effect on the mean received power levels.

It was also important for us to look at two other criterion measures (CM). These are the coefficient of variation (CV) and the K-factor. The received power level has an inherent bias in terms of the distance of the receiver from the transmitter, so in order to minimize this bias, we chose to perform an ANOVA analysis on the CV. The CV is the ratio of the standard deviation of the receiver power level over the mean or absolute value of the mean of the received power level. The K-factor is the ratio of the power in the direct path to the power in the scattered paths. Only the Pareto charts for these two analyses will be shown in this section.

The Pareto chart for the CV is shown in Figure C-18. In this chart, the road (LOS vs NLOS) appears to explain about 60% of the data, the combination of the transmitter height plus the road explains approximately 35% of the data for a cumulative effect due to these two factors of about 95%. The transmitter height explains another 4% of the data, for a cumulative effect due to these three factors of approximately 99%. All other effects explain only 1% of the data.

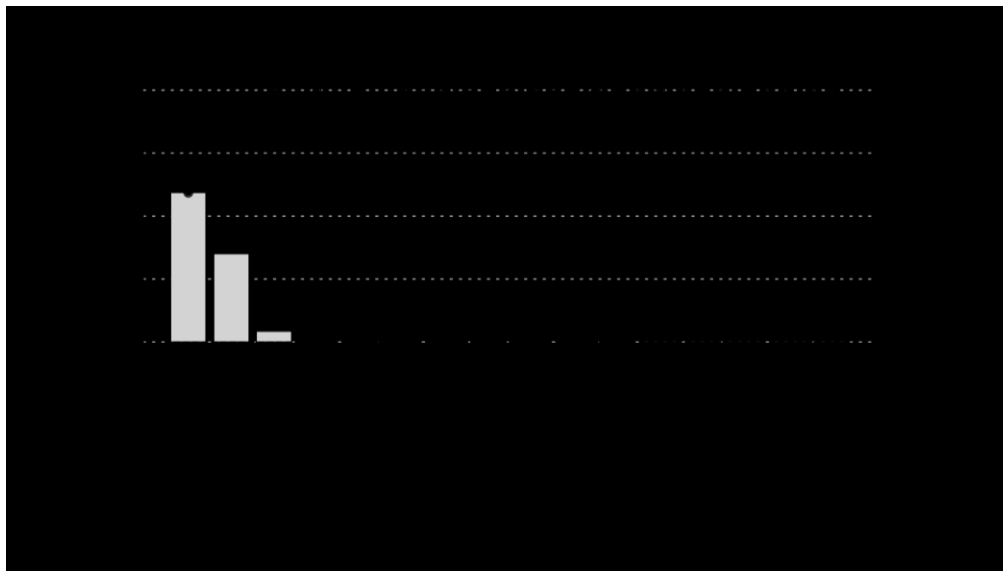


Figure C-18. Pareto chart showing the percentage influence of each main effect on the coefficient of variation (CV).

The Pareto chart for the K-factor is shown in Figure C-19. In this chart, the road (LOS vs NLOS) appears to explain about 73% of the data, the transmitter height explains approximately 12% of the data for a cumulative effect due to these two factors of about 85%. The combination of the transmitter height plus the road explains another 10% of the data, for a cumulative effect due to these three factors of approximately 95%. All other effects explain about 15% of the data.

These three Pareto charts show the road alone has the most influence on the measured data, transmitter height either independently or with the road has the second largest influence on the measured data and the transmitter height either independently or with the road has the third largest influence on the data.

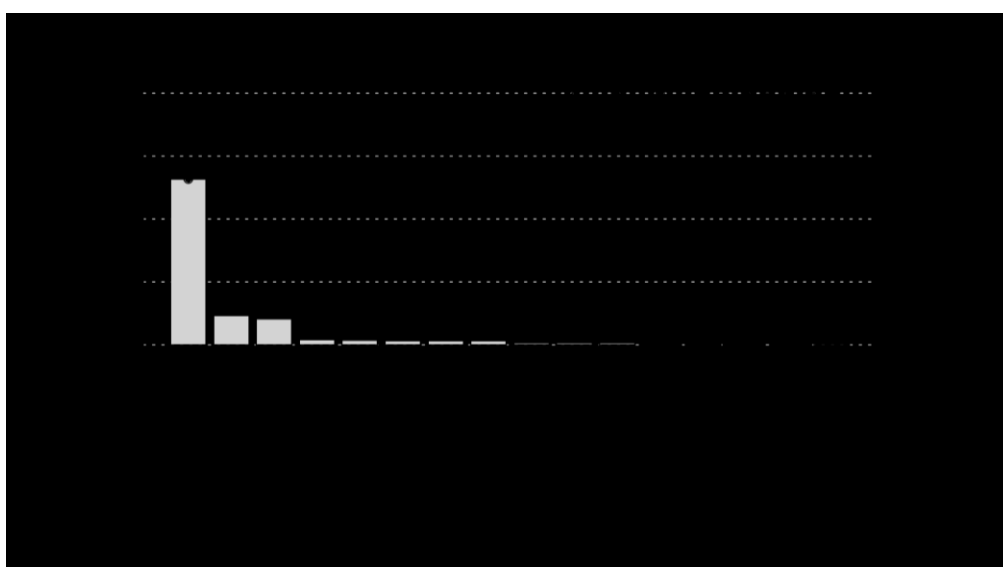


Figure C-19. Pareto chart showing the percentage influence of each main effect on the K-factor.

BIBLIOGRAPHIC DATA SHEET

| | | |
|---|---|--|
| 1. PUBLICATION NO. TM-19-535 | 2. Government Accession No. | 3. Recipient's Accession No. |
| 4. TITLE AND SUBTITLE Best Practices for Radio Propagation Measurements | | 5. Publication Date November 2018 |
| | | 6. Performing Organization Code NTIA/ITS.M |
| 7. AUTHOR(S) Chriss Hammerschmidt, Robert T. Johnk, Paul M. McKenna, Christopher R. Anderson | | 9. Project/Task/Work Unit No. 6786000-300 |
| | | 10. Contract/Grant Number. |
| 8. PERFORMING ORGANIZATION NAME AND ADDRESS Institute for Telecommunication Sciences National Telecommunications & Information Administration U.S. Department of Commerce 325 Broadway Boulder, CO 80305 | | 12. Type of Report and Period Covered |
| | | 11. Sponsoring Organization Name and Address National Telecommunications & Information Administration Herbert C. Hoover Building 14 th & Constitution Ave., NW Washington, DC 20230 |
| 14. SUPPLEMENTARY NOTES | | |
| 15. ABSTRACT (A 200-word or less factual summary of most significant information. If document includes a significant bibliography or literature survey, mention it here.) This report describes a set of best practices for the preparation and verification of radio propagation measurement systems. We discuss advantages and disadvantages of various channel sounders, the common components used in these systems, and measurement of these components. We then move to system verification measurements both on the benchtop and in some preliminary outdoor propagation measurements. The appendices discuss uncertainty analysis, antenna measurements, and system repeatability and sensitivity analysis measurements. | | |
| 16. Key Words (Alphabetical order, separated by semicolons) measurements, radio propagation, radio propagation measurements, radio propagation measurement system, radio propagation uncertainties, radio measurement system performance verification | | |
| 17. AVAILABILITY STATEMENT <input checked="" type="checkbox"/> UNLIMITED. <input type="checkbox"/> FOR OFFICIAL DISTRIBUTION. | 18. Security Class. (This report) Unclassified | 20. Number of pages 133 |
| | 19. Security Class. (This page) Unclassified | 21. Price: |

NTIA FORMAL PUBLICATION SERIES

NTIA MONOGRAPH (MG)

A scholarly, professionally oriented publication dealing with state-of-the-art research or an authoritative treatment of a broad area. Expected to have long-lasting value.

NTIA SPECIAL PUBLICATION (SP)

Conference proceedings, bibliographies, selected speeches, course and instructional materials, directories, and major studies mandated by Congress.

NTIA REPORT (TR)

Important contributions to existing knowledge of less breadth than a monograph, such as results of completed projects and major activities.

JOINT NTIA/OTHER-AGENCY REPORT (JR)

This report receives both local NTIA and other agency review. Both agencies' logos and report series numbering appear on the cover.

NTIA SOFTWARE & DATA PRODUCTS (SD)

Software such as programs, test data, and sound/video files. This series can be used to transfer technology to U.S. industry.

NTIA HANDBOOK (HB)

Information pertaining to technical procedures, reference and data guides, and formal user's manuals that are expected to be pertinent for a long time.

NTIA TECHNICAL MEMORANDUM (TM)

Technical information typically of less breadth than an NTIA Report. The series includes data, preliminary project results, and information for a specific, limited audience.

For information about NTIA publications, contact the NTIA/ITS Technical Publications Office at 325 Broadway, Boulder, CO, 80305 Tel. (303) 497-3572 or e-mail ITSinfo@ntia.doc.gov.